ABSTRACT

Title of Dissertation: INVESTIGATION OF POLY-N-ACETYL GLUCOSAMINE BIOSYNTHESIS INITIATION AND SPATIAL DISTRIBUTION IN BACTERIAL BIOFILMS THROUGH MICROFLUIDIC FLUORESCENT MICROSCOPY

Steven Hong, Doctor of Philosophy, 2026

Dissertation directed by: Dr. Myles Poulin, Department of Chemistry and Biochemistry

Bacterial cells surface is rich in diverse polysaccharides that encapsulate the cells involved in crucial roles such as regulating cell permeability, mediating surrounding interactions, and offering protection. Key classes of bacterial surface polysaccharides include teichoic acids (TAs), lipopolysaccharides (LPS), capsular polysaccharides (CPS), and exopolysaccharides (EPS). These surface polysaccharides are predominately synthesized by three conserved pathways: the Wzx/Wzy-dependent pathway, the ATP-binding cassette (ABC) transporter-dependent pathway, and the synthase-dependent pathway. The initiation of polysaccharide biosynthesis in the Wzx/Wzy-dependent and ABC transporter pathways is well documented to employ a lipid initiator

substrate. However, the initiations of synthase-dependent systems have yet to be eluted, with speculation of undergoing a "self-initiating" mechanism by employing a free monosaccharide as the first acceptor molecule.

Here, we investigate the initiation of poly-β-D-(1→6)-N-acetyl-glucosamine (PNAG) in Gram-negative bacteria through synthase-dependent pathway via PgaCD complex. PgaCD is a transmembrane heterodimer within the glycosyl transferase (GT) 2 family, catalyzing the transfer of GlcNAc residues from activated sugar nucleotides onto an acceptor substrate. We begin by isolating active PgaCD complex and measuring its activity *in vitro* (Chapter 2). First, we employ an expression system that successfully incorporates both proteins within the same membrane bilayer and demonstrated positive enzymatic activity through the hydrolysis of UDP from its cognate substrate UDP-GlcNAc (2.2.1). Additional ^{13}C NMR analysis of *in vitro* product confirmed the polymerization of PNAG and revealed chemical shifts characteristic of unsaturated lipids (2.2.4). Localization experiments of the *de novo* PNAG demonstrated membrane association mechanism after polymerization suggesting possible interactions with the membrane lipids (3.2.1). Furthermore, high concentrations of free GlcNAc residues had no effect on enzymatic activity of PgaCD, ruling out its role as a possible initiator substrate (3.2.2). Taken together, the evidence suggests that the PgaCD complex may employ a primer-dependent initiation strategy analogous to other surface polysaccharide biosynthetic systems.

Stratification of biofilms could impact how EPS is spatially distributed throughout; thus, it is imperative to study biofilms *in situ*, without disrupting their architecture. By utilizing a microfluidic device with an integrated cell seeding zone, it allowed for simultaneous cultivation, labeling, and dispersal monitoring of bacterial biofilms (4.2.1). Through using this platform, we compared PNAG distributions in biofilms produced by different bacteria (4.2.3). Dispersal by

PNAG hydrolysis using DspB wt revealed alternative cohesion profiles between the two species, showcasing the versatility of the microfluidic platform for simultaneous cultivation, imaging, and targeted dispersal of diverse bacterial biofilms.

INVESTIGATION OF POLY-N-ACETYL GLUCOSAMINE BIOSYNTHESIS INITIATION AND SPATIAL DISTRIBUTION IN BACTERIAL BIOFILMS THROUGH MICROFLUIDIC FLUORESCENT MICROSCOPY

by

Steven Hong

Thesis submitted to the Faculty of the Graduate School of the
University of Maryland, College Park, in partial fulfillment
of the requirements for the degree of

Doctor of Philosophy

2026

Advisory Committee:

Professor Myles Poulin, Chair

Professor Paul Paukstelis

Professor Lai-Xi Wang

Professor Yanxin Liu

Professor Vincent Lee

Acknowledgements

As I reflect on my journey, it was very clear to me that it was the support I have received throughout the years that has allowed me the opportunity and privilege to purse and obtain this degree. I am truly grateful to have been in an environment that allowed me to ponder, to question, to fail, and to laugh, all thanks to the people that make up the Poulin Lab. To Alexandra Peterson, Teodora Kljaic, Laura Kuperman, and Shaochi Wang for welcoming me to the lab – I will always to grateful for your advice and friendship. To Luan Vo, the self-proclaimed "most senior member", it was an honor to be in your presence day in and day out for the past 5 years. To Sureshee Liyanaarachchi, its was your protein factory that allowed my labelling experiments to succeed. To Sashika Fernando, Kwaku Obeng, Prince Tetteh, Maddy Plank, Wonder Acquah, Saul Flores, Fathima Faiz, and Mark Eshun – I am thankful for your friendship. It wouldn't be the Poulin Lab without our brigade of talented and hardworking undergraduates, Lucas Barry, Jack Yang, Kick Monahan, Ashley Chan, and many others. To Dr. Myles Poulin, I am grateful to have been a student in your lab. It was through your expertise, mentorship, compassion, and support that has made this journey possible – thank you.

To the University of Maryland, for being my home for the last 5 years. Thank you to all the committee members, Professors Douglas Julin, David Fushman, Lai-Xi Wang, Paul Paukstelis, and Vincent Lee for your guidance and helping hand. To the Fab Lab staff members Mark Lecates and Jonathan Hummel for helping me navigate all the equipment as a novice.

This Ph.D. would not have been possible without the unwavering support from my family and friends. To my partner, Jasmine Grey, your talent, wisdom, and intelligence pushed me to better myself throughout the years and always believing in me. To my parents, Ling Di Hong and

Qiao Ling Weng, for all your sacrifices that granted me this opportunity. To my favorite sister, Vicki Weng, who taught me that you only live once. To the Grey and Snow family, for always treating me like family. What a journey it has been.

Table of Contents

List of Figures

List of Tables

List of Abbreviations

Exopolysaccharides (EPS)

Teichoic acids (TA)

Lipopolysaccharides (LPS)

Capsular polysaccharides (CPS)

ATP-binding cassette (ABC)

Nucleotide-binding domains (NBDs)

Hyaluronic acid synthase (HAS)

Bacterial cellulose synthase (Bcs)

Deoxyribonucleic acid (DNA)

Scanning electron microscopy (SEM)

Hyaluronan (HA)

Quorum sensing (QS)

N-acyl-l-homoserine lactones (AHLs)

Diffusible signal factor (DSF)

Dispersin B (DspB)

β-1,6-poly-N-acetylglucosamine (PNAG)

Cyclic diguanosine (c-di-GMP)

Cyclic guanosine monophospnate (cGMP)

Cyclic adenosine monophosphate (cAMP)

Diguanylate cyclases (DGCs)

Cross polarization magic angle spinning (CP-MAS)

Nuclear magnetic resonance (NMR)

Glycoside hydrolase (GH)

Luria broth (LB)

Bovine serum albumin (BSA)

Confocal laser scanning microscopy (CLSM)

Atomic force microscopy (AFM)

Transmission electron microscopy (TEM)

Carbon storage regulator A (CsrA)

High-performance liquid chromatography (HPLC)

Amphiphilic polymer (AMPHIPOL)

N-Dodecyl-phosphocholine (FC-12)

Immobilized metal affinity chromatography (IMAC)

Inverted membrane vesicles (IMVs)

Proteoliposome (PL)

Gray value (GV)

Chapter 1: Introduction to bacterial cell surface polysaccharides and bacterial biofilms

1.1 Cell surface polysaccharides in bacteria

Bacteria surfaces are predominately composed of polysaccharides that encapsulate cells and are essential of their survival.[1] These surface polysaccharides are highly diverse in structure and play crucial roles in regulating cell permeability and mediating interactions with the surrounding environment.[2] The initial characterization of bacterial surface polysaccharides dates back to the early 1900s, with the isolation of a "soluble specific substance" from *pneumococcus* Type II strains associated with pneumonia.[3] Subsequent studies have elucidated the precise morphological localization and functional significance of these macromolecules.

Surface polysaccharides are often described as forming a "capsule" around the bacteria, contributing to 60% of the bacterial dry weight. This capsule is biochemically and structurally distinct from the bacterial cell wall which includes a complex of proteins, lipids, and polysaccharides essential for cell integrity and viability. Alternatively, enzymatic degradation/removal of these polysaccharides does not compromise cell viability. The capsule is highly hydrated, containing as much as 98% water, and possess a characteristic sticky, gelatinous texture.[4]

These polysaccharide capsules contribute to multiple aspects of the bacterial lifecycle, including modulation of immune system interactions, maintenance of structural integrity, and control of cellular permeability. Key classes of bacterial surface polysaccharides include teichoic acids (TAs), lipopolysaccharides (LPS), capsular polysaccharides (CPS), and exopolysaccharides (EPS) (Fig 1.1).[5–7] Teichoic acids are anionic polymers found exclusively in Gram-positive bacteria, and are subdivided into wall teichoic acids (WTAs), which are covalently linked to peptidoglycan, and lipoteichoic acids (LTAs), which are anchored to membrane lipids.[8] In Gram-negative bacteria, LPS molecules constitute a major component of the outer membrane and consist

of three distinct regions: Lipid A, serving as the lipid anchor and consisting of a β-1,6-linked disaccharide of glucosamine attached to fatty acids; a core oligosaccharide containing residues such as 3-deoxy-D-manno-oct-2-ulosonic acid (Kdo) and heptose residues that confer structural stability; and the O-antigen, a highly variable polysaccharide chain composed of repeated oligosaccharide units.[9,10] CPS are tightly associated with the cell surface, linked via lipid anchors in Gram-negative bacteria or covalently bound to peptidoglycan in Gram-positive bacteria. These large acidic polymers exhibit extensive structural variation, providing the basis for bacterial

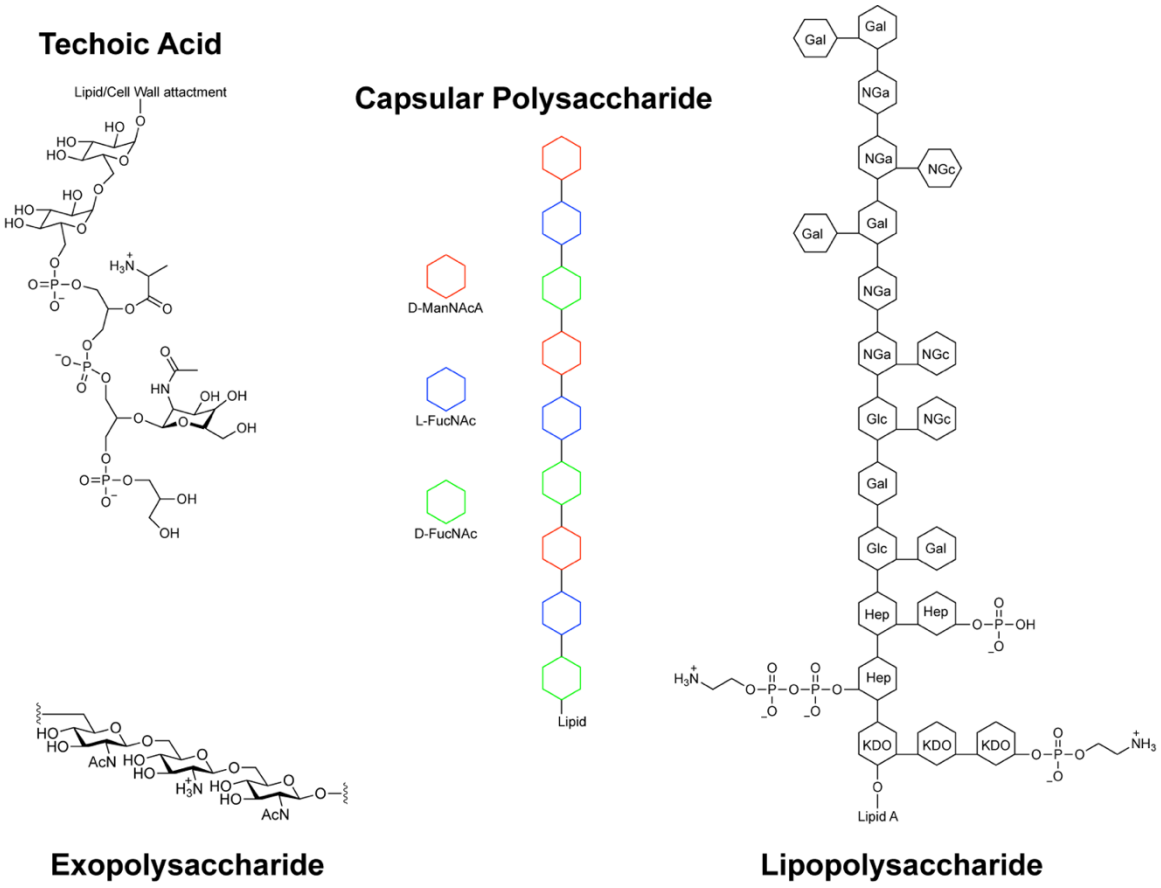

Figure 1.1: Common surface polysaccharides produced by bacteria. Majority of surface polysaccharides are displayed on cell surfaces through covalent linkages to lipid substrate/peptidoglycans. Abbreviations: FucNAc: N-Acetyl-Fucosamine; ManNAcA: N-acetyl-Mannosaminuronate; Gal: Galactose; Nga: N-glycolylneuraminic acid; KDO: 3-deoxy-α-D-mannooctulosonic acid; Hep: Heptulose; NGa: Galactosamine; NGc: Glucosamine.

serotyping.[11] EPS are long-chain polysaccharides that contribute significantly to biofilm matrix formation in both Gram-positive and Gram-negative bacteria, with structural diversity arising from variations in branching, glycosidic linkages, and chemical modifications such as deacetylation, succinylation, and phosphorylation.[12–14]

Biosynthesis of bacterial surface polysaccharides is primarily mediated through three conserved pathways: the Wzx/Wzy-dependent pathway, the ATP-binding cassette (ABC) transporter-dependent pathway, and the synthase-dependent pathway (Fig 1.2).[15–17] While these pathways govern the synthesis and export of polysaccharides, the specific biochemical characteristics of the polysaccharide and their final assembly and display determine how they are classified and their function.

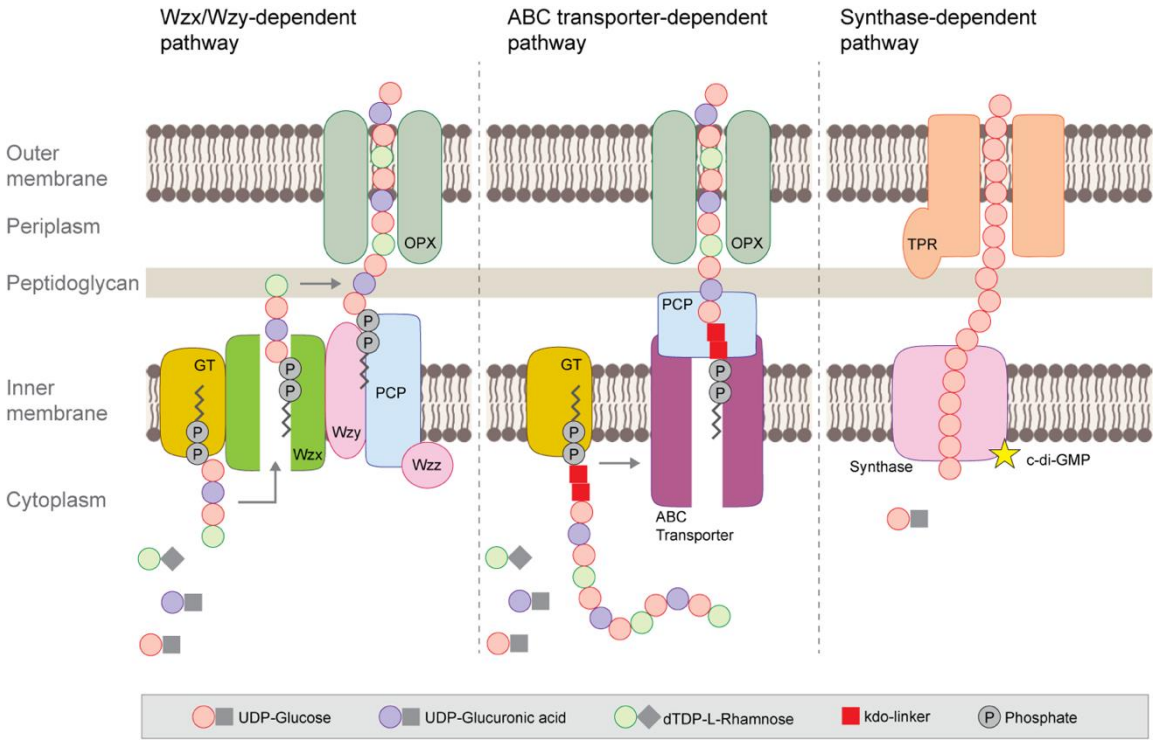

Figure 1.2: Biosynthetic pathways for surface polysaccharides. All surface polysaccharides in bacteria are biosynthesized by 3 pathways: Wzx/Wzy-dependent, ABC transporter-dependent, and Synthase-dependent. Depiction of all 3 pathways in Gram-negative bacterium.

1.2 Wzx/Wzy dependent pathway

Of the three pathways responsible for surface polysaccharide biosynthesis, the Wzx/Wzy pathway is responsible for the synthesis of the majority of the heteropolysaccharides including the LPS O-antigen , CPS, and EPS.[18] The initiation of the pathway typically begins with the transfer of a monosaccharide 1-phosphate from activated sugar nucleotide (NDP-glycoses) onto undecaprenyl phosphate (Und-P) forming undecaprenyl pyrophosphate monosaccharide (Und-PP-monosaccharide) which serves as the foundational acceptor for the polysaccharide assembly.[19] Glycosyltransferase polymerizes upon the lipid linked monosaccharide in the cytoplasm, after which the growing oligosaccharide is translocated across the cytoplasmic membrane by the Wzx flippase into the periplasmic space. Polymerization continues in the periplasm, catalyzed by the putative polymerase Wzy.[20] Upon completion of polymerization, the polysaccharide follows distinct routes depending on the biosynthetic pathway. In LPS biosynthesis, the fully assembled O-antigen is attached to the core oligosaccharide by the ligase WaaL and incorporated into the outer leaflet of the outer membrane. In CPS biosynthesis, the completed polymer is exported through the outer membrane via the translocon Wza.[21]

1.3 ABC-transport dependent pathway

ABC transporters perform diverse functions in biological systems, including the export of various polysaccharides. These large transmembrane proteins contain 4 essential domains: two transmembrane domains (TMDs) and two nucleotide-binding domains (NBDs). The TMDs facilitates polysaccharides export and typically comprise up to 12 transmembrane helices.[22] The nucleotide-binding domains contain a highly conserved LSGGQ motif, a feature that has aided the identification of multiple surface polysaccharide transporters such as Wzt (O-antigen transport), KpsT (Group 2 capsular polysaccharides), and TagH (teichoic acid transport).[15]

In ABC transporter-dependent pathways, polysaccharide polymerization occurs entirely within the cytoplasm. Similar to the Wzx/Wzy pathway, polymer synthesis begins with an Und-PP-monosaccharide intermediate, which is extended through the action of glycosyltransferase (GT) enzymes to assemble a Und-PP-linked polysaccharide product. The completed polysaccharide is subsequently transported across the membrane by the ABC transporter through ATP hydrolysis-driven translocation.[11,23]

1.4 Synthase dependent pathway

The synthase-dependent pathway represents the third major mechanism for bacterial surface polysaccharide synthesis and export.[17] Unlike the Wzx/Wzy and ABC transporter systems, synthase-dependent systems utilize a GT enzyme that is responsible for both polymerization and translocation of the polysaccharide across the membrane.[24] The activity of synthase dependent systems is often regulated by the second messenger cyclic di-guanosine monophosphate (c-di-GMP) in response to environmental signals.[25] In Gram-negative bacteria, the biosynthetic operon frequently contains an outer membrane porin to facilitate polysaccharide export. Many biofilm-associated polysaccharides, such as alginate in *Pseudomonas* species, bacterial cellulose in *Escherichia coli*, and poly-*N*-acetylglucosamine in *Staphylococcal* species, are synthesized via this pathway.[26–28] These enzymes typically use nucleotide diphosphate sugars (NDP-glycoses) as substrates for polysaccharide polymerization. Notably, certain synthases can produce heteropolysaccharides using different substrates. For example, hyaluronic acid synthase (HAS) alternately incorporates UDP-glucuronic acid (UDP-GlcUA) and UDP-N-acetylglucosamine (UDP-GlcNAc) to generate a polysaccharide with repeating disaccharide units.[29] The initiation mechanism of polysaccharide synthesis in synthase-dependent pathways remains under investigation. Current hypotheses suggest a “self-initiation” process where hydrolysis of the NDP-

sugar releases a free monosaccharide that serves as the nucleus for chain elongation. *In vitro* studies have demonstrated reconstituted synthase activity for enzymes such as bacterial cellulose synthase (Bcs), hyaluronic acid synthase (HAS), and alginate synthase.[24,30] However, whether this is the mechanism *in vivo* remains under speculation.

The Bcs system is responsible for the synthesis and translocation of bacterial cellulose, a linear polymer of β-(1→4)-linked glucose (Glc) subunits, across the cellular membrane within Gram-negative bacteria, including in *E. coli* and *Rhodobacter sphaeroides*.[31] The BcsA–BcsB complex forms the active synthase and translocation pore for bacterial cellulose, and its function is allosterically regulated by c-di-GMP binding.[30,32] The BcsA–BcsB complex catalyzes the transfer of Glc from UDP-Glc to the growing polysaccharide. Studies from the Zimmer lab using purified recombinantly expressed BcsA/B from *R. sphaeroides* have shown that the complex is sufficient to produce cellulose polysaccharides in the presence of cellobiose (a dimer of Glc) and UDP-Glc. Similarly, HAS catalyzes the alternate transfer of UDP-N-acetylglucosamine (UDP-GlcNAc) and UDP-glucuronic acid (UDP-GlcUA) to the growing HA chain, forming repeating disaccharide subunits containing alternating β-(1→3) and β-(1→4) glycosidic linkages, respectively.[24]

1.5 PNAG structure, function, and initiation

Poly-β-(1→6)-N-acetyl-D-glucosamine (PNAG) is a widely distributed EPS found in both Gram-positive and Gram-negative bacterial biofilms, with minor structural variations between species (Table 1).[33,34] In Gram-positive bacteria, PNAG synthesis is regulated by the *ica* operon,

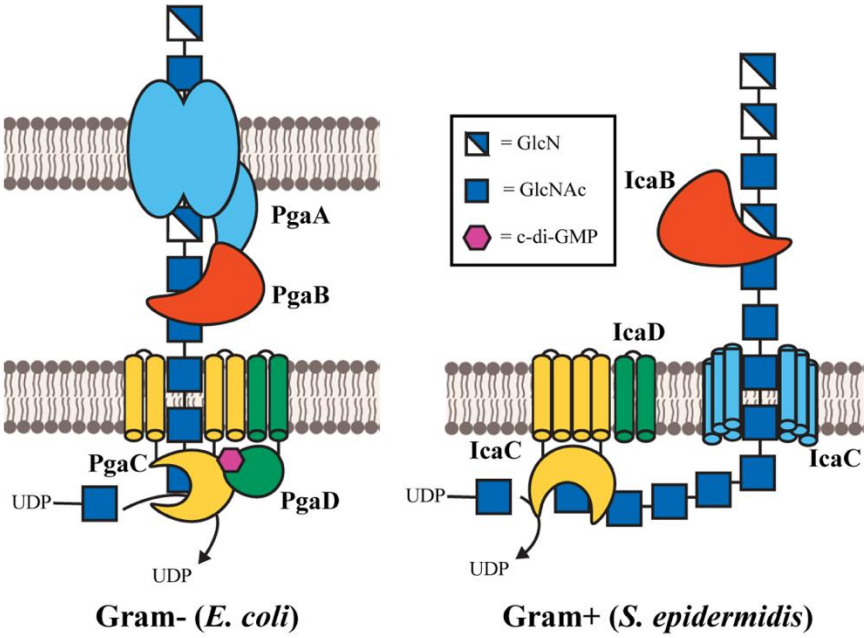

Figure 1.3: PNAG biosynthetic pathway in Gram-negative and Gram-positive bacteria. In Gram-negative bacteria the glycosyl transferase enzyme performs both polymerization and translocation through the membrane. In Gram-positive bacteria, PNAG is polymerized by the glycosyl transferase then exported out by a separate outer porin protein.

which is conserved in *Staphylococcal* species such as *S. epidermidis* and *S. aureus*.[35,36] The operon is comprised of 4 genes: *icaA, icaD, icaB, icaC*.[35,37,38] The IcaA protein is predicted to contain 4 transmembrane helices and a cytosolic domain, and function as the GT enzyme responsible for PNAG polymerization (Fig 1.3).[39] IcaD is a small unknown protein with 2 transmembrane helices, that is required for optimal IcaA activity.[40] IcaC is a large integral membrane protein that was initially predicted to aid in the export of PNAG,[37] though more recent studies suggest it might serve as a succinyl transferase adding succinate esters to the growing PNAG polysaccharide in

Staphylococcal species. Lastly, IcaB is classified as a carbohydrate esterase enzyme responsible for catalyzing the de-*N*-acetylation of PNAG generating glucosamine (GlcN) residues in the mature polysaccharide.[41]

Table 1.1: Different PNAG producing species.[56]

SPECIES TYPE	SPECIES
GRAM-NEGATIVE	*Actinobacillus pleuropneumoniae, Escherichia coli, Acinetobacter baumannii, Aggregatibacter actinomycetemcomitans, Vibrio parahemolyticus, Yersinia pestis, Bordetella pertussis, Klebsiella pneumoniae, B. parapertussis, Shigella spp., B. bronchiseptica, Stenotrophomonas maltophilia, Burkholderia cepacia, Yersinia entercolitica, Enterobacter cloacae, Yersinia pseudotuberculosis, Bacteroides fragilis, Neisseria meningitides, Hemophilus ducreyi, Hemophilus influenzae, Neisseria gonorrhoeae*
GRAM-POSITIVE	*Staphylococcus aureus, Staphylococcus epidermidis, Bacillus subtilis, Streptococcus pyogenes, Streptococcus agalactiae, Streptococcus pneumoniae, Listeria monocytogenes, Mycobacterium tuberculosis*
EUKARYOTIC ORGANISMS	*Candida albicans, Plasmodium spp., Trichmonas vaginalis*

In Gram-negative bacteria, PNAG biosynthesis is mediated by the *pga* operon which also encodes four genes: *pgaA, pgaB, pgaC, and pgaD* (Fig 1.3).[42] Of these the PgaC protein is the inner membrane-associated GT responsible for the polymerization of PNAG by transferring the GlcNAc residue from UDP-GlcNAc to the growing chain.[14] PgaD, analogous to IcaD, is essential

for the GT activity.[14,43] PgaA is a large outer membrane β-barrel porin protein responsible for the secretion of mature PNAG through the outer membrane and features a TPR repeat domain within the periplasm that has been shown to interact with PgaB.[44] PgaB is a soluble, bifunctional periplasmic protein with both carbohydrate esterase (CE) and glycosyl hydrolase (GH) activities. It is responsible for both the de-*N*-acetylation of PNAG as well as PNAG hydrolysis. Its hydrolytic activity is thought to prevent unwanted aggregation of PNAG within the bacterial periplasm.[14]

Despite significant advances in structural and biochemical characterization of PNAG and its associated enzymes, a key aspect of the initial process of PNAG polymerization remains unclear. While the functions of the individual proteins and the structure of the polysaccharide have been elucidated, the identity of the native initiator substrate for PNAG synthase is still unknown.

To our knowledge, there are no reports of fully reconstituted *in vitro* activity for the PgaC/D complex. Previous work by the Nitz group showed that purified complexes solubilized in detergent micelles exhibited much lower activity compared to crude enzyme preparations from membrane fractions.[45] This observation raises questions about whether synthase-based EPS systems employ initiation mechanisms analogous to those of other bacterial surface polysaccharides and whether critical initiator molecules are lost during enzyme purification. This thesis will focus on detailing the biosynthetic pathway of PNAG in Gram-negative bacteria and developing tools to study its function in biofilm assembly, dynamics, and disassembly.

1.6 Exopolysaccharides in bacterial biofilms

Bacterial biofilms consist of sessile cells encapsulated in a self-secreted extracellular matrix composed of nucleic acids, proteins, and EPS. [46–48] EPS have been found to play a crucial role during bacterial biofilm formation by providing physical stability and resistance against shear force.[49] These polysaccharides function as adhesins, promoting cell-to-cell adhesion and

facilitating attachment to surfaces.[50] Several distinct EPS including Pel, Psl, alginate, cellulose, Vps, PNAG and Bacillus EPS have been linked to the development of mature bacterial biofilms.[33,51–54] In most studies, mutants lacking the machinery to synthesize these EPS exhibit significantly reduced biofilm formation capabilities.[35] Beyond conferring physical stability, EPS also play important roles in bacterial pathogenicity.[49,55,56] For example, alginate, a polysaccharide consisting of a linear chain of β-(1→4)-linked D-mannuronic acid that is further modified through isomerization and O-acetylation, has been linked to host immune evasion and has been shown to contribute to pathogenesis in patients suffering from cystic fibrosis.[57]

It is not uncommon for bacteria to contain machinery to synthesize multiple types of EPS structures. For example, *E. coli* harbors at least three distinct synthase pathways encoded by the *pga*, *bcs*, and *nfr* operons.[14,32,58] Together these pathways are responsible for the biosynthesis of PNAG, bacterial cellulose, and a novel poly-*N*-acetylmannosamine (poly-ManNAc) polysaccharide, respectively. For all three pathways, the activity of the synthase enzyme is allosterically modulated through binding to the bacterial second messenger c-di-GMP.[59] In *E. coli*, the production of c-di-GMP is catalyzed by at least 14 diguanylate synthase (Dgc) enzymes in response to environmental signals, serving as part of the bacterial stress response.[60,61] The

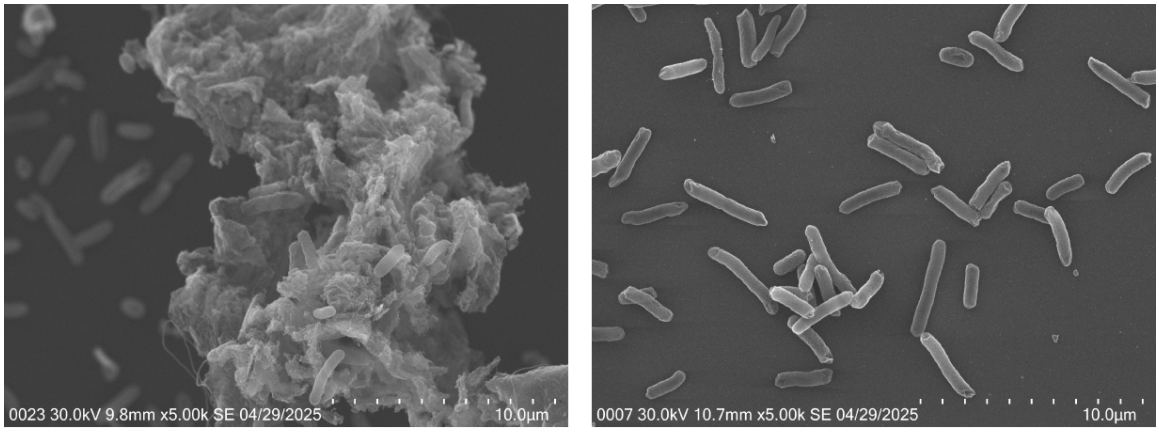

Figure 1.4: Scanning Electron Microscopy of E. coli cells. Biofilm inducing growth conditions (left) reveals cells encased in extracellular matrix with planktonic cells shown on the right. Imaging studies were performed by Saul Flores.

downstream effects of increased c-di-GMP production include decreased cell motility, enhanced synthesis of adhesion-related proteins such as pili and fimbriae, and upregulated biosynthesis of EPS.[62–65] While PNAG and bacterial cellulose are well-established contributors to biofilm formation, the precise role of the poly-ManNAc polysaccharide assembled by the proteins encoded in the *nfr* operon remains unclear. If and how these synthase-dependent EPS biosynthesis pathways are independently regulated during biofilm formation also remains a mystery, and to date, there have been no studies that investigate the interactions, colocalization, or dynamics or these EPS systems.

1.7 Biofilm development and architecture

Bacterial biofilm formation is typically described as a five-stage process that begins with the reversible attachment of planktonic cells to a surface via non-specific interactions, such as van der Waals force s(Figure 1.5).[66,67] Following this initial attachment, the process advances to stage two, irreversible attachment.[68,69] Here, bacteria utilize specific proteins or lipopolysaccharides to anchor themselves more firmly through ionic interactions with the surface.[70,71] During stage 3, attached cells begins to proliferate forming microcolonies and begin secreting extracellular matrix that includes EPS, proteinaceous fimbriae, and extracellular nucleic acids, including eDNA and eRNA.[72–74]

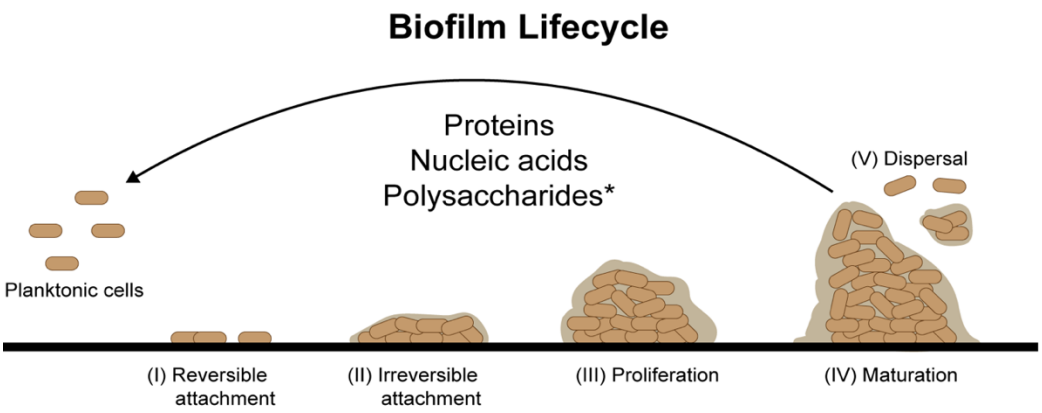

Figure 1.5: Lifecycle of bacterial biofilm. Stage 1 begins with reversible attachment of planktonic cells. Stage 2 is the irreversible attachment through secreting surface adhesins (polysaccharides/fimbriae proteins). Followed by stage 3 where cells undergo proliferation. As the biofilm matures in stage 4, stratification occurs. Stage 5 cells undergo active/inactive dispersal.

As microcolony matures through further cell division in stage IV, the development of a three-dimensional biofilm architecture becomes evident.[75] Stratification within the biofilm occurs due to nutrient gradients, regulated by both external and internal signals.[76] Cell-to-cell communication is conducted through quorum sensing (QS) a density-dependent signaling process where bacteria secrete and detect extracellular chemical signals.[77] In Gram-negative bacteria, QS is often mediated by N-acyl-L-homoserine lactones (AHLs), while Gram-positive bacteria primarily utilize cyclic peptides.[78–81] Additional small molecule signals also include quinolones in *P. aeruginosa*, and diffusible signal factor (DSF) cis-11-methyl-dodecenoic acid in *Xanthomanas campestris*.[82,83]

During maturation, biofilms often develop a mushroom-like structure, with immotile cells forming the stalk and motile cells migrating to create the characteristic cap.[84] The maturation timeline is highly variable ranging from hours to weeks depending on bacterial species and environmental conditions.[85] Mature biofilms contain a complex system of water channels responsible for carry nutrients throughout the structure.[86] Variations in nutrient availability across

the biofilm produce distinct microenvironments where cells in the nutrient-poor biofilm core display reduced metabolic activity, whereas those at the periphery experience higher rates of division due to greater nutrient access.[87] These regions may also differ in oxygen, pH, and cell density.[87] In fully developed biofilms, the extracellular matrix comprises 75–95% of the total biomass, the majority of which is water (up to 97%), with the remainder consisting of proteins, nucleic acids, and EPS. The bacterial cells themselves constitute only 5–25% of the biomass.[88,89]

The final stage of the biofilm lifecycle is dispersal, in which portions of the biofilm are released and cells revert to a planktonic state.[90] This mechanism can occur passively, as cells are naturally carried away by environmental factors such as shear forces, or actively through matrix degradation by secreting enzymes such as glycosidases, proteases, and nucleases.[91,92] Active dispersal is thought to be a regulatory mechanism in response to changes in nutrient availability, oxygen levels, or increases in nitric oxide levels.[93,94] Following dispersal, freed cells migrate and colonize new, more favorable environments. Notably, even biofilms in optimal environments can undergo active dispersal to facilitate expansion and survival.[95]

1.8 Biofilm imaging techniques

The first recorded observation of biofilms dates back to the late 1600s, when Dutch lens maker Antony van Leeuwenhoek used light microscopy to study aggregated microorganisms from scrapings of his teeth and tongue.[96] This work led to the earliest descriptions of dental plaque and the native microbial communities present in oral mucosa. Since then, advances in microscopy have enabled high-resolution imaging of bacterial biofilms and their three-dimensional structures. Techniques such as fluorescence-based microscopy, electron microscopy, and scanning probe microscopy are now commonly used to visualize and study biofilms.[97–99]

Perhaps the most advanced fluorescence-based technique is the confocal laser scanning microscopy (CLSM) which employs laser excitation of fluorophores at defined focal planes within the sample *in situ*, enabling 3-dimensional reconstruction of biofilm architecture without destroying or disrupting the sample.[100] This allows researchers to measure biofilm shape, thickness, and volume over time. Multiple fluorescent probes can used simultaneously to target distinct biofilm components in a single sample. Typically, samples are incubated with fluorophores or fluorescent stains, and excited by lasers. The emitted signals are converted into grayscale pixel values and recorded at different Z-heights, resulting in layered micrographs that are processed into complete 3D images.[101]

Examples of confocal images of biofilm extracellular matrix have been achieved by implementing fluorophore/stains that target the specific components such as polysaccharides, extracellular nucleic acids (eDNA/eRNA), and proteins.[100,102] For example, a fusion protein of carbohydrate binding module 3 (CBM3) from a *Paenibacillus curdlanolyticus* cellulase with GFP has enabled detection of bacterial cellulose in *E. coli*.[102] A widely adopted stain for eDNA is 3-dichloro-7hydroxy-9,9-dimethyl-2(9H)-acridinone (DDAO), after the initial reported use to visualize eDNA from *P. aeruginosa* biofilms. However, it was later discovered that propidium iodine, TOTO®-1, or SYTOX® Green yielded more reliable results as DDAO exhibits some cell permeability in *Pseudomonas*, *Staphylococcus* and *Bacillus* species.[100] Extracellular proteins can be imaged using nonspecific protein stains (ie. FilmTracer™ SyPro®) or by using monoclonal antibodies conjugated to fluorophores for the visualization of specific proteins.[100]

For high-resolution morphological studies, scanning electron microscopy (SEM) remains a powerful tool.[103] Conventional SEM requires dehydrating samples, heavy metal coating and operating under high vacuum, which can cause collapse of the biofilm matrix due to water

loss.[98] Variable pressure (VP) SEM overcomes this issue by allowing imaging of fully hydrated samples under moderate vacuum, without need for heavy metal coating.[104] Alternatively, ruthenium red is used to visualize extracellular matrix.[104] Studies comparing conventional SEM and VP SEM have revealed clear morphological differences, with VP SEM offering superior visualization of hydrated biofilm structures, such as those formed by *P. aeruginosa.*[105]

While fluorescence and electron microscopy methods excel in identifying biofilm morphology and volume, they provide limited information on the chemical and physical properties of the sample. Atomic force microscopy (AFM) addresses this by scanning the sample surface with a physical probe that measures interactive forces, such as van der Waals interactions, and surface roughness.[106] AFM can be performed on untreated biological samples, preserving their native structure, and allows for *in situ* measurements. The technique has been successfully used to monitor changes in biofilm height, surface topography, and roughness during biofilm growth, aging, or in response to antimicrobial agents in *S. aureus*, *P. aeruginosa*, and *Nocardia brasiliensis*.[106]

1.9 Thesis Overview

This section outlines the scope, goals, and experimental approaches addressed in this thesis. Exopolysaccharides serve a pivotal role in bacterial biofilm formation, providing essential structural support and protection. Biofilms formation poses a threat in modern medicine with higher antibiotic resistance compared to planktonic variants as well as industrial disruptions such as biofouling. These properties are largely attributed to the extracellular matrix that surrounds and protects the cells with EPS, which are often produced through synthase-dependent biosynthetic pathways, being the dominant component. Despite their importance, the mechanism by which synthase-dependent EPS secretion systems initiate polysaccharide biosynthesis remains poorly

understood. This work seeks to elucidate the mechanism of initiation for PNAG biosynthesis using a combination of *in vitro* kinetic measurements and blotting analyses, and to develop tools and approaches that enable us to monitor the utilization, 3D distribution, and dissociation dynamics of PNAG within live bacterial biofilms via fluorescence microscopy.

In Chapter 2, I will describe our initial objective to design an optimal plasmid construct for the recombinant overexpression of a functional PgaC/D glycosyltransferase complex, which is responsible for PNAG biosynthesis in Gram-negative bacteria. Enzyme activity was quantified by measuring the conversion of native UDP-GlcNAc substrate to free UDP following glycosyl group transfer for polysaccharide elongation. Once minimal requirements for observable enzymatic activity were established, we aimed to purify the glycosyl transferase complex. Chapter 2 will detail the methods used for solubilization of membrane proteins including using traditional detergent micelle solubilization, which encases proteins in synthetic lipid environments, and the use of amphiphilic polymers that preserve native membrane lipids in nano discs.[107]

Since most surface polysaccharides are initiated via lipid-linked substrates, in Chapter 3 we examined whether the PNAG produced *in vitro* contained evidence of a lipid initiator. Solid-state NMR comparisons were made between *de novo* synthesized PNAG and endogenous PNAG isolated from *S. epidermidis* RP62A, a Gram-positive bacterium. Due to Gram-positive bacteria possessing a thick peptidoglycan layer, surface-attached PNAG was sheared off by sonication, enabling high-purity isolation without cell lysis.[108] Localization studies of synthesized PNAG post-polymerization were performed using dot blot analysis. To detect PNAG, we utilized a fusion protein composed of catalytically inactive DspB (E184A mutant), a PNAG hydrolase enzyme, fused to ascorbic acid peroxidase APEX2 ($DspB_{E184A}$–APEX2).[109] This enabled direct detection of PNAG through dot blot analysis. To further investigate initiation mechanisms, kinetic studies

were conducted in the presence and absence of free GlcNAc monosaccharides, assessing their impact on enzymatic activity.

Finally, in chapter 4 we sought to develop tools that would allow us to understand EPS distribution within biofilm colonies. As synthase-based exopolysaccharide synthesis is regulated by the second messenger c-di-GMP, we were interested in exploring how spatial stratification within biofilms influences polysaccharide localization. To address this, we developed a platform for *in situ* cultivation, labeling, and observation of biofilm dispersal.[110] Flow-based devices are ideal for biofilm cultivation, mimicking natural shear forces and enabling direct visualization through integrated glass windows. However, traditional biofilm flow cells rely on the random association of bacterial cells to the flow cell surface. Using a custom-designed microfluidic device, we established specific seeding zones to predict biofilm formation and coupled these studies with fluorescent labeling of PNAG using $DspB_{E184A}$–eGFP.[111] This allowed us to observe the spatial distribution of PNAG in biofilms formed by Gram-negative *E. coli* and Gram-positive *S. epidermidis,* highlighting differences in utilization and organization of PNAG within these distinct bacterial communities.

References

1. Silhavy, T. J., Kahne, D. & Walker, S. The Bacterial Cell Envelope. *Cold Spring Harb. Perspect. Biol.* 2, a000414 (2010).

2. Cooper, C. A., Mainprize, I. L. & Nickerson, N. N. Prokaryotic Systems Biology. *Adv. Exp. Med. Biol.* 883, 295–315 (2015).

3. Heidelberger, M. & Avery, O. T. THE SOLUBLE SPECIFIC SUBSTANCE OF PNEUMOCOCCUS. *J. Exp. Med.* 38, 73–79 (1923).

4. Wilkinson, J. F. THE EXTRACELLULAR POLYSACCHARIDES OF BACTERIA. *Bacteriol. Rev.* 22, 46–73 (1958).

5. Bertani, B. & Ruiz, N. Function and Biogenesis of Lipopolysaccharides. *EcoSal Plus* 8, 10.1128/ecosalplus.ESP-0001–2018 (2018).

6. Potekhina, N. V., Streshinskaya, G. M., Tul'skaya, E. M. & Shashkov, A. S. 6 Cell Wall Teichoic Acids in the Taxonomy and Characterization of Gram-positive Bacteria††Dedicated to the memory of Professor L.V. Backinowsky (1938–2011) – friend and colleague, whose inspiration and insight problems contributed to the writing of this chapter. *Methods Microbiol.* 38, 131–164 (2011).

7. Roberts, I. S. THE BIOCHEMISTRY AND GENETICS OF CAPSULAR POLYSACCHARIDE PRODUCTION IN BACTERIA. *Annu. Rev. Microbiol.* 50, 285–315 (1996).

8. Swoboda, J. G., Campbell, J., Meredith, T. C. & Walker, S. Wall Teichoic Acid Function, Biosynthesis, and Inhibition. *ChemBioChem* 11, 35–45 (2010).

9. Caroff, M. & Novikov, A. Lipopolysaccharides: structure, function and bacterial identifications☆☆☆. *OCL* 27, 31 (2020).

10. Ascari, A. & Morona, R. Recent insights into Wzy polymerases and lipopolysaccharide O-antigen biosynthesis. *J. Bacteriol.* e0041724 (2025) doi:10.1128/jb.00417-24.

11. Willis, L. M. & Whitfield, C. Structure, biosynthesis, and function of bacterial capsular polysaccharides synthesized by ABC transporter-dependent pathways. *Carbohydr. Res.* 378, 35–44 (2013).

12. Verma, P., Ho, R., Chambers, S. A., Cegelski, L. & Zimmer, J. Insights into phosphoethanolamine cellulose synthesis and secretion across the Gram-negative cell envelope. *Nat. Commun.* 15, 7798 (2024).

13. Mack, D. *et al.* The intercellular adhesin involved in biofilm accumulation of Staphylococcus epidermidis is a linear beta-1,6-linked glucosaminoglycan: purification and structural analysis. *J. Bacteriol.* 178, 175–183 (1996).

14. Itoh, Y. *et al.* Roles of pgaABCD genes in synthesis, modification, and export of the Escherichia coli biofilm adhesin poly-beta-1,6-N-acetyl-D-glucosamine. *J Bacteriol* 190, 3670–80 (2008).

15. Cuthbertson, L., Kos, V. & Whitfield, C. ABC Transporters Involved in Export of Cell Surface Glycoconjugates. *Microbiol. Mol. Biol. Rev.* 74, 341–362 (2010).

16. Schmid, J., Sieber, V. & Rehm, B. Bacterial exopolysaccharides: biosynthesis pathways and engineering strategies. *Front. Microbiol.* 6, 496 (2015).

17. Whitney, J. C. & Howell, P. L. Synthase-dependent exopolysaccharide secretion in Gram-negative bacteria. *Trends Microbiol.* 21, 63–72 (2013).

18. Whitfield, C., Wear, S. S. & Sande, C. Assembly of Bacterial Capsular Polysaccharides and Exopolysaccharides. *Annu. Rev. Microbiol.* 74, 1–23 (2020).

19. Romano, K. P. & Hung, D. T. Targeting LPS biosynthesis and transport in gram-negative bacteria in the era of multi-drug resistance. *Biochim. Biophys. Acta (BBA) - Mol. Cell Res.* 1870, 119407 (2023).

20. Woodward, R. *et al.* In vitro bacterial polysaccharide biosynthesis: defining the functions of Wzy and Wzz. *Nat. Chem. Biol.* 6, 418–423 (2010).

21. Weckener, M. *et al.* The lipid linked oligosaccharide polymerase Wzy and its regulating co-polymerase, Wzz, from enterobacterial common antigen biosynthesis form a complex. *Open Biol.* 13, 220373 (2023).

22. Wilkens, S. Structure and mechanism of ABC transporters. *F1000Prime Rep.* 7, 14 (2015).

23. Kuklewicz, J. & Zimmer, J. Molecular insights into capsular polysaccharide secretion. *Nature* 628, 901–909 (2024).

24. Hubbard, C., McNamara, J. T., Azumaya, C., Patel, M. S. & Zimmer, J. The Hyaluronan Synthase Catalyzes the Synthesis and Membrane Translocation of Hyaluronan. *J. Mol. Biol.* 418, 21–31 (2012).

25. Jenal, U., Reinders, A. & Lori, C. Cyclic di-GMP: second messenger extraordinaire. *Nat. Rev. Microbiol.* 15, 271–284 (2017).

26. Augimeri, R. V., Varley, A. J. & Strap, J. L. Establishing a Role for Bacterial Cellulose in Environmental Interactions: Lessons Learned from Diverse Biofilm-Producing Proteobacteria. *Front. Microbiol.* 6, 1282 (2015).

27. Nivens, D. E., Ohman, D. E., Williams, J. & Franklin, M. J. Role of Alginate and Its O Acetylation in Formation of Pseudomonas aeruginosa Microcolonies and Biofilms. *J. Bacteriol.* 183, 1047–1057 (2001).

28. Vuong, C. *et al.* Polysaccharide intercellular adhesin (PIA) protects Staphylococcus epidermidis against major components of the human innate immune system. *Cell. Microbiol.* 6, 269–275 (2004).

29. DeAngelis, P. L. Hyaluronan synthases: fascinating glycosyltransferases from vertebrates, bacterial pathogens, and algal viruses. *Cell. Mol. Life Sci. CMLS* 56, 670–682 (1999).

30. Omadjela, O. *et al.* BcsA and BcsB form the catalytically active core of bacterial cellulose synthase sufficient for in vitro cellulose synthesis. *Proc. Natl. Acad. Sci.* 110, 17856–17861 (2013).

31. Römling, U. Molecular biology of cellulose production in bacteria. *Res. Microbiol.* 153, 205–212 (2002).

32. Acheson, J. F., Ho, R., Goularte, N. F., Cegelski, L. & Zimmer, J. Molecular organization of the E. coli cellulose synthase macrocomplex. *Nat. Struct. Mol. Biol.* 28, 310–318 (2021).

33. Roux, D. *et al.* Identification of Poly-N-acetylglucosamine as a Major Polysaccharide Component of the Bacillus subtilis Biofilm Matrix*. *J. Biol. Chem.* 290, 19261–19272 (2015).

34. Pérez, M. M. *et al.* Protection from Staphylococcus aureus mastitis associated with poly-N-acetyl β-1,6 glucosamine specific antibody production using biofilm-embedded bacteria. *Vaccine* 27, 2379–2386 (2009).

35. Cramton, S. E., Gerke, C., Schnell, N. F., Nichols, W. W. & Götz, F. The Intercellular Adhesion (ica) Locus Is Present in Staphylococcus aureus and Is Required for Biofilm Formation. *Infect Immun* 67, 5427–5433 (1999).

36. Cue, D., Lei, M. G. & Lee, C. Y. Genetic regulation of the intercellular adhesion locus in staphylococci. *Front. Cell. Infect. Microbiol.* 2, 38 (2012).

37. Heilmann, C. *et al.* Molecular basis of intercellular adhesion in the biofilm-forming Staphylococcus epidermidis. *Mol Microbiol* 20, 1083–1091 (1996).

38. McKenney, D. *et al.* The ica Locus of Staphylococcus epidermidis Encodes Production of the Capsular Polysaccharide/Adhesin. *Infect. Immun.* 66, 4711–4720 (1998).

39. Atkin, K. E., MacDonald, S. J., Brentnall, A. S., Potts, J. R. & Thomas, G. H. A different path: Revealing the function of staphylococcal proteins in biofilm formation. *FEBS Lett.* 588, 1869–1872 (2014).

40. Gerke, C., Kraft, A., Süßmuth, R., Schweitzer, O. & Götz, F. Characterization of theN-Acetylglucosaminyltransferase Activity Involved in the Biosynthesis of the Staphylococcus epidermidisPolysaccharide Intercellular Adhesin*. *J Biol Chem* 273, 18586–18593 (1998).

41. Pokrovskaya, V. *et al.* Functional Characterization of Staphylococcus epidermidis IcaB, a De-N-acetylase Important for Biofilm Formation. *Biochemistry* 52, 5463–5471 (2013).

42. Wang, X., Preston, J. F. & Romeo, T. The pgaABCD Locus of Escherichia coli Promotes the Synthesis of a Polysaccharide Adhesin Required for Biofilm Formation. *J. Bacteriol.* 186, 2724–2734 (2004).

43. Steiner, S., Lori, C., Boehm, A. & Jenal, U. Allosteric activation of exopolysaccharide synthesis through cyclic di-GMP-stimulated protein–protein interaction. *Embo J* 32, 354–368 (2013).

44. Pfoh, R. *et al.* The TPR domain of PgaA is a multifunctional scaffold that binds PNAG and modulates PgaB-dependent polymer processing. *PLoS Pathog.* 18, e1010750 (2022).

45. Morrison, Z. A., Eddenden, A., Subramanian, A. S., Howell, P. L. & Nitz, M. Termination of Poly-N-acetylglucosamine (PNAG) Polymerization with N-Acetylglucosamine Analogues. *Acs Chem Biol* (2022) doi:10.1021/acschembio.1c00855.

46. Fong, J. N. C. & Yildiz, F. H. Biofilm Matrix Proteins. *Microbiol. Spectr.* 3, 10.1128/microbiolspec.mb-0004–2014 (2015).

47. Campoccia, D., Montanaro, L. & Arciola, C. R. Extracellular DNA (eDNA). A Major Ubiquitous Element of the Bacterial Biofilm Architecture. *Int. J. Mol. Sci.* 22, 9100 (2021).

48. Vu, B., Chen, M., Crawford, R. J. & Ivanova, E. P. Bacterial Extracellular Polysaccharides Involved in Biofilm Formation. *Molecules* 14, 2535–2554 (2009).

49. Vuong, C. *et al.* A Crucial Role for Exopolysaccharide Modification in Bacterial Biofilm Formation, Immune Evasion, and Virulence*. *J Biol Chem* 279, 54881–54886 (2004).

50. Böhning, J., Tarafder, A. K. & Bharat, T. A. M. The role of filamentous matrix molecules in shaping the architecture and emergent properties of bacterial biofilms. *Biochem. J.* 481, 245–263 (2024).

51. Colvin, K. M. *et al.* The Pel and Psl polysaccharides provide Pseudomonas aeruginosa structural redundancy within the biofilm matrix. *Environ. Microbiol.* 14, 1913–1928 (2012).

52. York, A. Naturally modified cellulose in bacterial biofilms. *Nat. Rev. Microbiol.* 16, 123–123 (2018).

53. Yildiz, F., Fong, J., Sadovskaya, I., Grard, T. & Vinogradov, E. Structural Characterization of the Extracellular Polysaccharide from Vibrio cholerae O1 El-Tor. *PLoS ONE* 9, e86751 (2014).

54. Arbour, C. A. *et al.* Defining early steps in Bacillus subtilis biofilm biosynthesis. *mBio* 14, e00948-23 (2023).

55. Costerton, J. W., Stewart, P. S. & Greenberg, E. P. Bacterial Biofilms: A Common Cause of Persistent Infections. *Science* 284, 1318–1322 (1999).

56. Limoli, D. H., Jones, C. J. & Wozniak, D. J. Bacterial Extracellular Polysaccharides in Biofilm Formation and Function. *Microbiol Spectr* 3, (2015).

57. Ramsey, D. M. & Wozniak, D. J. Understanding the control of Pseudomonas aeruginosa alginate synthesis and the prospects for management of chronic infections in cystic fibrosis. *Mol. Microbiol.* 56, 309–322 (2005).

58. Junkermeier, E. H. & Hengge, R. A Novel Locally c-di-GMP-Controlled Exopolysaccharide Synthase Required for Bacteriophage N4 Infection of Escherichia coli. *mBio* 12, e03249-21 (2021).

59. Boehm, A. *et al.* Second messenger signalling governs Escherichia coli biofilm induction upon ribosomal stress. *Mol Microbiol* 72, 1500–1516 (2009).

60. Perkins, A. *et al.* A Bacterial Inflammation Sensor Regulates c-di-GMP Signaling, Adhesion, and Biofilm Formation. *mBio* 12, 10.1128/mbio.00173-21 (2021).

61. Yu, Z. *et al.* Gas and light: triggers of c-di-GMP-mediated regulation. *FEMS Microbiol. Rev.* 47, fuad034 (2023).

62. Lindenberg, S., Klauck, G., Pesavento, C., Klauck, E. & Hengge, R. The EAL domain protein YciR acts as a trigger enzyme in a c-di-GMP signalling cascade in E. coli biofilm control. *EMBO J.* 32, 2001–2014 (2013).

63. Opoku-Temeng, C. & Sintim, H. O. Targeting c-di-GMP Signaling, Biofilm Formation, and Bacterial Motility with Small Molecules. *Methods Mol. Biol. (Clifton, NJ)* 1657, 419–430 (2017).

64. Schmid, J. *et al.* Screening of c-di-GMP-Regulated Exopolysaccharides in Host Interacting Bacteria. *Methods Mol. Biol. (Clifton, NJ)* 1734, 263–275 (2017).

65. Nicastro, G. G. *et al.* c-di-GMP-related phenotypes are modulated by the interaction between a diguanylate cyclase and a polar hub protein. *Sci. Rep.* 10, 3077 (2020).

66. Bryers, J. & Characklis, W. Early fouling biofilm formation in a turbulent flow system: Overall kinetics. *Water Res.* 15, 483–491 (1981).

67. Stoodley, P., Sauer, K., Davies, D. G. & Costerton, J. W. BIOFILMS AS COMPLEX DIFFERENTIATED COMMUNITIES. *Annu. Rev. Microbiol.* 56, 187–209 (2002).

68. Pearce, W. A. & Buchanan, T. M. Bacterial Adherence. 289–344 (1980) doi:10.1007/978-94-009-5863-0_10.

69. Costerton, J. W. *et al.* Bacterial Biofilms in Nature and Disease. *Annu. Rev. Microbiol.* 41, 435–464 (1987).

70. Matilla-Cuenca, L. *et al.* Bacterial biofilm functionalization through Bap amyloid engineering. *npj Biofilms Microbiomes* 8, 62 (2022).

71. Rather, M. A., Gupta, K. & Mandal, M. Microbial biofilm: formation, architecture, antibiotic resistance, and control strategies. *Braz. J. Microbiol.* 52, 1701–1718 (2021).

72. Malone, J. A. & Caldwell, D. E. Evaluation of surface colonization kinetics in continuous culture. *Microb. Ecol.* 9, 299–305 (1983).

73. Chiba, A. *et al.* Staphylococcus aureus utilizes environmental RNA as a building material in specific polysaccharide-dependent biofilms. *npj Biofilms Microbiomes* 8, 17 (2022).

74. Mugunthan, S. *et al.* RNA is a key component of extracellular DNA networks in Pseudomonas aeruginosa biofilms. *Nat. Commun.* 14, 7772 (2023).

75. Donlan, R. M. Biofilms: Microbial Life on Surfaces - Volume 8, Number 9—September 2002 - Emerging Infectious Diseases journal - CDC. *Emerg. Infect. Dis.* 8, 881–890 (2002).

76. Vlamakis, H., Aguilar, C., Losick, R. & Kolter, R. Control of cell fate by the formation of an architecturally complex bacterial community. *Genes Dev.* 22, 945–953 (2008).

77. Wagner, V. E., Gillis, R. J. & Iglewski, B. H. Transcriptome analysis of quorum-sensing regulation and virulence factor expression in Pseudomonas aeruginosa. *Vaccine* 22, S15–S20 (2004).

78. Rutherford, S. T. & Bassler, B. L. Bacterial Quorum Sensing: Its Role in Virulence and Possibilities for Its Control. *Cold Spring Harb. Perspect. Med.* 2, a012427 (2012).

79. Miyashiro, T. & Ruby, E. G. Shedding light on bioluminescence regulation in Vibrio fischeri: Shedding light on bioluminescence regulation in Vibrio fischeri. *Mol. Microbiol.* 84, 795–806 (2012).

80. Billot, R. *et al.* Engineering acyl-homoserine lactone-interfering enzymes toward bacterial control. *J. Biol. Chem.* 295, 12993–13007 (2020).

81. Mukherjee, S. & Bassler, B. L. Bacterial quorum sensing in complex and dynamically changing environments. *Nat. Rev. Microbiol.* 17, 371–382 (2019).

82. Ryan, R. P., An, S., Allan, J. H., McCarthy, Y. & Dow, J. M. The DSF Family of Cell–Cell Signals: An Expanding Class of Bacterial Virulence Regulators. *PLoS Pathog.* 11, e1004986 (2015).

83. Pesci, E. C. *et al.* Quinolone signaling in the cell-to-cell communication system of Pseudomonas aeruginosa. *Proc. Natl. Acad. Sci.* 96, 11229–11234 (1999).

84. Miller, J. K. *et al.* Development of the Pseudomonas aeruginosa mushroom morphology and cavity formation by iron-starvation: A mathematical modeling study. *J. Theor. Biol.* 308, 68–78 (2012).

85. Sauer, K. *et al.* The biofilm life cycle: expanding the conceptual model of biofilm formation. *Nat. Rev. Microbiol.* 20, 608–620 (2022).

86. Zhao, A., Sun, J. & Liu, Y. Understanding bacterial biofilms: From definition to treatment strategies. *Front. Cell. Infect. Microbiol.* 13, 1137947 (2023).

87. Stoodley, P., Dodds, I., Boyle, J. D. & Lappin-Scott, H. M. Influence of hydrodynamics and nutrients on biofilm structure. *J. Appl. Microbiol.* 85, 19S-28S (1998).

88. Wickramasinghe, N. N. *et al.* Characterization of the biofilm matrix composition of psychrotrophic, meat spoilage pseudomonads. *Sci. Rep.* 10, 16457 (2020).

89. Agarwal, H., Gurnani, B., Pippal, B. & Jain, N. Capturing the micro-communities: Insights into biogenesis and architecture of bacterial biofilms. *BBA Adv.* 7, 100133 (2025).

90. Hall-Stoodley, L., Costerton, J. W. & Stoodley, P. Bacterial biofilms: from the Natural environment to infectious diseases. *Nat. Rev. Microbiol.* 2, 95–108 (2004).

91. Ymele-Leki, P. & Ross, J. M. Erosion from Staphylococcus aureus Biofilms Grown under Physiologically Relevant Fluid Shear Forces Yields Bacterial Cells with Reduced Avidity to Collagen. *Appl. Environ. Microbiol.* 73, 1834–1841 (2007).

92. Choi, Y. C. & Morgenroth, E. Monitoring biofilm detachment under dynamic changes in shear stress using laser-based particle size analysis and mass fractionation. *Water Sci. Technol. : a J. Int. Assoc. Water Pollut. Res.* 47, 69–76 (2003).

93. Gjermansen, M., Ragas, P., Sternberg, C., Molin, S. & Tolker-Nielsen, T. Characterization of starvation-induced dispersion in Pseudomonas putida biofilms. *Environ. Microbiol.* 7, 894–904 (2005).

94. Sauer, K. *et al.* Characterization of Nutrient-Induced Dispersion in Pseudomonas aeruginosa PAO1 Biofilm. *J. Bacteriol.* 186, 7312–7326 (2004).

95. Landini, P., Antoniani, D., Burgess, J. G. & Nijland, R. Molecular mechanisms of compounds affecting bacterial biofilm formation and dispersal. *Appl. Microbiol. Biotechnol.* 86, 813–823 (2010).

96. DOBELL, C. ANTONY VAN LEEUWENHOEK AND HIS "LITTLE ANIMALS." *Am. J. Méd. Sci.* 186, 287 (1933).

97. Darvishi, S., Pick, H., Oveisi, E., Girault, H. H. & Lesch, A. Soft-probe-scanning electrochemical microscopy reveals electrochemical surface reactivity of E. coli biofilms. *Sens. Actuators B: Chem.* 334, 129669 (2021).

98. Rimal, B. *et al.* Scanning Electron Microscopy and Energy-Dispersive X-ray Spectroscopy of Staphylococcus aureus Biofilms. *ACS Omega* 9, 37610–37620 (2024).

99. Barbosa, A., Miranda, S., Azevedo, N. F., Cerqueira, L. & Azevedo, A. S. Imaging biofilms using fluorescence in situ hybridization: seeing is believing. *Front. Cell. Infect. Microbiol.* 13, 1195803 (2023).

100. Schlafer, S. & Meyer, R. L. Confocal microscopy imaging of the biofilm matrix. *J. Microbiol. Methods* 138, 50–59 (2017).

101. Mhade, S. & Kaushik, K. S. Tools of the Trade: Image Analysis Programs for Confocal Laser-Scanning Microscopy Studies of Biofilms and Considerations for Their Use by Experimental Researchers. *ACS Omega* 8, 20163–20177 (2023).

102. Nguyen, M. H., Ojima, Y., Sakka, M., Sakka, K. & Taya, M. Probing of exopolysaccharides with green fluorescence protein-labeled carbohydrate-binding module in Escherichia coli biofilms and flocs induced by bcsB overexpression. *J. Biosci. Bioeng.* 118, 400–405 (2014).

103. Priester, J. H. *et al.* Enhanced visualization of microbial biofilms by staining and environmental scanning electron microscopy. *J. Microbiol. Methods* 68, 577–587 (2007).

104. Relucenti, M. *et al.* Microscopy Methods for Biofilm Imaging: Focus on SEM and VP-SEM Pros and Cons. *Biology* 10, 51 (2021).

105. Weber, K., Delben, J., Bromage, T. G. & Duarte, S. Comparison of SEM and VPSEM imaging techniques with respect to Streptococcus mutans biofilm topography. *FEMS Microbiol. Lett.* 350, 175–179 (2014).

106. Chatterjee, S., Biswas, N., Datta, A., Dey, R. & Maiti, P. Atomic force microscopy in biofilm study. *Microscopy* 63, 269–278 (2014).

107. Marconnet, A. *et al.* Influence of Hydrophobic Groups Attached to Amphipathic Polymers on the Solubilization of Membrane Proteins along with Their Lipids. *Anal. Chem.* 94, 14151–14158 (2022).

108. Joyce, J. G. *et al.* Isolation, structural characterization, and immunological evaluation of a high-molecular-weight exopolysaccharide from Staphylococcus aureus. *Carbohyd Res* 338, 903–922 (2003).

109. Vo, L. H. *et al.* Mapping protein–exopolysaccharide binding interaction in Staphylococcus epidermidis biofilms by live cell proximity labeling. *bioRxiv* 2023.08.29.555326 (2023) doi:10.1101/2023.08.29.555326.

110. Zhang, Y. *et al.* A Microfluidic Approach for Quantitative Study of Spatial Heterogeneity in Bacterial Biofilms. *Small Sci.* 2, (2022).

111. Eddenden, A., Kitova, E. N., Klassen, J. S. & Nitz, M. An Inactive Dispersin B Probe for Monitoring PNAG Production in Biofilm Formation. *ACS Chem. Biol.* 15, 1204–1211 (2020).

Chapter 2: Mechanistic insight of PgaCD glycosyltransferase enzyme

Contribution of other authors:

Merrit Scott and Michal Tyrlik both aided in the initial generation of various Pga protein constructs and activity assay parameters. Dr. Fu Chen for CP MAS NMR of *de novo* PNAG from PgaCD.

2.1 Introduction

Bacterial biofilms can accumulate in diverse medical environments ranging from dental plaques to prosthetics, and other medical instruments, resulting in chronic and persistent infections that remain an issue in modern medicine.[1,2] Biofilm formation occurs when planktonic bacterial cells adhere to a biotic or abiotic surface, where they transition into a sessile multicellular community encased in a self-produced extracellular cellular matrix (ECM) containing secreted proteins, extracellular DNA, and exopolysaccharides (EPS).[3,4] Previous studies have attributed the protective nature and virulence factor of biofilms to the EPS within the ECM.[5–7]

Many biofilm exopolysaccharides have been identified from various bacterial species.[8] These include highly anionic alginate[9] neutral polysaccharides such as cellulose[10] and cationic poly-(1,6)-β-*N*-acetylglucosamine (PNAG).[11,12] Of these different exopolysaccharides, PNAG is of particular interest due to its prevalence within common human pathogens. This includes Gram-positive *Staphylococcus aureus*, where it is also referred to as the polysaccharide intercellular adhesin (PIA), and Gram-negative bacteria such as *Escherichia coli* and *Klebsiella pneumoniae*.[13,14] While PNAG biosynthesis was first identified in *Staphylococci*, pioneering work by the Romeo lab lead to the identification and characterization of genes responsible for PNAG biosynthesis in Gram-negative bacteria and established the role of PNAG biosynthesis in biofilm formation.[12,15] The lab was able to initially identify the *pgaABCD* genes (formally *ycdSRQP*) as the operon responsible for PNAG production and export.[15] PgaA is an outer membrane porin responsible for PNAG secretion, PgaB is a periplasmic localized deacetylase/hydrolase enzyme. PgaC and PgaD complex is classified as a GT2 family enzyme which is responsible for PNAG polymerization and is allosterically activated by second messenger c-di-GMP.[15] Polymerization of of the polysaccharide by GT enzymes can undergo an inverting or retaining mechanism (Fig

2.1).[16] Retaining mechanism involves a double displacement mechanism with the formation of the glycosyl-enzyme intermediate.[16] While the inverting mechanism involves a S_N2-like displacement of the nucleotide involving an enzymatic base catalyst that activates the incoming glycosyl residue, forming an oxocarbenium ion-like transition state.[16] GT2 enzymes typically employ the inverting mechanism as most nucleotide activated sugars exist in the α-anomeric form while its products are in the β-anomeric form.[16]

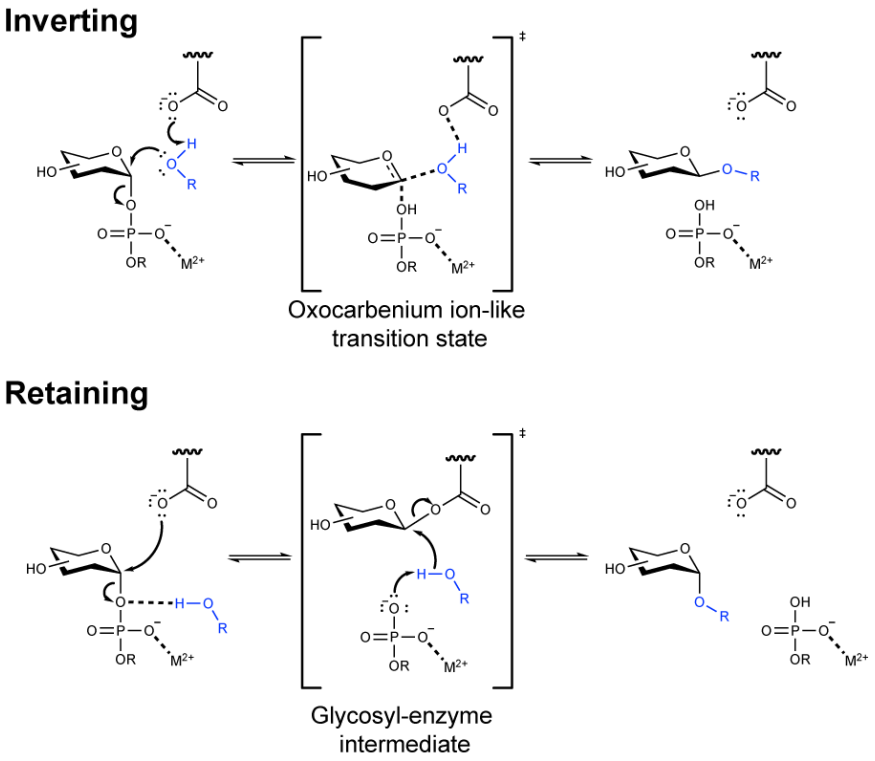

Figure 2.1: Schematic of inverting and retaining mechanism of glycosyltransferase enzymes.

Characterization of the polysaccharide confirmed its shared structure with previously described *Staphylococcal* PIA. In *E. coli*, PNAG biosynthesis is heavily regulated, with one of the most critical factors being the RNA-binding protein carbon storage regulator A (CsrA).[17] CsrA functions as a global regulator, exerting broad influence over cellular processes in bacteria. It promotes motility, glycolysis, and virulence while simultaneously repressing biofilm-associated

phenotypes, including exopolysaccharide (EPS) production.[17] The duality of CsrA helps balance bacterial adaptation between planktonic growth and surface-associated lifestyles.

CsrA functions as a homodimer, with each subunit containing an identical RNA-binding site, which bind to mRNA and directly compete with ribosomal binding.[18] Repression of PNAG biosynthesis by CsrA is multifaceted. At the post-transcriptional level, CsrA binds to six regions within the 5′ untranslated leader sequence of the *pga* operon mRNA and destabilizes the *pgaABCD* transcript, thereby reducing its stability and overall translation efficiency.[18] In addition to this direct regulation, CsrA indirectly downregulates PNAG production by targeting cation-responsive protein (NhaR), a transcriptional regulator that binds to the promoter region of the *pga* operon.[19] NhaR is required for adaptation to alkaline pH and high-salt conditions.[19] By interfering with NhaR, CsrA provides an additional layer of control over *pga* operon expression under stress conditions. Another mechanism by which CsrA represses PNAG biosynthesis is through the regulation of c-di-GMP production. The PgaCD complex, which is responsible for PNAG polymerizing from activated UDP-GlcNAc sugar nucleotide substrates, requires c-di-GMP binding for activation.[20] Synthesis of c-di-GMP occurs through the cyclization of two guanosine triphosphates (GTP) performed by diguanylate cyclase (DGC) enzymes containing a conserved GGDEF motif.[21] Repression of DGC enzymes leads to decreased intracellular c-di-GMP concentrations, thereby limiting PgaCD complex activation and reducing PNAG synthesis.[22] Together, these overlapping regulatory mechanisms–direct mRNA binding, control of transcriptional regulators, and modulation of second messenger signaling–underscore the central role of CsrA in repressing biofilm matrix production and fine-tuning bacterial adaptation to diverse environments.

Although the genes that biosynthesize PNAG and regulate its production have been well characterized, the exact mechanism for how the PgaCD complex initiates PNAG biosynthesis remains unknown. PNAG polymerization is facilitated by the PgaCD complex, which transfers a glycosyl group from UDP-GlcNAc to a glycosyl acceptor substrate. During polymerization, this acceptor is the growing PNAG polymer, but it is unclear what serves as the native acceptor to initiate PNAG biosynthesis by this enzyme. Many cell surface polysaccharide pathways often utilize a lipid intermediate to serve as primers for polymerization. For instance, group II and III CPS synthesis is initiated by a conserved glycolipid anchor composed of phosphatidylglycerol linked to 5-9 Kdo sugars.[23] Additionally, LPS and TA are added onto undecaprenyl phosphate (Und-P) and undecaprenyl pyro phosphate (Und-PP) carriers.[24,25]

Here we aimed to investigative the initiation of PNAG EPS by PgaCD complex in Gram-negative bacteria. Enzymes were expressed and characterized through HPLC assays, followed by isolation of *de novo* synthesized PNAG to confirm EPS polymerization. Various membrane protein solubilization methods were performed to isolated purified variants of the enzyme complex within detergent micelles and native lipid nano discs. However, quenching of the enzymatic activity following purification suggest the loss of an initiator substrate supported by solid state ^{13}C NMR analysis of the *de novo* PNAG.

2.2 Results

2.2.1 Overexpression of PgaCD complex and its variants

Previous studies have demonstrated the synthesis of PNAG is dependent on the presence of both PgaC and PgaD. To build upon the previous findings, we aimed to determine if co-localization of the protein within the same membrane is required for the activation of the complex. Investigation of the glycosyltransferase enzyme begins by isolating PgaC and PgaD proteins under various expression conditions. PgaC and PgaD were co-expressed from a pETduet vector, facilitating the integration of both membrane proteins into the same membrane, and were also expressed individually from separate plasmids. In addition, a previous report by the Jenal lab demonstrated that a direct C-teminual to N-terminal the fusion of the PgaC and PgaD proteins, hereafter referenced as PgaCDf, was functionally active and yielded a similar biofilm phenotype as the native PgaCD complex.[20] AlphaFold prediction revealed the unstructured regions of the C-

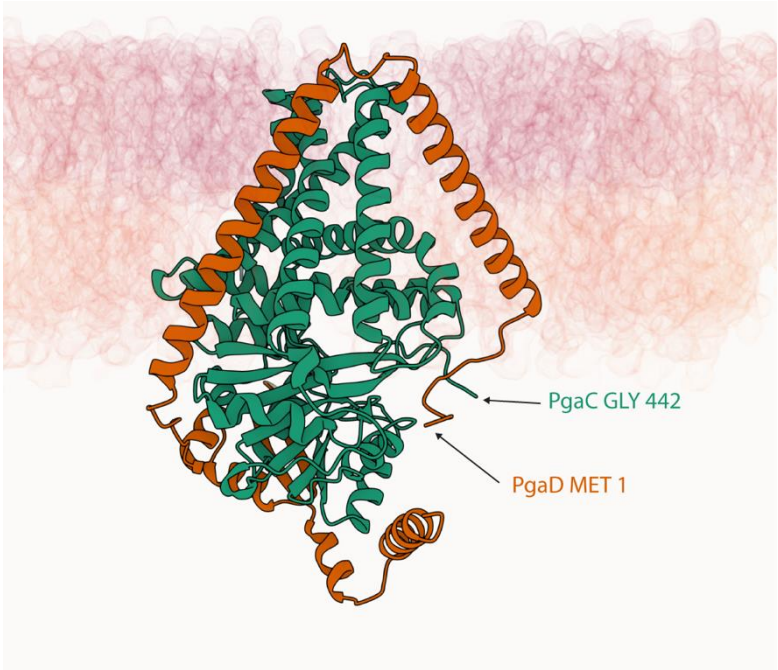

Figure 2.2: AlphaFold prediction of PgaCD complex in lipid bilayer. PgaC (green) C-terminal Gly144 and Pga (orange) D N-terminal Met1 in close proximity within cytoplasmic region.

terminus from PgaC and N-terminus of PgaD coincide within the cytosolic space in close proximity (Figure 2.2). Thus, we generated a fusion protein of PgaCD complex by direct C-to-N terminal fusion to ensure proper oligomerization ratio (Figure 2.3). To more easily assess proper protein expression and folding, we additionally prepared a PgaCDf construct containing a C-terminal enhanced green fluorescent protein (eGFP) fusion.

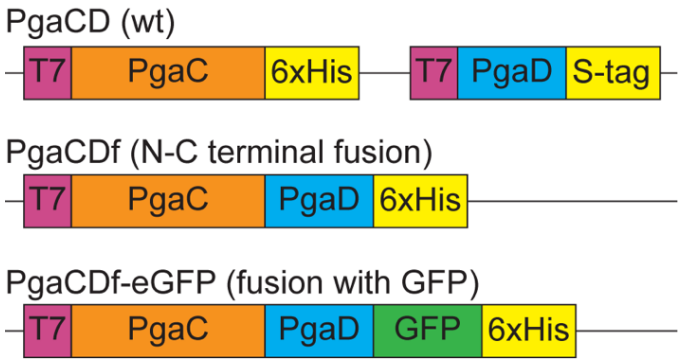

Figure 2.3: Different PgaCD plasmid constructs. PgaCD wt, direct C-N fusion of PgaC to PgaD (PgaCDf), and a fluorescent fusion protein conjugate (PgaCDf-eGFP).

2.2.3 PgaCD enzymatic activity characterization by HPLC

Following the isolation of the proteins, enzyme activities were measured using a high-performance liquid chromatography (HPLC) based assay. The activity of each protein was measured based on conversion of the substrate UDP-GlcNAc to form free UDP upon polymerization of the GlcNAc residues. Notably, UDP production, and thus enzymatic activity was only observed in membrane fractions containing both PgaC and PgaD in the presence of c-di-GMP. Importantly, no activity was observed for membrane fractions containing PgaC and PgaD in the absence of c-di-GMP, indicating that the release of UDP in this assay is exclusively the result of the PgaCD complex, and activity is only observed when it is allosterically activated by c-di-GMP. Moreover, membrane fractions containing PgaC alone or PgaD alone displayed no activity in the presence or absence of c-di-GMP, highlighting the importance of both proteins for

PNAG biosynthesis. Finally, when membrane fractions containing either PgaC alone or PgaD alone were combined in the same reaction mixture, no observable enzymatic activity was detected. This finding indicates that both PgaC and PgaD proteins must be present within the same membrane environment for catalytic activity to occur (Figure 2.4A).

We also evaluated the activity of membrane fractions expressing either PgaCDf or the PgaCDf-eGFP fusion protein. Both fusion proteins exhibited similar enzymatic activity in this assay (Figure 2.4C), and any differences in the rates measured are likely the result of slight differences in the concentration of the recombinant protein present in each membrane fraction.

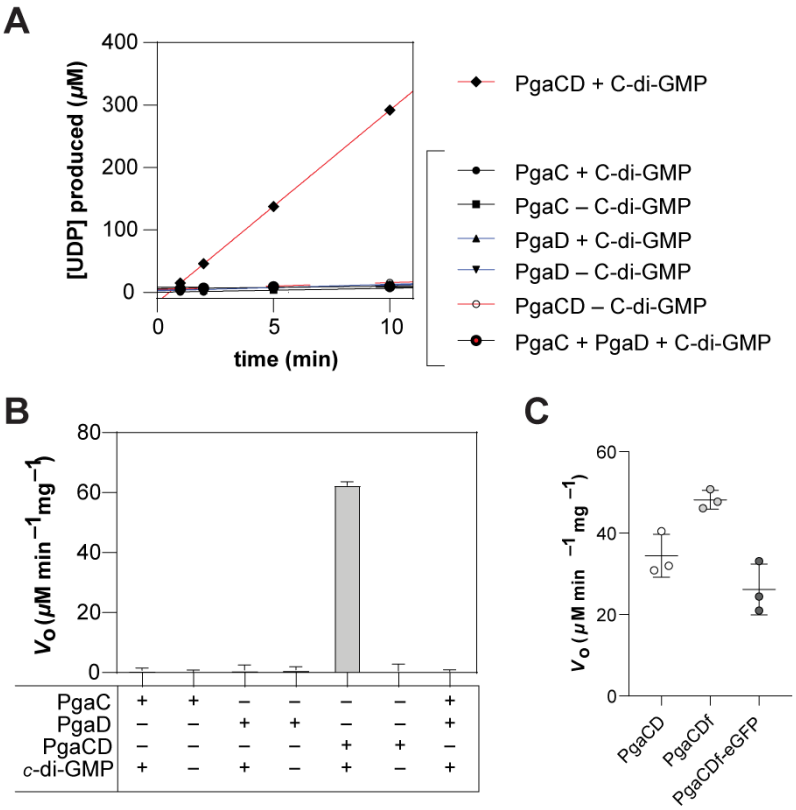

Figure 2.4: Enzymatic acitivty of PgaCD. (A) Reaction time course of various plasmids encoding PgaC, PgaD, or both PgaC and PgaD in a pETduet vector. Reactions were performed with or without the presence of c-di-GMP, a known allosteric activator of the GT enzyme. (B) Enzymatic rates for the different protein variant with/without the addition of c-di-GMP. (C) Enzymatic rate comparison between PgaCD WT, fusion protein PgaCDf, and fluorescent tagged fusion conjugate PgaCDf-eGFP.

2.2.4 Solid State NMR analysis of *de novo* PNAG isolated from active PgaCD complex

Previous measurements of PgaCD enzymatic activity relied on quantifying the release of free UDP. To ensure PNAG polymerization, we sought to isolate the *de novo* product for structural analysis. Isolation of the *de novo* synthesized PNAG begun with incubating 10mM UDP-GlcNAc with 200 mg of membrane fraction containing PgaCD. Following overnight incubation, the reaction mixture was quenched by the addition of a 1:1 ratio of MeOH, resulting in the precipitation of the polysaccharide as an insoluble white fibrous solid. The solid was separated from the soluble reaction mixture by centrifugation and washed using both water and methanol. The isolated solid material was subsequently treated with DNase1 followed by proteinase K to digest any DNA or proteinatious contaminants, respectively.

Table 2.1: 13C chemical shift comparison of de novo PNAG vs endogenous isolates.

CARBON	*de novo*	*E. coli* [15]	*S. aureus* [26]
C1	103.3	104	104
C2	54.9	58	59
C3,C5	75.2	76-78	76-77
C4,C6	70.5	71-73	72-73
CH_3	23.5	24	--
C=O	173.4	--	--

The solid material was then lyophilized before being subjected to analysis by solid state cross polarization magic angle spinning (CP-MAS) ^{13}C NMR spectroscopy. The one-dimensional ^{13}C CP-MAS NMR spectrum of our *de novo* synthesize PNAG sample displayed chemical shifts

(δ) consistent with those previously reported for authentic PNAG exopolysaccharide isolated from *E. coli* and *S. aureus* (Table 2.1). In addition to the expected CS, the NMR spectra from the *de novo* PNAG displayed additional peaks observed at 30.4, 60.9, 129.8 ppm. These δ do not correspond to protein carbonyl (172-176 ppm) or alpha carbon regions (53-56 ppm), making protein contamination unlikely.[27] Instead, the observed δ are characteristic of unsaturated lipid carbons, glycerol backbone, and aliphatic carbons which are typically located between 124-134, 60-72, and 10-35 ppm, respectively.[28]

2.2.2 Purification of glycosyl transferase complex solubilized in detergents/amphipathic polymers

We first sought to isolate and purify the recombinant PgaCD complex after overexpression in *E. coli*. To facilitate the purification, we conducted a detergent screen using various neutral or zwitterionic membrane solubilizing detergents (Fig 2.5). The results identified n-Dodecyl-phosphocholine (FC-12) and n-dodecyl-ß-D-maltoside (DDM) as the best surfactants for efficient solubilization of both PgaC and PgaD. Purification of the complex was achieved using immobilized metal chromatography (IMAC) with Ni-NTA. Interestingly, despite PgaD lacking a poly-His tag, it co-purified with PgaC, suggesting a protein-protein interaction (PPI) between PgaC and PgaD was preserved during the purification process. However, when the purified PgaCD

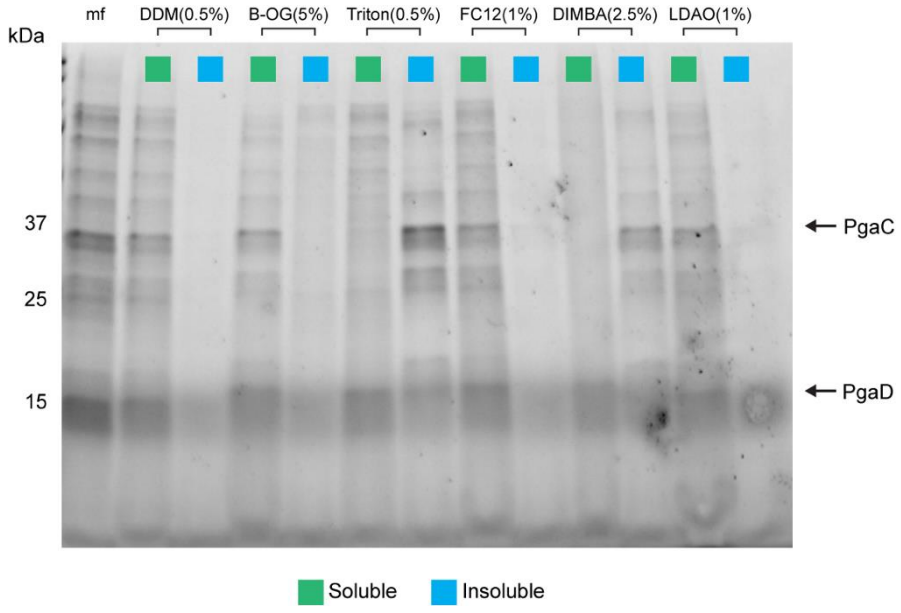

Figure 2.5: Detergent screen of PgaCD complex. Equal volumes of inverted membrane vesicles were incubated with various detergents with the final percentages shown above. Mixed on rotator overnight at 4°C. Reactions were centrifuged at 60,000 x g to isolate solubilized complex. Abbreviations: DDM: n-dodecyl-β-maltoside; B-OG: n-Octyl-β-D-glucoside; FC12: fos-choline-12; DIMBA: Diisobutylene-maleic acids; LDAO; N,N-Dimethyl-n-dodecylamine N-oxide.

complex was incubated with UDP-GlcNAc no consumption of the substrate was observed (Fig 2.6B). This result was also true for the fusion variant of the enzyme, PgaCDf.

There have been reports of reconstituting enzymatic activity of other membrane associated GT2 family synthase dependent polysaccharide biosynthesis systems. This includes the bacterial cellulose synthase (Bcs) and the hyaluronic acid synthase (HAS). Similar to PgaCD, BcsAB and HAS are transmembrane glycosyltransferases that facilitate the polymerization and transmembrane export of the polysaccharide.[29,30] BcsAB synthesizes cellulose by polymerizing UDP-Glc to form β-1→4 glucose while HAS utilizes both UDP-GlcNAc and UDP-GlcA to form the heteropolysaccaride composed of D-glucuronic acid and N-acetyl-D-glucosamine, with alternating β-(1→4) and β-(1→3) linkages.[31–33] Both enzymes have been successfully purified

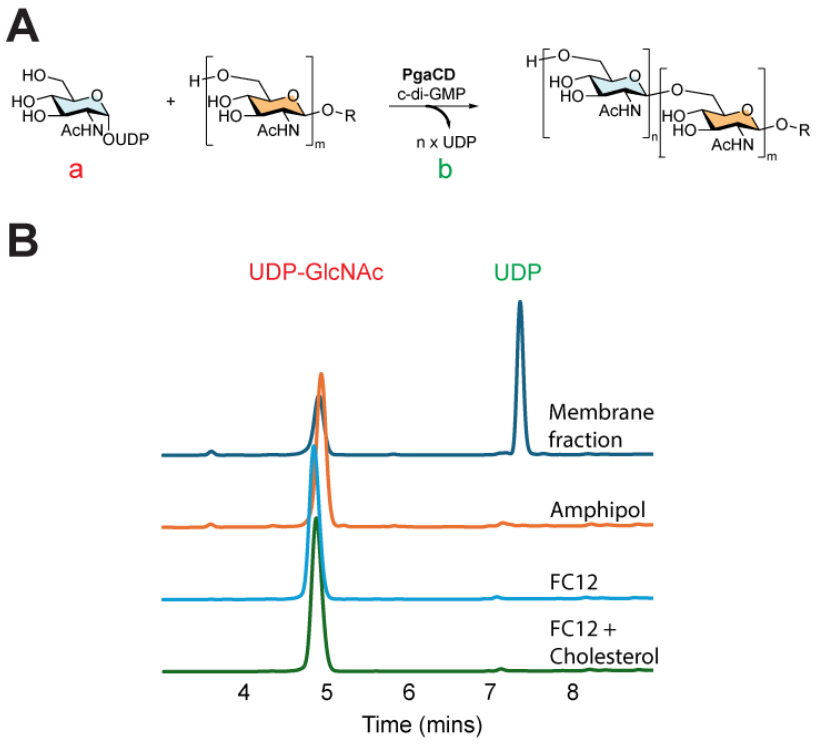

Figure 2.6: Chromatogram of PgaCD activity. A) mechanism of transferring glycosyl group onto acceptor, releasing UDP. B) HPLC chromatogram of UDP conversion from UDP-GlcNAc of various PgaCD samples. Crude membrane fraction contained glycosyltransferase activity while detergent/polymer solubilized complex did not exhibit observable activity.

using resolubilization in detergent micelles, lysoFosCholine Ether 14 for BcsAB and dodecyl maltoside for HAS, followed by reconstitution in lipid nano discs or proteolipososmes.[29,34–36] Adding UDP-GlcNAc and UDP-GlcA to purified HAS was sufficient to restore activity, while BcsAB activity could be measured in the presence of UDP-Glc and cellobiose.

A possible explanation is the solubilization of the PgaCD complex through detergent micelles could potentially create a non-native lipid environment for the enzyme, thereby inhibiting its activity. The solubilization of membrane proteins using polymeric detergents to generate native lipid nano-discs has emerged as a promising strategy to isolate membrane proteins in the presence of native lipids.[37]

This approach involved the use of an amphiphilic polymer (AMPHIPOL) to encapsulate the enzyme within its native lipids, forming lipid nano discs (Fig 2.7).[38] The direct fusion variant of

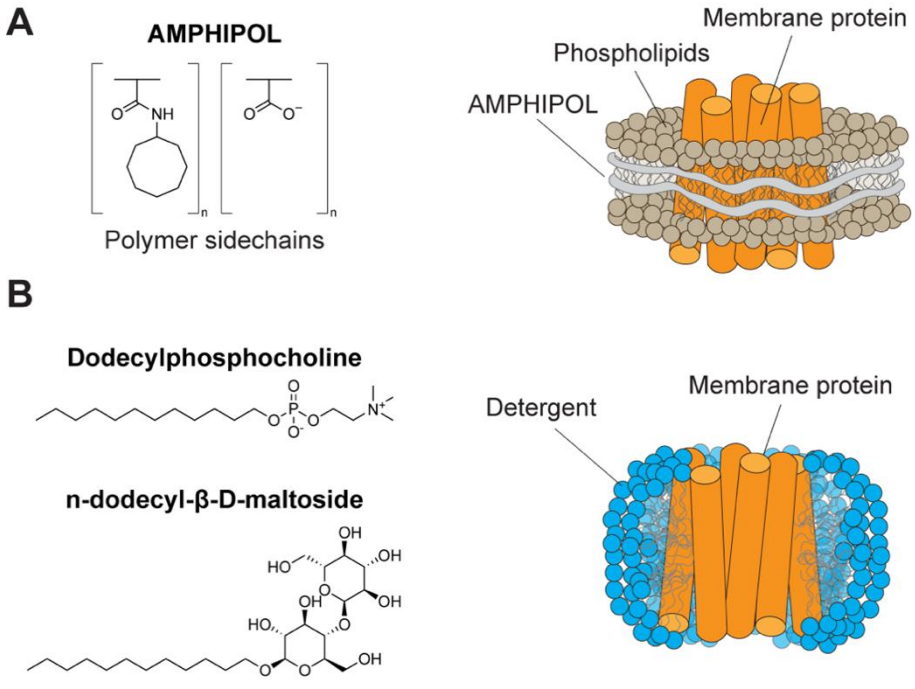

Figure 2.7: Solubilization methods of PgaCD complex. A) Amphiphilic polymer solubilization through nano disc particle comprised of native phospholipids. B) Detergent micelle solubilization, encasing transmembrane regions with hydrophobic tail groups.

PgaCD ensures proper 1:1 oligomerization ratio during expression for subsequent reactions. The lipid nano discs were purified by the same immobilized metal affinity chromatography as described previously. Cryo-electron microscopy (cryo-EM) images of the purified sample revealed uniform nano disc particles averaging 18 nm in diameter (Figure 2.8). However, despite this effort to preserve the complex within its native lipid environment, the purified complex did not yield any observable catalytic activity. It is important to note that activity assays after detergent/polymer solubilization were conducted both prior and after IMAC purification. This includes all detergents and polymers used during screening.

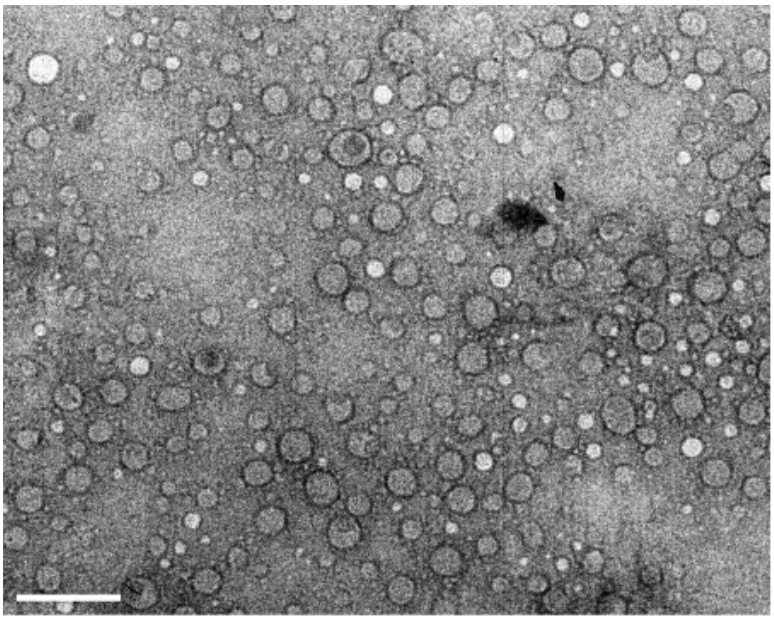

Figure 2.8: Cryo transmission electron microscopy (Cryo-EM) image of uniform nano discs containing PgaCDf-eGFP after purification. Particles are estimated to be around 18 nm in diameter. Scale bar 100nm.

2.3 Conclusion

Given the widespread integration of EPS within bacterial biofilms, the biochemical mechanism that initiates the biosynthesis of these polysaccharides remains an area of active investigation with speculations that synthase-dependent polysaccharide synthesis undergoes self-initiation process. Specifically, the *pga* operon encodes the machinery for PNAG biosynthesis in

Gram-negative bacterial biofilms.[15] The biosynthesis is performed by the PgaCD complex. While there has been a number of studies on the role of PgaCD in PNAG biosynthesis, there are conflicting reports about how To date, there have been no reports of fully rescuing enzymatic activity after purification.

There have been reports of reconstituting enzymatic activity of other membrane associated GT2 family synthase dependent polysaccharide biosynthesis systems including Bcs and HAS. While activity was rescued within these systems, it remains unclear if these mechanisms occur *in vivo*. In the case of the PgaCD complex, efforts to reconstitute its activity *in vitro* have largely been unsuccessful. Initially, the lack of activity was attributed to improper lipid environment and oligomerization state after purification. This was addressed by solubilizing the complex within native lipids using amphiphilic polymer (AMPHIPOL) as well as fusing the PgaC and PgaD enzyme to ensure proper oligomerization. However, neither approach was able to rescue enzymatic activity. Subsequent NMR characterization of *de novo* synthesized PNAG from activity revealed additional peaks characteristic to unsaturated lipid carbons, glycerol backbone, aliphatic carbons which are typically located between 124-134, 60-72, and 10-35ppm, respectively.[28] It is entirely possible that the additional signals observed originates from a lipid-based initiator. WbbF is a O-polysaccharide synthase found in *Salmonella enterica* has been identified to utilize a lipid initiator substate undecaprenyl pyro phosphate (Und PP) GlcNAc similar to other cell surface polysaccharides in Wzx/Wzy and ABC transporter dependent pathways.[39] The combination of expression and purification conditions suggests that PgaCD complex does not utilize a self-initiating mechanism. Instead, the loss of activity is due to the lack of an acceptor substrate, which is likely involves a lipidated molecule based on NMR spectra of *de novo* PNAG.

2.4 Experimental Procedures

General procedure

All chemicals were purchased as reagent grade and used without further purification, unless otherwise noted. Regents, pipettes, and collection tubes were sterilized (unless sterile from manufacture) for any work involving cells and DNA/RNA. Cell work and PCR reactions were performed in biosafety cabinets. Protein overexpression was performed using BL21 (DE3) cells cultured in Luria Broth (LB). Ampicillin (100µg/ml) was used for cells containing pET21/pETduet vectors while Kanamycin (50µg/mL) was used for cells carrying pET28 vectors. Antibiotic solutions were sterilized via syringe filter (0.22µm) and stored in -20^{o}C.

SDS-PAGE samples were prepared from loading dye and 20x reducing agent from Bio-rad. Heat denatured at 95^{o}C for 5 mins, followed by centrifugation. 10µL of sample were loaded onto 12% Mini-PROTEIN TGX Stain-Free polyacrylamide gel (Bio-Rad). Gels were run in 1x Tris-Glycine-SDS running buffer (Bio-Rad) for 35 min or until completion at 200 V.

Plasmid construction

PgaCD wt is encoded within a pETduet vector, containing dual T7 promotor regions to accommodate the individual expression of PgaC and PgaD within the same cell line. PgaCDf (direct C-N fusion of PgaCD) was encoded within a pET28 vector. PgaCDf-eGFP was generated by amplifying the PgaCDf sequence and inserted into a pET28 vector containing eGFP. Restriction sites include NcoI (Fwd) and EcoRI (Rev).

Table 2.2 PgaCDf primers

PgaCDf primer pair	Fwd 5'-CAGTCCATGGTCAACCGTATCGTTAGCTTCTTTATTCTGTGCC Rev 5'- CTGAGAATTCCGCACGCACCAGCGCTTTTTC

Protein expression and preparation of inverted membrane vesicles

Starter cultures were prepared by inoculating 50 mL of Luria broth (LB) from a glycerol stock and incubating at 37 ^{o}C while shacking at 200 rpm for 18 hrs. 5 mL of the overnight starter culture was used to inoculate 500 mL of LB and the cells were grown at 37 ^{o}C until reaching an OD_{600} of 0.5-0.6. The culture was cooled to room temperature for 10 min before inducing by adding 200-400 µM isopropyl-β-D-thiogalactopyranoside (IPTG). The culture was then incubated at 18 ^{o}C at 200 rpm for an additional 18 hrs.

Cells were harvested through centrifugation at 5500 x g and resuspended to 10 g cell/mL of phosphate buffered saline (PBS). The cells were lysed by sonication, and inverted membrane vesicles (IMV) were prepared as previously described.[29] Briefly, cells were harvested and resuspended to 1g/10mL of 1x PBS and lysed using the Fisherband^{TM} Model 505 Sonic Dismembrator set at; 1 sec on, 3 sec off, 30% amp for 2:30. Lysate was centrifuged at 13,000 x g for 20 mins to remove cell debris. Supernatant was floated on 1.8M sucrose solution and centrifugation at 60,000 x g for 1 hr. After centrifugation, 3 layers will be observed with the middle layer containing the membrane vesicles. The middle layer was removed and centrifuged for an additional 60,000 x g for 1 hr before resuspension in storage buffer at 200mg/mL. The IMV fraction pellet was resuspended to a final concentration of 200 mg of pellet/mL of 50 mM Tris-HCl, 150 mM NaCl, 5 % glycerol, pH 7.4 and stored at –80 ^{o}C until use.

Reconstitution in detergent micelles/nano discs for IMAC purification

IMV fractions were incubated with FC-12 (1 % w/v) and AMPHIPOL polymer (1 % w/v) overnight with gentle rotation. The mixture was centrifuged at 60,000 x g for 1 hr, and the supernatant containing the solubilized membrane protein was collected. The solubilized proteins

were incubated with Ni-NTA resin overnight at 4 ^{o}C with gentle rotation. The resin was then loaded onto a spin column and subject to a stepwise imidazole gradient (10, 30, 50, 70, 100, 200mM) elution in 25mM Sodium phosphate, 150mM NaCl, pH 7.4 in 400µL fractions. Each imidazole concentration was performed twice to obtain the purified membrane proteins verified by SDS gel electrophoresis. All proteins were aliquoted and stored in –80 ^{o}C for future use.

Cryo-TEM

IMAC column purified nano discs containing 1mg/mL PgaCD complex was added to copper grid and submerged into liquid ethane. The grid was blotted for 5 seconds then imaged with JEOL JEM 2100 LaB6 TEM assisted by Dr. Wen-An Chiou at the Advanced Imaging & Microscopy laboratory (AIM Lab) located in the Jeong H. Kim Engineering Building.

Activity assay

Reaction progress was monitored through HPLC. Reactions were conducted in 50mM Tris-HCl buffer pH 7.5 containing 1 mM UDP-GlcNAc, 2 mM c-di-GMP, and 1 mM $MgCl_2$. Reactions were initiated through the addition of membrane proteins (5 µL) and incubated at 37 ^{o}C. To analyze reaction progress, a 10 µL of the reaction mixture was removed after 1–30 min incubation and quenched by adding 10 µL of MeOH followed by centrifugation at 17,000 x g for 2 min to remove any insoluble material. The quenched mixture was diluted 3-fold with Milli-Q water before HPLC analysis. 20µL of the diluted samples were injected in Kinetex 5µm C18 reverse phase column. Analytes were resolved using a gradient of Buffer A (20mM potassium phosphate, 2mM tetrabutyl ammonium persulfate, pH 6.0) and Buffer B (10 mM potassium phosphate, 1mM tetrabutyl ammonium persulfate, and 50% HPLC-grade acetonitrile, pH 6.0) shown below. Reaction progression is monitored though the conversion of UDP-GlcNAc to free UDP.

Table 2.2 HPLC conditions for resolving UDP and UDP-GlcNAc

Time (min)	Flow rate (mL/min)	% Buffer B
0	1	0
1	1	0
6	1	100
10	1	100
11	1	0
15	1	0
15.5	0	0

Isolation of *de novo* synthesized PNAG

A 10 mL reaction containing 200 mg of PgaCD containing IMV was incubated in 50 mM Tris-HCl pH 7.4 containing 10 mM UDP-GlcNAc and 2 µM c-di-GMP overnight at 37ºC. The de novo synthesized PNAG was precipitated upon the addition of MeOH (10 mL). The precipitate was washed and vortexed with 1:1 ratio of MeOH:water before being thoroughly dried using vacuum centrifugation. The dried pellet was resuspended in 500uL of 50 mM Tris-HCl, at pH 7.4, containing 1 mM of $MgCl_2$ and 1 mM $CaCl_2$ before treating with DNAse1 (50 µg/mL) and proteinase K (100 µg/mL) for 60 mins at 37ºC. The polysaccharide pellet was again washed and dried with the same method described above and stored in –20 ºC until use.

CP-MAS NMR

De novo PNAG was analyzed using a Bruker AVANCE NEO solid-state 500 MHz (SS500) NMR spectrometer. 15 mg of the polysaccharide was grounded, packed into a CP-MAS probe, and analyzed at 5, 7, and 12 kHz. Adamantane was used as the reference compound for chemical shift calibration.

References

1. Marsh, P. D. & Zaura, E. Dental biofilm: ecological interactions in health and disease. *J Clin Periodontol* 44, S12–S22 (2017).

2. Rohde, H. *et al.* Polysaccharide intercellular adhesin or protein factors in biofilm accumulation of Staphylococcus epidermidis and Staphylococcus aureus isolated from prosthetic hip and knee joint infections. *Biomaterials* 28, 1711–1720 (2007).

3. Flemming, H.-C. *et al.* Biofilms: an emergent form of bacterial life. *Nat. Rev. Microbiol.* 14, 563–575 (2016).

4. Schmid, J., Sieber, V. & Rehm, B. Bacterial exopolysaccharides: biosynthesis pathways and engineering strategies. *Front. Microbiol.* 6, 496 (2015).

5. Jamal, M. *et al.* Bacterial biofilm and associated infections. *J Chin Med Assoc* 81, 7–11 (2018).

6. Limoli, D. H., Jones, C. J. & Wozniak, D. J. Bacterial Extracellular Polysaccharides in Biofilm Formation and Function. *Microbiol Spectr* 3, (2015).

7. Vuong, C. *et al.* Polysaccharide intercellular adhesin (PIA) protects Staphylococcus epidermidis against major components of the human innate immune system. *Cell. Microbiol.* 6, 269–275 (2004).

8. Maunders, E. & Welch, M. Matrix exopolysaccharides; the sticky side of biofilm formation. *FEMS Microbiol. Lett.* 364, fnx120 (2017).

9. Evans, L. R. & Linker, A. Production and Characterization of the Slime Polysaccharide of Pseudomonas aeruginosa. *J. Bacteriol.* 116, 915–924 (1973).

10. Thongsomboon, W. *et al.* Phosphoethanolamine cellulose: A naturally produced chemically modified cellulose. *Science* 359, 334–338 (2018).

11. McKenney, D. *et al.* The ica Locus of Staphylococcus epidermidis Encodes Production of the Capsular Polysaccharide/Adhesin. *Infect. Immun.* 66, 4711–4720 (1998).

12. Itoh, Y. *et al.* Roles of pgaABCD genes in synthesis, modification, and export of the Escherichia coli biofilm adhesin poly-beta-1,6-N-acetyl-D-glucosamine. *J Bacteriol* 190, 3670–80 (2008).

13. Skurnik, D. *et al.* Extended-spectrum antibodies protective against carbapenemase-producing Enterobacteriaceae. *J. Antimicrob. Chemother.* 71, 927–935 (2016).

14. Cywes-Bentley, C. *et al.* Antibody to a conserved antigenic target is protective against diverse prokaryotic and eukaryotic pathogens. *Proc. Natl. Acad. Sci.* 110, E2209–E2218 (2013).

15. Wang, X., Preston, J. F. & Romeo, T. The pgaABCD Locus of Escherichia coli Promotes the Synthesis of a Polysaccharide Adhesin Required for Biofilm Formation. *J. Bacteriol.* 186, 2724–2734 (2004).

16. Lairson, L. L., Henrissat, B., Davies, G. J. & Withers, S. G. Glycosyltransferases: Structures, Functions, and Mechanisms. *Annu Rev Biochem* 77, 521–555 (2008).

17. Vakulskas, C. A., Potts, A. H., Babitzke, P., Ahmer, B. M. M. & Romeo, T. Regulation of Bacterial Virulence by Csr (Rsm) Systems. *Microbiol. Mol. Biol. Rev.* 79, 193–224 (2015).

18. Romeo, T., Vakulskas, C. A. & Babitzke, P. Post-transcriptional regulation on a global scale: form and function of Csr/Rsm systems. *Environ. Microbiol.* 15, 313–324 (2013).

19. Goller, C., Wang, X., Itoh, Y. & Romeo, T. The Cation-Responsive Protein NhaR of Escherichia coli Activates pgaABCD Transcription, Required for Production of the Biofilm Adhesin Poly-β-1,6-N-Acetyl-d-Glucosamine. *J. Bacteriol.* 188, 8022–8032 (2006).

20. Steiner, S., Lori, C., Boehm, A. & Jenal, U. Allosteric activation of exopolysaccharide synthesis through cyclic di-GMP-stimulated protein–protein interaction. *Embo J* 32, 354–368 (2013).

21. Ryjenkov, D. A., Tarutina, M., Moskvin, O. V. & Gomelsky, M. Cyclic Diguanylate Is a Ubiquitous Signaling Molecule in Bacteria: Insights into Biochemistry of the GGDEF Protein Domain. *J. Bacteriol.* 187, 1792–1798 (2005).

22. Jonas, K. *et al.* The RNA binding protein CsrA controls cyclic di-GMP metabolism by directly regulating the expression of GGDEF proteins. *Mol. Microbiol.* 70, 236–257 (2008).

23. Martinson, J. N. V. & Walk, S. T. Escherichia coli Residency in the Gut of Healthy Human Adults. *EcoSal Plus* 9, 10.1128/ecosalplus.ESP-0003–2020 (2020).

24. Caroff, M. & Novikov, A. Lipopolysaccharides: structure, function and bacterial identifications☆☆☆. *OCL* 27, 31 (2020).

25. Swoboda, J. G., Campbell, J., Meredith, T. C. & Walker, S. Wall Teichoic Acid Function, Biosynthesis, and Inhibition. *ChemBioChem* 11, 35–45 (2010).

26. Joyce, J. G. *et al.* Isolation, structural characterization, and immunological evaluation of a high-molecular-weight exopolysaccharide from Staphylococcus aureus. *Carbohyd Res* 338, 903–922 (2003).

27. Andrade, F. D., Forato, L. A., Filho, R. B. & Colnago, L. A. Quantification of protein secondary structure by 13C solid-state NMR. *Anal. Bioanal. Chem.* 408, 3875–3879 (2016).

28. Alexandri, E. *et al.* High Resolution NMR Spectroscopy as a Structural and Analytical Tool for Unsaturated Lipids in Solution. *Molecules* 22, 1663 (2017).

29. Omadjela, O. *et al.* BcsA and BcsB form the catalytically active core of bacterial cellulose synthase sufficient for in vitro cellulose synthesis. *Proc. Natl. Acad. Sci.* 110, 17856–17861 (2013).

30. Hubbard, C., McNamara, J. T., Azumaya, C., Patel, M. S. & Zimmer, J. The Hyaluronan Synthase Catalyzes the Synthesis and Membrane Translocation of Hyaluronan. *J. Mol. Biol.* 418, 21–31 (2012).

31. Nishiyama, Y., Sugiyama, J., Chanzy, H. & Langan, P. Crystal Structure and Hydrogen Bonding System in Cellulose Iα from Synchrotron X-ray and Neutron Fiber Diffraction. *J. Am. Chem. Soc.* 125, 14300–14306 (2003).

32. Valachová, K., Hassan, M. E. & Šoltés, L. Hyaluronan: Sources, Structure, Features and Applications. *Molecules* 29, 739 (2024).

33. Mitra, A. K., Arnott, S. & Sheehan, J. K. Hyaluronic acid: Molecular conformation and interactions in the tetragonal form of the potassium salt containing extended chains. *J. Mol. Biol.* 169, 813–827 (1983).

34. DeAngelis, P. L. & Zimmer, J. Hyaluronan synthases; mechanisms, myths, & mysteries of three types of unique bifunctional glycosyltransferases. *Glycobiology* 33, 1117–1127 (2023).

35. Maloney, F. P. *et al.* Structure, substrate recognition and initiation of hyaluronan synthase. *Nature* 604, 195–201 (2022).

36. Morgan, J. L. W., Strumillo, J. & Zimmer, J. Crystallographic snapshot of cellulose synthesis and membrane translocation. *Nature* 493, 181–186 (2013).

37. Marconnet, A. *et al.* Solubilization and Stabilization of Membrane Proteins by Cycloalkane-Modified Amphiphilic Polymers. *Biomacromolecules* 21, 3459–3467 (2020).

38. Marconnet, A. *et al.* Influence of Hydrophobic Groups Attached to Amphipathic Polymers on the Solubilization of Membrane Proteins along with Their Lipids. *Anal. Chem.* 94, 14151–14158 (2022).

39. Wear, S. S., Hunt, B. A., Clarke, B. R. & Whitfield, C. Analysis of the Topology and Active-Site Residues of WbbF, a Putative O-Polysaccharide Synthase from Salmonella enterica Serovar Borreze. *J. Bacteriol.* 202, (2020).

Chapter 3: PNAG localization and initiation studies

Contributing of other authors:

Luan Vo for providing DspB wt and DspB-APEX2 for PNAG dot blot analysis. Dr. Fu Chen for CP MAS NMR of endogenous PNAG from *S. epidermidis*.

3.1 Introduction

Synthase-dependent exopolysaccharides (Fig. 3.1) are recognized as key components of bacterial biofilms, contributing to both cellular adhesion and virulence.[1] It is estimated that approximately 65% of all microbial infections involve biofilm formation, underscoring their significance in modern medicine.[2,3] Despite this importance, the precise mechanism of polysaccharide initiation in synthase-dependent systems remains unsolved, as no initiator molecule has yet been conclusively identified.

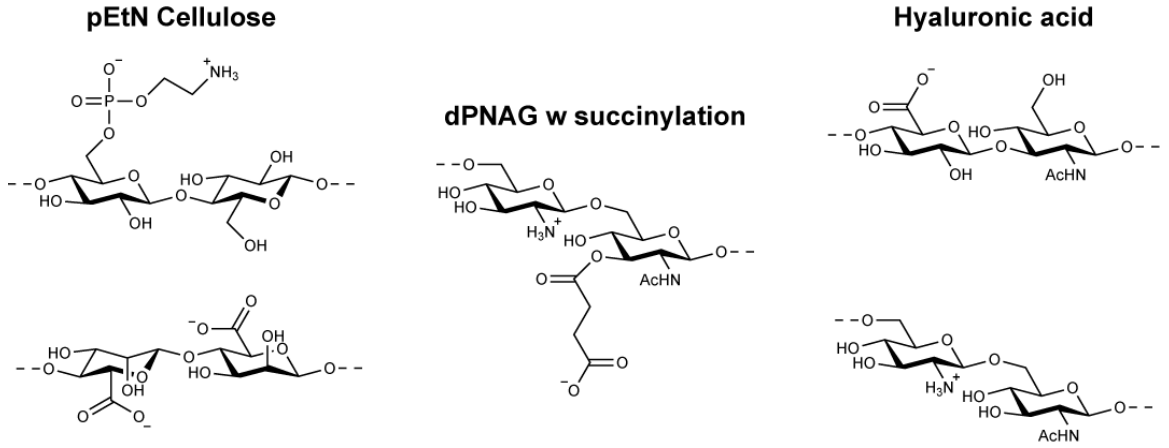

Figure 3.1: Different exopolysaccharides from synthase dependent pathways.

Both primer-dependent and primer-independent mechanisms have been proposed. Evidence for primer involvement includes early findings in 1995, when extracts of *Agrobacterium tumefaciens* harboring mutations in the bacterial cellulose synthase operon were shown to incorporate radiolabeled substrate onto a lipid-linked intermediate.[4] This was later supported in 2002, when yeast membrane fractions expressing recombinant cellulose synthase A subunit 1 (CesA1) extended radiolabeled sitosterol-β-glucoside in the presence of UDP-glucose.[5] More recently, studies on O-antigen biosynthesis demonstrated that O:54 synthase (WbbF), a GT2-family enzyme with homology to PgaC, CesA1 and BcsA (Fig. 3.2), was shown to initiate

polymerization using an undecaprenyl-diphosphate (Und-PP) linked disaccharide as the acceptor substrate.[6] Given the sequence similarity of PgaC to both cellulose synthase and WbbF, it is plausible that PNAG synthesis may also require a lipid- or sterol-linked primer.

In contrast, accumulating evidence also supports primer-independent, self-initiation mechanisms, particularly from *in vitro* reconstitution studies of enzymes such as Bacterial cellulose synthase A (BcsA) and Hyaluronic acid synthase (HAS).[7,8] Both of these enzymes have been proposed to "self initiate" polymer biosynthesis through the hydrolysis of the first equivalent

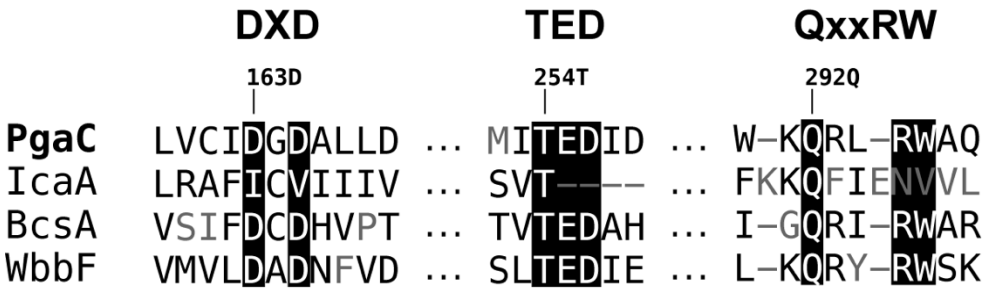

Figure 3.2: Sequence alignment of GT 2 family enzymes. Highlighted conservative motifs with GT enzymes including magnesium ion stabilizer (DXD), reaction catalytic site (TED), and the polymer stabilization (QXXRW).

of sugar-nucleotide substrate, generating a free reducing sugar monosaccharide as the initiator. Whether these self-initiating activities reflect the physiological mechanism of polysaccharide initiation *in vivo* remains an open question requiring further investigation.

3.2 Results

3.2.1 PNAG remains associated to membrane fraction after polymerization

As we described in Chapter 2, cross polarization magic angle spinning (CP-MAS) ^{13}C NMR analysis of PNAG polysaccharide produced via the *de novo* reaction of the PgaCD complex in E. coli inverted membrane vesicles (IMVs), revealed additional peaks corresponding with unsaturated lipids within the *de novo* synthesized PNAG spectra. Thus, we decided to investigate the localization of de novo synthesized PNAG following the polymerization via dot blot analysis. Reaction mixtures of IMVs containing PgaCD, PgaCDf or PgaCDf-eGFP incubated with UDP-

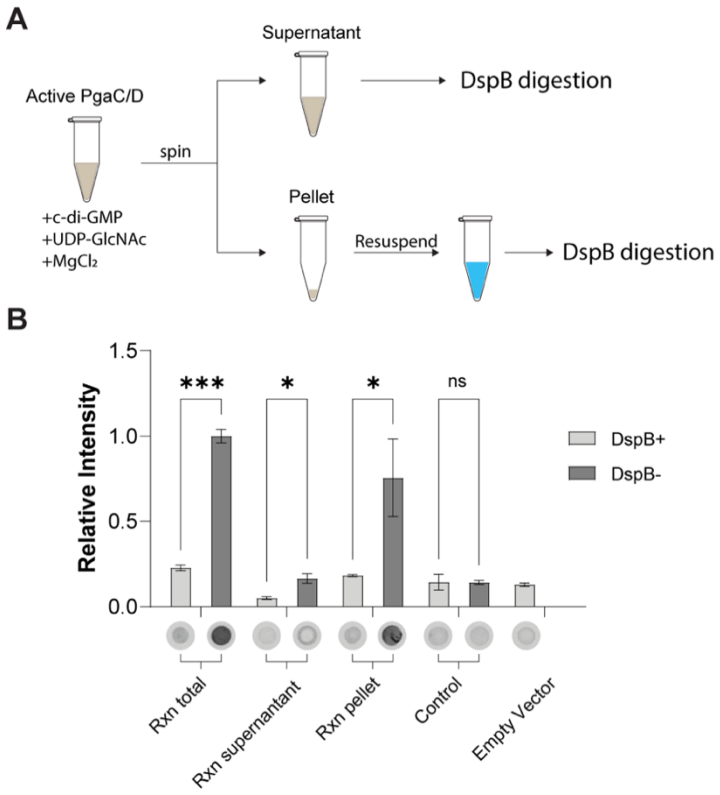

Figure 3.3: PNAG localization after polymerization. A) Reaction workflow for separating proteoliposomes after reaction. B) Different reaction fractions were spotted onto nitrocellulose membrane and blocked with 5% BSA for 1 hour while rotating at room temperature. After blocking, the membrane was washed 3 times with PBS tween then incubated with catalytically inactive DspBE184Q mutant conjugated to ascorbate peroxidase APEX2 (DspB-APEX2) for 1 hour rotating at room temperature. The membrane was washed 3 times with PBS tween before visualization by Opi-4CN from Bio-Rad.

GlcNAc and c-di-GMP were incubated for 0.5 hrs and then centrifuged to separate the supernatant from the membrane fraction (Fig 3.3A). The pellet, containing the IMVs, was then resuspended in the same reaction buffer and both fractions were incubated in the presence (+) or absence (–) of the PNAG hydrolase enzyme DspB to ensure that signals correspond to the presence of PNAG and no other unrelated glycans potentially present in the IMVs. Aliquots from each fraction were spotted on nitrocellulose membrane and probed with previously reported PNAG detection reagent DspB-APEX2 and visualized with Bio-Rad Opti 4CN substrate.[9] The DspB-APEX2 is a fusion protein of catalytically inactive $DspB_{E184A}$ fused with an engineered ascorbic acid peroxidase, which maintains the ability to bind to and detect PNAG in biological samples. Densitometric analysis of the spots was performed using Fiji (ImageJ), with pixel densities converted to relative gray values (GV) for comparison. Each spot was analyzed in technical replicate, and error bars represent the variance in spot pixel density among replicates. This dot blot analysis revealed that the majority of the *de novo* synthesized PNAG remained associated with the membrane fraction (Fig. 3.3B).

It is possible that the *de novo* synthesized PNAG was not directly membrane-associated but instead became encapsulated within the proteoliposome (PL) IMVs formed during sonication, thereby co-localized with the membrane fraction. To obtain active PgaCD enzyme complexes, cells harboring the overexpression vector were harvested and lysed by sonication, followed by sucrose density-based centrifugation to isolate IMVs. It has been well established that spontaneous vesicle formation will occur upon bacterial lysis, and sonication is known to induce the formation of IMV PLs containing membrane proteins.[10]

If PNAG were sequestered within PLs, the polymer would be inaccessible and resistant to degradation by an exogenously added glycosyl hydrolase enzyme like DspB. However, we

observed robust hydrolysis of PNAG in both the crude reaction mixture and the centrifuged membrane pellet without prior membrane disruption. These results indicate that PNAG was not encapsulated within PLs and thus must be association with the IMV via an alternative mechanism.

3.2.2 Presence of free GlcNAc does not influence enzymatic activity

Many proposed "self-initiating" mechanism involves the hydrolysis of the UDP-sugars, leaving the free sugar to serve as the initial acceptor for polymerization. This concept is supported by the observed activity from purified glycosyl transferase enzymes incubated with just their cognate nucleotide-sugar substrates. For example, HAS catalyzes HA polymerization upon addition of UDP-GlcNAc and UDP-GlcA. In this system, the inclusion of free GlcNAc monosaccharides has been shown to enhance UDP-GlcA hydrolysis, thereby accelerating HA polymerization.[11]

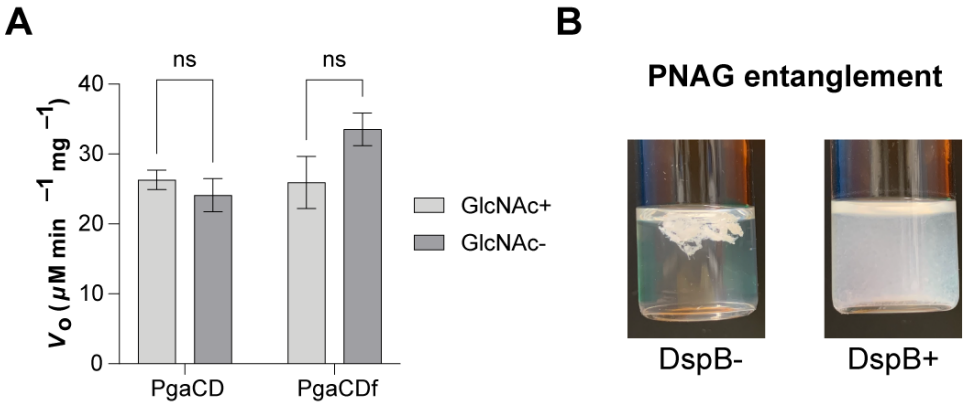

Figure 3.4: Effects of free GlcNAc on PNAG polymerization. A) Membrane vesicles containing either PgaCD wt or PgaCDf were incubated in the presence of UDP-GlcNAc, $MgCl_2$, c-di-GMP, and (+/-) 50 mM of free GlcNAc. B) Precipitation of PNAG by isopropanol. Comparison of product after DspB (+/-) hydrolysis.

To investigate whether a similar mechanism applies to PNAG biosynthesis, we examined the activity of the PgaCD complex in the presence or absence of exogenous free GlcNAc. Due to

the loss of enzymatic activity upon purification, assays were performed using membrane fractions containing active PgaCD complex or active PgaCDf. Reactions containing an excess of free GlcNAc (50 mM) and 1 mM UDP-GlcNAc were ran in parallel with reactions containing the same concentration of IMV but lacking free GlcNAc as controls. No significant differences were observed in enzymatic activity between the two conditions (Fig. 3.4A). This result was consistent for both wild-type PgaCD complex and using a PgaCDf variant. These findings suggest that free GlcNAc monosaccharide does not serve as a primer substrate for PNAG biosynthesis catalyzed by PgaCD.

3.2.3 PNAG is associated to cell surface *S. epidermidis* RP62A

Solid-state NMR analysis of *de novo* synthesized PNAG revealed additional peaks that suggested a possible lipid-linked intermediate could be used in the mechanism of PNAG biosynthesis. To investigate this, PNAG was isolated from S. *epidermidis* for comparison with the *in vitro* product (Fig. 3.4B). The clinical strain *S. epidermidis* RP62A exhibits a robust biofilm phenotype when grown at 37 °C under slow agitation for 72 hours. Although previous reports have primarily detected PNAG in the culture supernatant, we hypothesized that a fraction of the polymer remains associated with the cell surface and contributes directly to biofilm formation.

To isolate surface-associated PNAG, *S. epidermidis* cells were harvested and resuspended in low-salt buffer, followed by sonication. In Gram-positive bacteria, sonication can effectively shear surface polysaccharides from the thick peptidoglycan matrix without causing cell lysis. Following sonication, cells were pelleted, and the clarified supernatant was subjected to dialysis, followed by DNase1 and proteinase K treatments. PNAG was subsequently precipitated by isopropanol and recovered as an off-white powder.

Solid-state NMR spectra of the isolated material revealed characteristic signals consistent with purified PNAG and minimal background peaks (Fig. 3.5). PNAG isolated from *Staphylococcus* species is known to undergo O-succinylation at the 3′ position, and in the NMR spectra we observed weak but distinct resonance contributions from the succinate group: methylene carbons at ~29 ppm and a shoulder carbonyl peak at ~175 ppm overlapping with the acetyl signal. These signals were relatively minor, consistent with previous estimates that only ~6 % of PNAG residues carry the succinyl modification.[12]

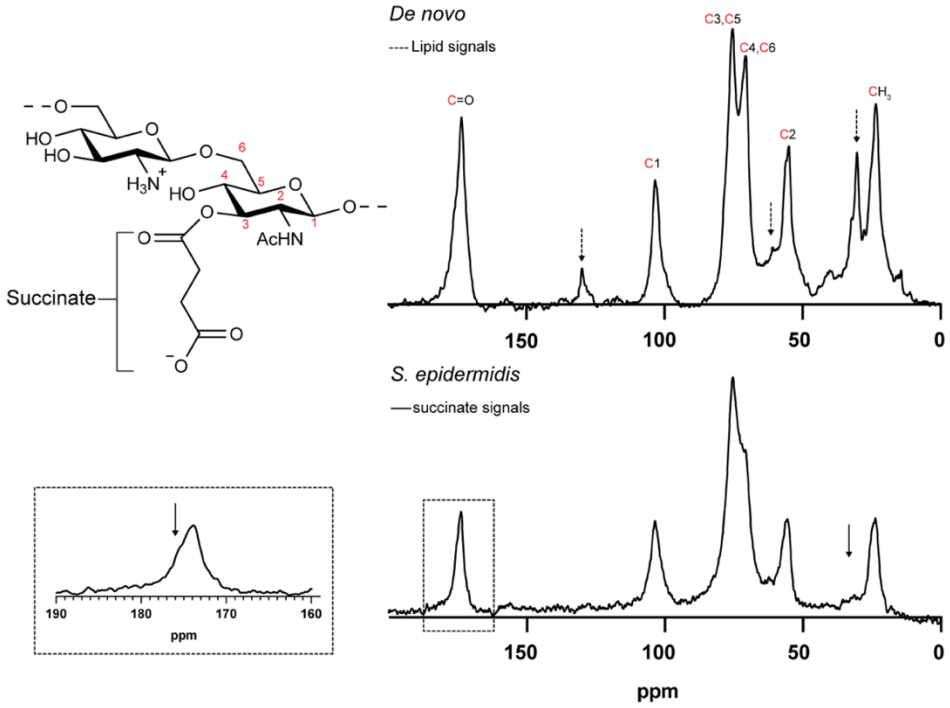

Figure 3.5: Solid State NMR comparison of *in vitro* vs endogenous cell surface PNAG from *S. epidermidis*. Lipid corresponding peaks found in *de novo* PNAG. Succinate modification can be found at 175 ppm (carbonyl) and 29 ppm (methylene).

Solid-state NMR spectra of the isolated material permitted direct comparison with *de novo* synthesized PNAG which revealed the lack of signals corresponding to lipids. It is important to note the yield for this method was relatively low (5-10 mg of PNAG per liter of culture). This was

not unexpected, as mechanical shearing during sonication likely disrupted only fragments of the polymer rather than extracting intact cell surface material.

Despite the modest yields, the isolation of PNAG tightly associated with the cell surface supports the hypothesis that *S. epidermidis* biofilm formation involves a mechanism of cell surface display. In fact, the presence of both cell surface displayed PNAG and secreted PNAG is consistent with initial reports on PNAG characterization in *S. epidermidis*. The retention of PNAG at the cell envelope raises the possibility of covalent linkage, analogous to teichoic acids in Gram-positive bacteria.

3.3 Conclusions

To date, no initiator substrate has been conclusively identified for PNAG biosynthesis. Both primer-dependent and primer-independent mechanism have been proposed for synthase-dependent polysaccharide systems. Our data strongly suggest that PNAG biosynthesis in Gram-negative bacteria does not proceed via a self-priming mechanism.

Our localization studies demonstrated that PNAG biosynthesized *in vitro* remains membrane associated after polymerization. This observation was not due to encapsulation within PLs, as PNAG hydrolysis by DspB occurred without any prior membrane disruption. In contrast, previous studies with hyaluronic acid synthase (HAS) demonstrated that intact PLs provided significant protection, up to 80% against hyaluronidase degradation, with polysaccharides becoming accessible only after solubilization with detergents (Triton X-100).[8] Given that DspB is unlikely to permeate proteoliposome bilayers and PNAG itself would not freely cross the membrane, the observed hydrolysis suggests that nascent PNAG does not translocate into PLs but rather remains exposed and membrane associated.

Self-priming mechanisms in glycosyltransferases are often supported by *in vitro* reconstitution using their cognate UDP-sugars. For example, HA synthase exhibits enhanced UDP-GlcA hydrolysis in the presence of free GlcNAc, and the purified BcsA/B complex from bacterial cellulose synthesis can polymerize cellulose when supplied with cellobiose.[7,11] However, when active PgaC/D complexes in membrane fractions were supplied with excess GlcNAc, no change in enzymatic activity was observed. These results indicate that free GlcNAc does not function as a priming acceptor in PNAG biosynthesis, effectively ruling out a self-priming mechanism for PgaC/D.

Taken together, the evidence suggests that the PgaCD complex may employ a primer-dependent initiation strategy analogous to other surface polysaccharide biosynthetic systems. Specifically, it is plausible that PNAG biosynthesis is primed by a lipid-linked monosaccharide, such as undecaprenyl pyrophosphate (Und-PP)–GlcNAc, or glycerol-phospholipid linked GlcNAc, which has been observed as an intermediate providing a mechanism consistent with other bacterial polysaccharide initiation pathways.

3.4 Experimental Procedures

Isolation of endogenous PNAG from *S. epidermidis*

S. epidermidis exopolysaccharide was isolated using a method adapted from a previous report.[13] Briefly, *S. epidermidis* glycerol stock was used to inoculate 500mL TSB buffered with 20mM Tris-HCl pH 7.5. The culture was grown for 72 hours rotating at 100 rpm and incubating at 37ºC. Cells were harvested by centrifuging at 2500 x g for 20mins and the pellet resuspended in 25 mL of cold PBS. The resuspended cells were sonicated using the FisherbandTM Model 505 Sonic Dismembrator set at; 5 seconds on, 10 seconds off, 3mins, 30% amp. The suspension was centrifuged at 6000 rpm for 20 mins to remove whole cells, and the supernatant was centrifuged

for an additional 12,000 rpm for 60 mins. The supernatant was dialyzed against 2L of 50mM Tris-HCl pH 7.5 overnight at 4^{o}C.

PNAG can be isolated as a precipitate by mixing the supernatant to ice cold isopropanol at a 1:3 ratio, respectively. The mixture was centrifuged at 4000 rpm to obtain the PNAG. The pellet was washed multiple times with Milli Q water before suspended in a buffer containing 1mM $MgCl_2$, 1mM $CaCl_2$, and 20mM Tris-HCl pH 7.4 followed by sonication bath to break up the precipitate. The suspension was then treated with DNase1 (50µg/mL) and Proteinase K (100µg/mL) for 2 hours at 37^{o}C. The pellet was washed with MilliQ water and isopropanol mixture described above and the solid was stored in -20^{o}C until use.

Dot blot analysis of PNAG localization

A reaction mixture previously described in the isolation of *de novo* synthesized PNAG was centrifuged at 17,000 x g for 10 minutes to pellet the membrane fraction. The pellet was resuspended in a buffer containing 1mM $MgCl_2$ in 50mM Tris-HCl pH 6. Fractions of the supernatant and pellet were treated with DspB (+/-) for 1hr rotating at room temperature. 1µL of each fraction was spotted on a nitrocellulose membrane and allowed to dry. The membrane was blocked using 5% BSA solution in PBS containing 0.05% tween for 2 hours at room temperature. PNAG localization was then determined by treating the membrane with a PNAG detection protein previously described, then visualized with Opti-4CN.

Densitometric analysis of the spots was performed using Fiji (ImageJ), with pixel densities converted to relative gray values (GV) for comparison. Each spot was analyzed in technical replicate, and error bars represent the variance in spot pixel density among replicates. Two-way ANOVA analysis were performed between DspB(+) and DspB(-) samples. Bar graphs of relative values were plotted in prism GraphPad.

References

1. Jamal, M. *et al.* Bacterial biofilm and associated infections. *J Chin Med Assoc* 81, 7–11 (2018).

2. Marsh, P. D. & Zaura, E. Dental biofilm: ecological interactions in health and disease. *J Clin Periodontol* 44, S12–S22 (2017).

3. Knobloch, J. K.-M., Osten, H. V., Horstkotte, M. A., Rohde, H. & Mack, D. Minimal attachment killing (MAK): a versatile method for susceptibility testing of attached biofilm-positive and -negative Staphylococcus epidermidis. *Med Microbiol Immun* 191, 107–14 (2002).

4. Matthysse, A. G., Thomas, D. L. & White, A. R. Mechanism of cellulose synthesis in Agrobacterium tumefaciens. *J Bacteriol* 177, 1076–81 (1995).

5. Peng, L., Kawagoe, Y., Hogan, P. & Delmer, D. Sitosterol-β-glucoside as Primer for Cellulose Synthesis in Plants. *Science* 295, 147–150 (2002).

6. Wear, S. S., Hunt, B. A., Clarke, B. R. & Whitfield, C. Analysis of the Topology and Active-Site Residues of WbbF, a Putative O-Polysaccharide Synthase from Salmonella enterica Serovar Borreze. *J. Bacteriol.* 202, (2020).

7. Omadjela, O. *et al.* BcsA and BcsB form the catalytically active core of bacterial cellulose synthase sufficient for in vitro cellulose synthesis. *Proc. Natl. Acad. Sci.* 110, 17856–17861 (2013).

8. Hubbard, C., McNamara, J. T., Azumaya, C., Patel, M. S. & Zimmer, J. The Hyaluronan Synthase Catalyzes the Synthesis and Membrane Translocation of Hyaluronan. *J. Mol. Biol.* 418, 21–31 (2012).

9. Vo, L. H. *et al.* Mapping protein–exopolysaccharide binding interaction in Staphylococcus epidermidis biofilms by live cell proximity labeling. *bioRxiv* 2023.08.29.555326 (2023) doi:10.1101/2023.08.29.555326.

10. Turnbull, L. *et al.* Explosive cell lysis as a mechanism for the biogenesis of bacterial membrane vesicles and biofilms. *Nat. Commun.* 7, 11220 (2016).

11. Maloney, F. P. *et al.* Structure, substrate recognition and initiation of hyaluronan synthase. *Nature* 604, 195–201 (2022).

12. Atkin, K. E., MacDonald, S. J., Brentnall, A. S., Potts, J. R. & Thomas, G. H. A different path: Revealing the function of staphylococcal proteins in biofilm formation. *FEBS Lett.* 588, 1869–1872 (2014).

13. Joyce, J. G. *et al.* Isolation, structural characterization, and immunological evaluation of a high-molecular-weight exopolysaccharide from Staphylococcus aureus. *Carbohyd Res* 338, 903–922 (2003).

Chapter 4: Unveiling PNAG dynamics in bacterial biofilms through microfluidics and fluorescence microscopy

Contributing of other authors:

Sureshee Liyanaarachchi for generating hydrolase-fluorescent protein conjugates and various wt hydrolase enzymes. Luan Vo for providing DspB wt for PNAG dispersal. Mark Lecates for providing guidance and expertise at the Fab Lab.

4.1 Introduction

Bacterial biofilm cultivation methods have evolved significantly, encompassing techniques ranging from microtiter plate assays to microcolony biofilm assays on agar plates.[1] Although these static systems are inexpensive and require minimal equipment, they fail to accurately model the dynamic conditions inherent to biofilm formation. Alternatively, flow-based platforms such as flow cells and microfluidic devices more closely emulate the native growth environment by introducing shear forces, constant nutrient supply, and waste removal.[2] A major limitation of conventional flow cells is the reliance on random bacterial adhesion within the growth chamber, introducing experimental variability. However, a recent study addressed this limitation by employing a dedicated seeding chamber adjacent to growth chamber enabling controlled cell seeding and reliable biofilm cultivation.[3] This improvement permits precise differentiation of internal and peripheral biofilm zones, thereby yielding spatial information critical for downstream analysis. One limitation of this design, however, is that the shallow growth chamber depth limits biofilm growth to two dimensions, which may not as accurately reflect the biomolecule distributions observed in native three-dimensional biofilm environments. The present work adapts this seeding approach to enable enhanced visualization of exopolysaccharide (EPS) distributions within bacterial biofilms using microfluidic flow devices with increased growth chamber depth.

Historically, EPS visualization included the use of lectin-based probes such as wheat germ agglutinin (WGA) for detection of N-acetylglucosamine (GlcNAc), Concanavalin A (ConA) for detection of mannose/glucose (Man/Glc), and griffonia simplicifolia lectin (GSL) for galactose (Gal) detection.[4,5] However, these lectins are often non-specific for EPS and bind to other glycans containing similar carbohydrate residues.[6] Small molecule fluorescent dyes such as Calcofluor

white, which binds cellulose and other β-glucans, and Congo red, which labels amyloids and β-linked polysaccharides, are similarly limited by non-specific interactions.[7]

An emerging strategy for developing EPS-specific probes involves mutating the catalytic residue of glycosidases, thereby preserving substrate binding while abolishing hydrolytic activity. For example, DspB a PNAG specific hydrolase, was inactivated via E184A mutation allowing targeted PNAG recognition in *S. epidermidis* and *E. coli* when fused with green fluorescent protein.[6] However, these imaging studies are still limited as they require stochastic attachment of the bacterial cells to a surface to enable imaging, limiting the reproducibility of these studies.

The combination of EPS specific probes with a microfluidic platform for biofilm growth aims to unveil the distributions of these exopolysaccharides within bacterial biofilms, provide novel insight on biofilm structure, and lead to new strategies for biofilm disruption.

4.2 Results

4.2.1 Microfluidic flow cells for three-dimensional biofilm growth

Microfluidic devices function as miniaturized analogs of traditional flow cells, possessing lower internal volumes and thereby reducing the consumption of media and reagents. Conventional flow cells typically use a single inlet for both media flow and cell introduction, which results in random bacterial adhesion to the surface of the flow cell and thus, significant variability between experiments (Fig 4.1A). In an attempt to address this, Jintao Liu and co-workers introduced an additional seeding chamber into the design of their microfluidic devices, providing a dedicated channel for cell introduction and enabling precise spatial placement of bacteria in the growth chamber (Fig 4.1B).[3,8] We further modified this design by increasing flow cell depth to enable the capacity for increased three-dimensional biofilm growth.

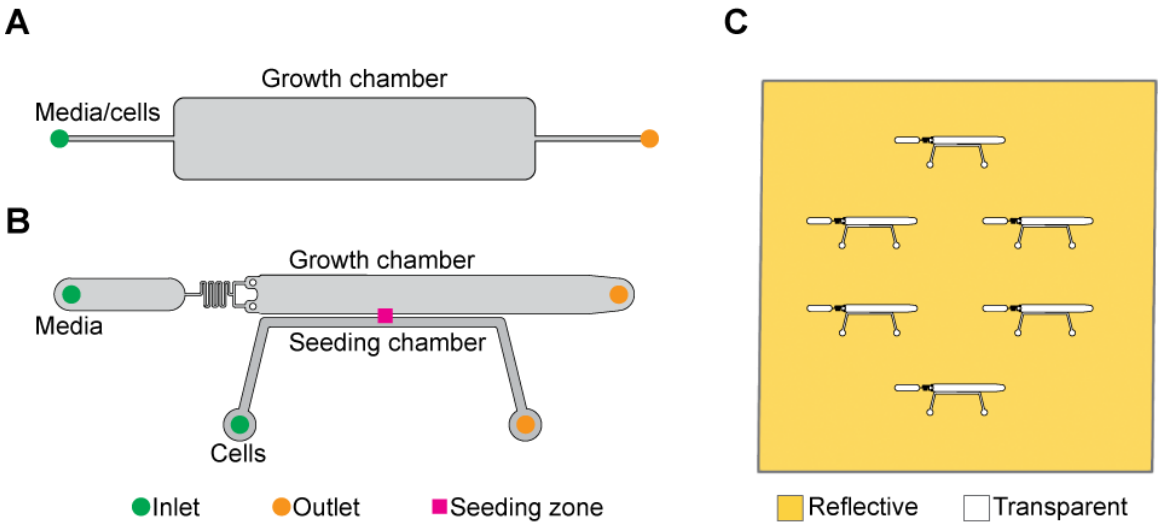

Figure 4.1: Design of microfluidic device. A) Conventional flow-device with single inlet and outlet. B) Improved design with the addition of seeding chamber, allowing for specific cell seeding. C) Photomask containing microfluidic device design. Yellow represents chromium plating and reflects incoming light, while the design is etched (white) to allow passing of UV light.

The microfluidic device design comprises two primary aspects: two-dimensional planar layout and three-dimensional height. The overall architecture was designed in AutoCAD and adapted from the original report with expanded dimensions to fit a standard glass slide foundation.[3] Inlet and outlet ports were elongated to reduce mechanical stress on tubing interfaces during operation. Device patterns were transferred onto a chromium-coated glass substrate to create the photomask (Fig 4.1C).

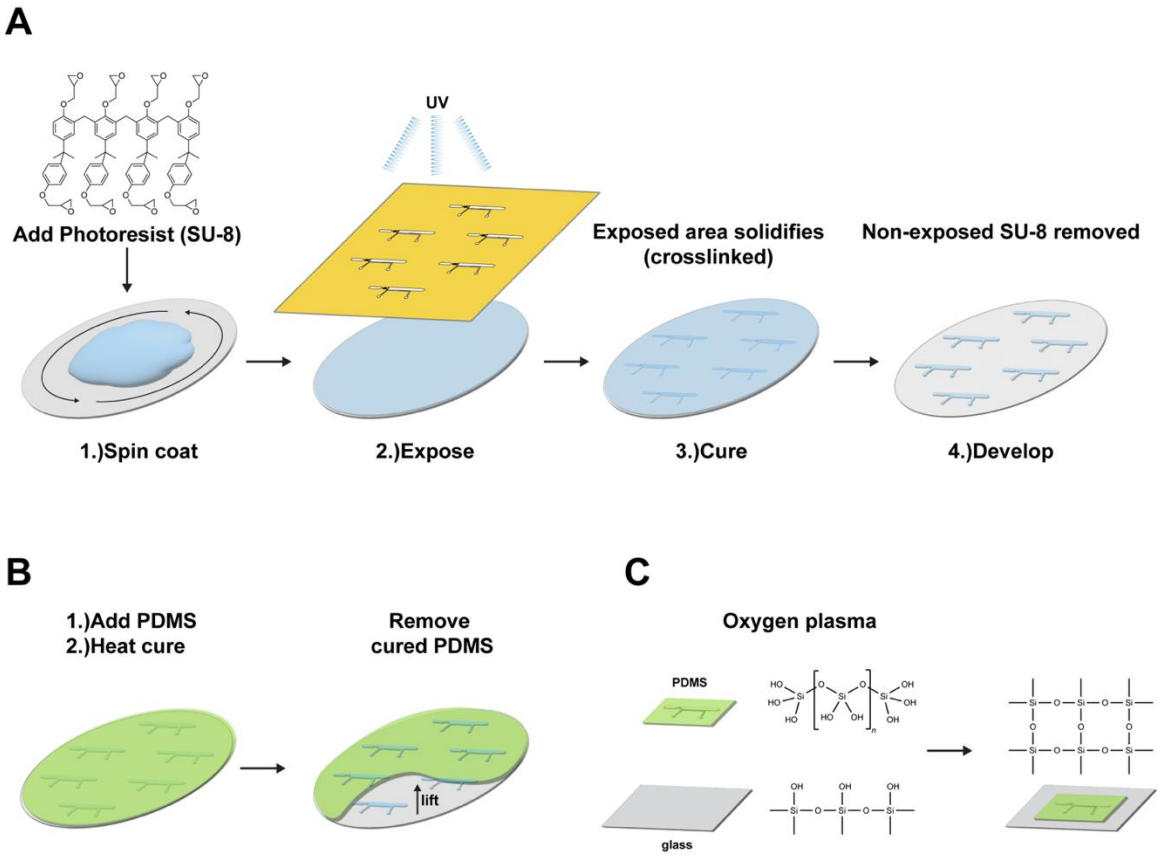

Figure 4.2: Microfluidic device fabrication. A) Master mold is created through spin-coating photoresist (SU-8) onto wafer, followed by exposing UV through photomask. The wafer is then rinsed with solvent to remove non-crosslinked SU-8, leaving behind the microfluidic design. B) PDMS is added onto the master and heat cured at 60ºC, before removal and trimming. C) Trimmed cells are plasma treated, oxidizing the surface, and ready for glass adherence yielding the completed device.

After the photomask was created, a mold (often referred to as the master) was fabricated using photolithography. A viscous photoresist (SU-8) was spin-coated onto a wafer to create the

negative mold, where the final device height depended on the spin-coating speed (Fig 4.2A). While previous versions featured a 6 μm channel height suitable for imaging biofilm layers ~3-6 cells thick, our design increased the height to ~300 μm, verified by profilometry, thus supporting three-dimensional biofilm growth and analysis. The resulting growth chamber measured 23 mm in length, 2.4 mm in width, and 0.1–0.3 mm in height, yielding an internal volume of ~15 μL.

Individual microfluidic cells are cast from this mold using polydimethylsiloxane (PDMS), a non-toxic transparent silicone polymer. The PDMS alongside a curing agent were combined, poured onto the master, and cured at 60 ^{o}C (Fig 4.2B). The cured polymer is then carefully removed and sectioned to size. At this point thin ~1mm scotch tape is placed at the wall that separates the growth and seeding chamber, preventing oxidation by oxygen plasma thus maintaining an accessible entry point for precise bacterial seeding (Fig 4.2C).

4.2.2 Biofilm cultivation conditions in microfluidic device

Common biofilm assays, such as those using microtiter or agar plates, often fail to replicate the dynamic physiological conditions found in natural environments. In contrast, microfluidic devices enable culturing, labeling, and real-time observation of biofilms *in situ*, facilitating a more authentic representation of biofilm structure. Using this approach, we sought to compare the PNAG exopolysaccharide distributions within model Gram-negative and Gram-positive bacterial biofilms. We selected *E. coli* MG1655Δ*csrA* and *S. epidermidis* RP62A strains as model Gram-negative and Gram-positive biofilm forming bacteria, respectively, as both display well documented PNAG production.[9,10]

Traditionally, laboratory strains of *E. coli* have demonstrated a diminished capacity to form robust biofilms which has led many researchers to utilize the *E. coli* MG1655ΔcsrA strain for studies of PNAG biosynthesis due to its enhanced biofilm phenotype.[11,12] The csrA gene encodes

for a global transcriptional regulatory protein, CsrA (carbon storage regulator), which represses several biofilm inducing pathways decreased motility and exopolysaccharide biosynthesis.[13,14] Collectively, the loss of these regulatory functions in the ΔcsrA mutant resulting in high exopolysaccharide production and reduced motility has led to its wide adoption in *E. coli* biofilm research.

S. epidermidis RP62A was originally isolated in the early 1980s during an outbreak of intravascular catheter-associated sepsis. Christensen and colleagues first described the strain's robust ability to adhere to smooth plastic surfaces.[15] Subsequently, complete genome sequencing of the RP62A strain confirmed the presence of the ica operon essential for PNAG biosynthesis. This genomic characterization provided a high-resolution map for transcriptomics (RNA-Seq) and proteomics, facilitating more precise genetic knockouts and regulatory studies compared to uncharacterized wild-type strains.[16,17]

Distinct cultivation protocols were optimized for each bacterial species to yield characteristic biofilm morphologies within the microfluidic device. For *S. epidermidis*, starter cultures were grown in Tryptic Soy Broth (TSB) and incubated at 37°C with continuous agitation at 100 rpm overnight. To prepare the inoculum for the microfluidic device, these cultures were concentrated to 1/10 of their original volume. Following seeding, the biofilms were matured at ambient temperature for 18–20 hours under a constant flow rate of 15 chamber volumes per hour.

The *E. coli* protocol utilized Luria-Bertani (LB) broth and a two-stage initial growth phase: an initial 5-hour incubation at 37°C with high-speed shaking (200 rpm), followed by a static overnight incubation at 37°C. The resulting cultures were concentrated ten-fold prior to seeding the microfluidic channels. Maturation of the biofilms were established after 18–20 hours at ambient temperature with a continuous flow of 15 chamber volumes per hour. All experimental

stages, including fluorescent labeling, were performed using TSB to maintain a consistent nutrient environment.

After the biofilms had matured, we next sought to visualize the distribution of PNAG within the biofilms and subsequently monitor the disruption of the biofilm upon treatment with a PNAG specific hydrolase enzyme DspB. For this the biofilms were subjected to a three-phase labeling, washing, and disruption protocol (Fig 4.3). In the initial labeling phase, PNAG within the biofilms was visualized by introducing growth media containing an appropriate concentration of a catalytically inactive $DspB_{E184A}$ mutant containing a C-terminal enhanced green fluorescent protein tag (*in*DspB-eGFP). This same protein design has previously been used shown to be highly specific for labeling PNAG in both *S. epidermidis* and *E. coli* biofilms.[6] The labeling was allowed to proceed under flow for 90 min, during which the fluorescence intensity within the biofilm was monitored at regular intervals. The labeling was subsequently followed by a washing phase to evaluate the retention of fluorescent probes within the biofilm matrix under continuous flow conditions. Finally, the labeled biofilms were treated with either catalytically active DspB or an inactive $DspB_{E184Q}$ mutant to observe structural and morphological changes in the biofilm

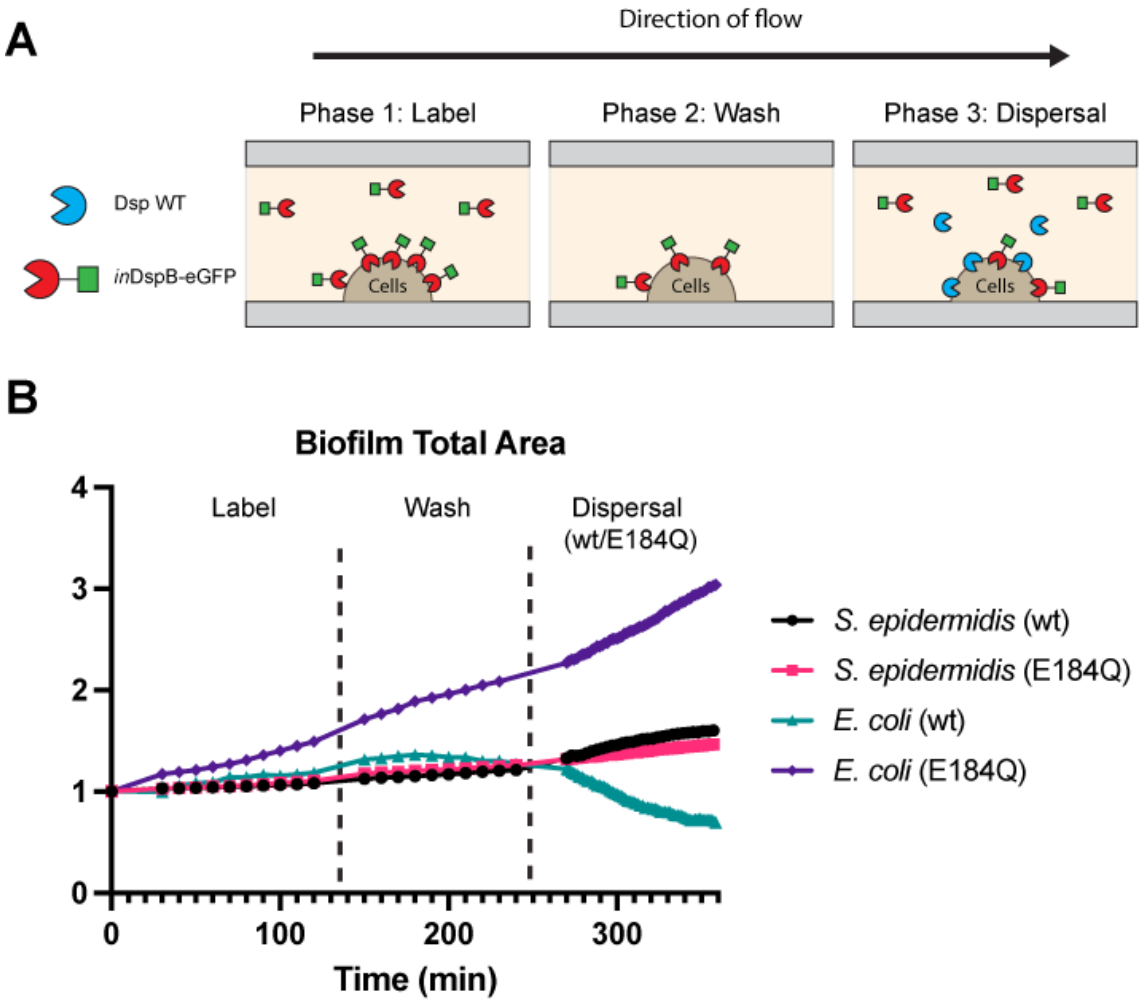

Figure 4.3: Total biofilm area. Biofilm area progression was monitored across three stages: labeling, washing, and dispersal. A) Schematic of the 3 phases. All experimental phases were conducted in growth media supplemented with the appropriate proteins. B) Each phase lasted approximately 90 minutes, with images captured at 10-minute intervals during labeling and washing, and at a higher frequency during the dispersal phase. The 30-minute gaps between phases account for the void volume during media exchanges. The total biofilm area was quantified using Fiji (ImageJ) by defining a region of interest around the biofilm and measuring the total gray value (GV) from brightfield images over time. By adjusting image thresholds, GVs were isolated for the cells while excluding background signal.

architecture upon the hydrolysis of PNAG. In addition to the catalytically active DspB or $DspB_{E184Q}$, *in*DspB-eGFP was also included in the growth media during this disruption phase to aid in monitoring PNAG distribution during disruption phase. For each phase of this labeling protocol, we continuously monitored the biofilms for 90 min. Time-laps images of the biofilm

were recorded on 10 min intervals during the labeling and washing stages, while the frequency of image acquisition was increased to every 1.5 min (for *E. coli*) or 3 min (for *S. epidermidis*) during the disruption phase. This accelerated acquisition rate was necessary to capture the rapid architectural shifts occurring during the dispersal process.

4.2.3 Effects of PNAG hydrolysis in *S. epidermidis* biofilms

To track the morphological shifts across each of the three growth phases, we measured the biofilm cross-sectional area. The biofilm cross-sectional area was quantified in Fiji (ImageJ) by defining a region of interest around the biofilm and applying a pixel density threshold to isolate gray values of the cells from the background. Perhaps unsurprisingly, we observed that the cross-sectional area of *S. epidermidis* biofilms expanded at a constant rate through both the labeling and washing stages (Fig 4.3B and Fig 4.4A). The biofilm areas were then compared before and after 90 min of treatment with the PNAG hydrolase DspB, or inactive $DspB_{E184Q}$ during the disruption phase (Fig 4.4B. As expected, we also observed no phenotypic changes when the biofilms were treated with inactive $DspB_{E184Q}$ during the disruption phase and the biofilm continued to grow at a near constant rate (Fig 4.4C). Previous publications have shown that treatment of *S. epidermidis* RP62A biofilms with DspB is sufficient to affect significant biofilm disruption. [18] Thus it was a surprise that we observed no loss in biofilm cross-sectional area for *S. epidermidis* biofilms treated with DspB. Instead, we observed an initial rapid increase in the biofilm cross-sectional area, despite visible cell shedding observed at the periphery of the biofilm, which eventually slowed to expand at the same rate as observed for the biofilm treated with $DspB_{E184Q}$ (Fig 4.4C and E). Throughout this disruption with DspB, we observed visible evidence of cells shedding from the surface of the biofilm, which was not observed when treated with $DspB_{E184Q}$, yet the core of the *S. epidermidis* biofilm remained intact and expanded in cross-sectional area upon prolonged DspB

treatment. These observations suggest that while PNAG hydrolysis effectively removes surface-associated cells, additional adhesion factors likely contribute to the overall integrity of the *S. epidermidis* biofilm core. This is perhaps unsurprising as both proteins, like Aap, Embp1, and BHP, and extracellular nucleic acids, have both been shown to contribute to biofilm cohesion in *S. epidermidis* biofilms.[19–22]

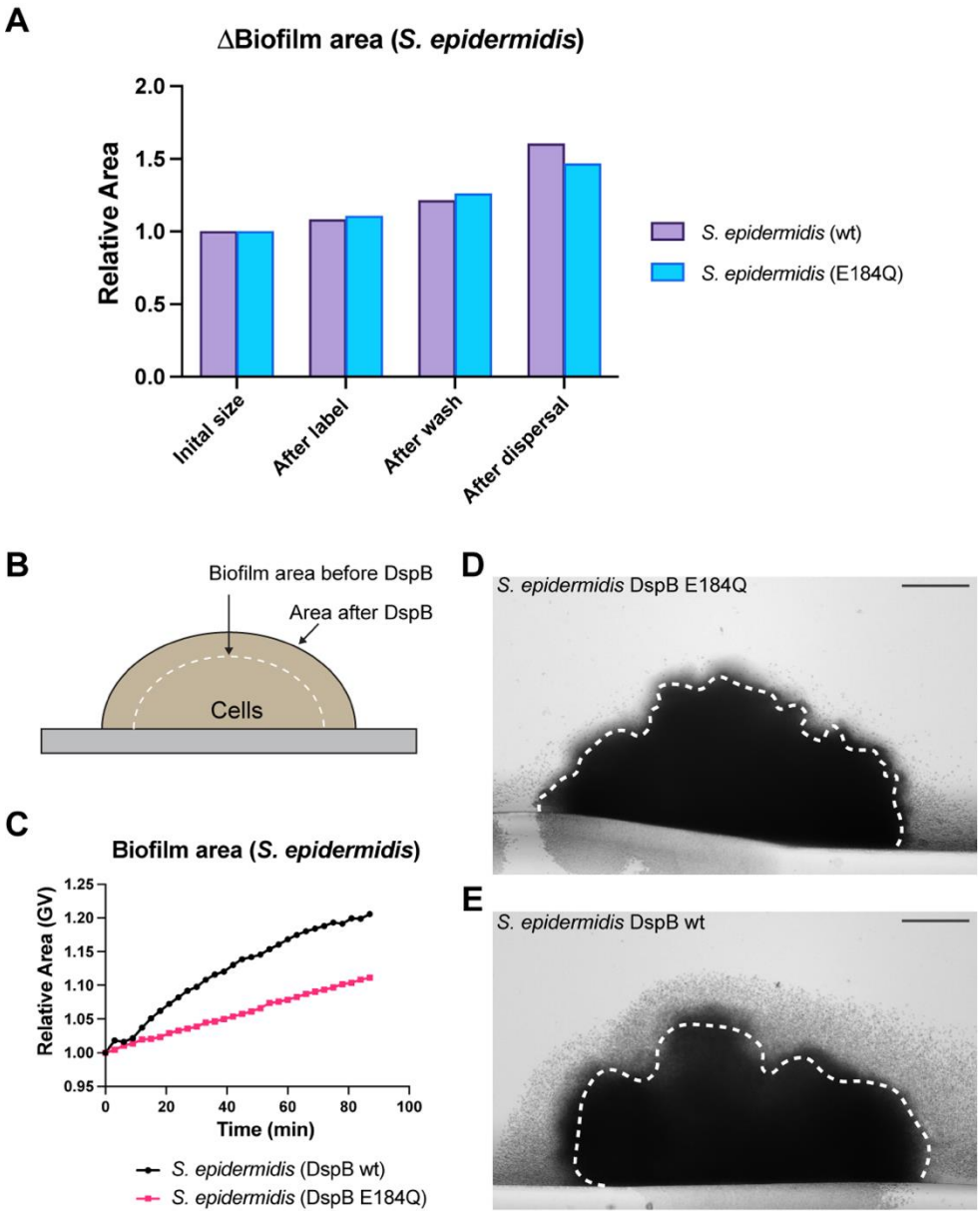

Figure 4.4: Effects of S. epidermidis biofilm area from PNAG hydrolysis by DspB. A) Total area of *S. epidermidis* biofilms after each phase; Label, wash, and DspB (wt/E184Q) treatment. Biofilm area was quantified in Fiji based on GV mentioned previously. B) White dotted line represents biofilm area prior to DspB(wt/E184Q) addition. C) Biofilm area over prolonged DspB (wt/E184) treatment. D) Biofilm sample treated with $DspB_{E184Q}$ exhibited no observable dispersal. E) Biofilm sample treated with DspB displayed peripheral cell shedding, but no decrease in overall size. Scale bar 100 µm.

4.2.4 PNAG distribution in *S. epidermidis* biofilms

To better visualize the PNAG distribution within the biofilm architecture, the *S. epidermidis* biofilms were labeled with growth media containing 0.5 µM of *in*DspB-eGFP under continuous flow for a total of 90 min. As seen in Fig 4.5B, the fluorescent signal initially increases at the biofilm perimeter before diffusing deeper into the biofilm core. However, even after prolonged exposure, the *S. epidermidis* biofilms exhibited the highest PNAG labelling primarily at the periphery (Fig 4.5), with significantly lower concentrations in the center. This localization

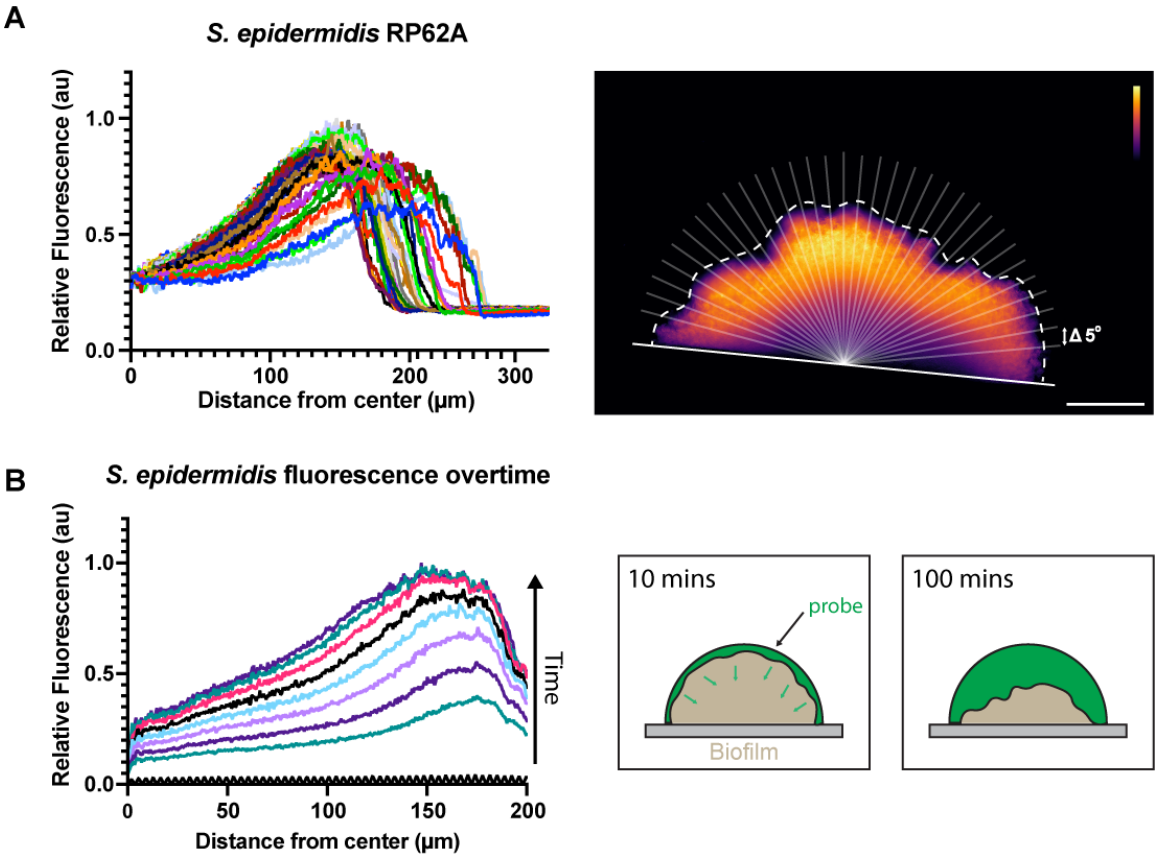

Figure 4.5: Fluorescent signal profiles of S. epidermidis biofilms after labeling with *in*DspB-eGFP (0.5 µM) for 90 mins under continuous flow. A) The center of the biofilm base was established by identifying the midpoint of a line drawn along the attachment surface. Radial lines were then extended through the biofilm at 5° intervals from this center point, with fluorescent signal intensity plotted along each path to map the protein distribution. Biofilm perimeter is highlighted by white dotted line. B) High concentrations of *in*DspB-eGFP localized at the peripheral of the biofilm structure during labelling phase. Scale bar 100 µm.

correlates with the observed dispersal pattern, in which cell shedding was restricted to the outer edges while the primary biofilm core remained intact. These findings suggest that PNAG may serve as a primary cohesive factor within the expansion zone of *S. epidermidis* biofilms, but that other adhesive factors, which may include protein and nucleic acids contribute to cohesion within the biofilm core.

Previous reports have characterized several *S. epidermidis* strains as either exopolysaccharide-dependent (1457) or protein-dependent (5179-R1 and 1585v).[23] Biofilms formed via protein processing, involving either extracellular matrix-binding protein (Embp1) or accumulation-associated protein (Aap), demonstrated dispersal only upon proteinase K treatment and remained resistant to DspB.[23] Additionally, confocal microscopy reveals that exopolysaccharide-dependent biofilms possess PNAG localized at the intercellular interface, a feature absent in protein-dependent biofilms.

4.2.5 Effects of PNAG hydrolysis in *E. coli* biofilms

A similar approach was applied to study PNAG contributions to *E. coli* biofilms. The addition of $DspB_{E184Q}$ to mature *E. coli* biofilms resulted in no phenotypic changes to the biofilm architecture, and the biofilm area grew consistently throughout the treatment (Fig 4.6B). Conversely, when *E. coli* biofilms were treated with active DspB, > 50% of the initial mass was lost within the 90 min dispersal phase (Fig 4.6B). The final frame of the DspB treatment revealed a loss of cells from both the exterior and interior of the structure, accompanied by a decrease in overall biofilm density. This result is consistent with the role of exopolysaccharide hydrolysis in other Gram-negative bacterial biofilms. For example, the use of endogenous endoglycosidase PslG effectively cleared *Pseudomonas aeruginosa* biofilms under flow conditions. In those studies, time-lapse imaging demonstrated a uniform loss of biomass throughout the entire biofilm

structure.[24] These results suggest that PNAG is a critical component for structural integrity within *E. coli* biofilms lacking the crsA transcriptional regulator. However, hydrolyzing the exopolysaccharide alone does not result in complete degradation, as roughly half of the biomass remained compared to pre-treatment levels (Fig 4.6A). Although PNAG hydrolysis disperses a large portion of the biomass, it does not achieve complete dissolution, as the center remains partially attached. These findings demonstrate the importance of PNAG while highlighting the heterogeneity of the biofilm matrix. Since the matrix consists of various materials, such as extracellular DNA, proteins, and exopolysaccharides, the degradation of a single component may not be sufficient for total dispersal.

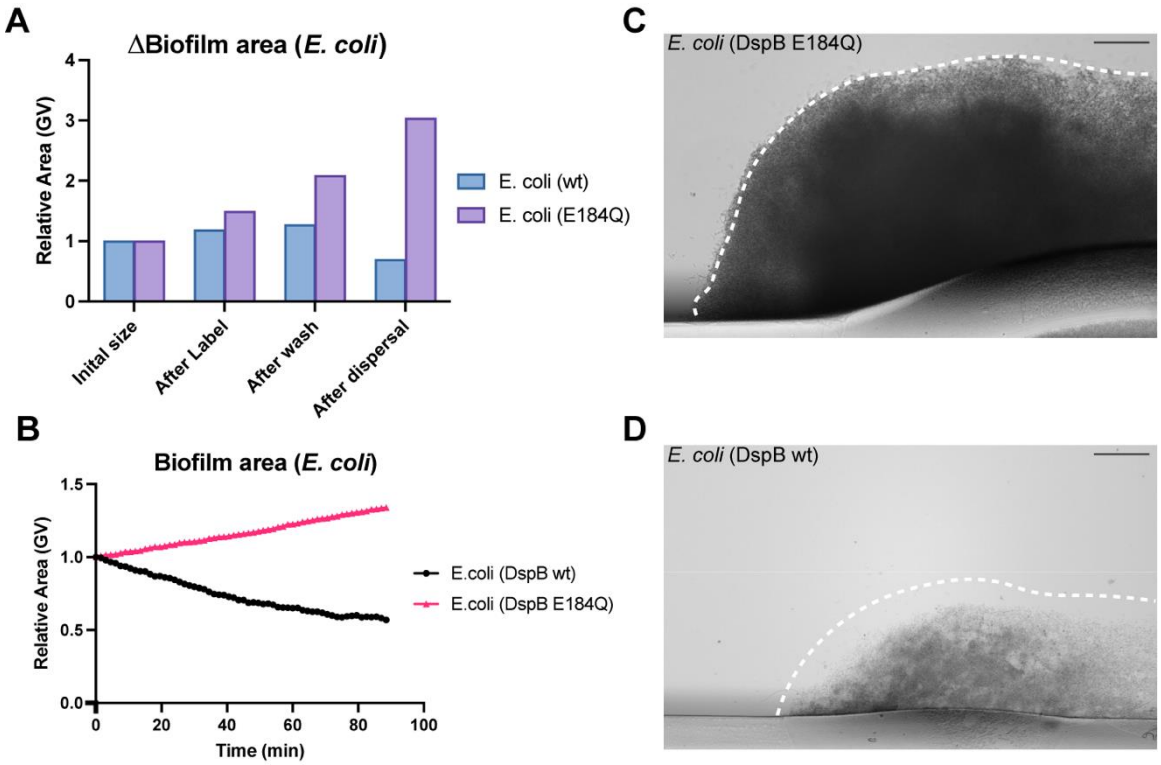

Figure 4.6: Effects of E. coli biofilm area from PNAG hydrolysis by DspB. A) Total area of *E.coli* biofilms after each phase; Label, wash, and DspB (wt/E184Q) treatment. B) Biofilm areas quantified by GV over the course of Dsp (wt/E184Q) treatment. Images display the final frame of the biofilm post-treatment, with the initial biofilm size indicated by a white dotted line. C) *E. coli* biofilm treated with inactive $DspB_{E184Q}$ displayed no observable dispersal. D) Biofilm treated with DspB exhibited significant dispersal of both internal and external regions. Scale bar 100 µm.

4.2.6 PNAG distribution in *E. coli* biofilms

For the labelling of *E. coli* biofilms, the fluorescent probe concentration was decreased to 0.2 µM of inDsp-eGFP. This lower probe concentration was selected to minimize background fluorescence. The probe localized primarily to the center of the biofilm structure (Fig 4.7), which is consistent with our dispersal observations. These findings highlight that *E. coli* biofilms lose significant biomass upon PNAG hydrolysis, underscoring the critical role of PNAG in maintaining their structural architecture.

Additionally, *E. coli* biofilms exhibited distinct regions of high PNAG concentration, characterized by punctate labeling following prolonged fluorescent probe exposure (Fig 4.7A).

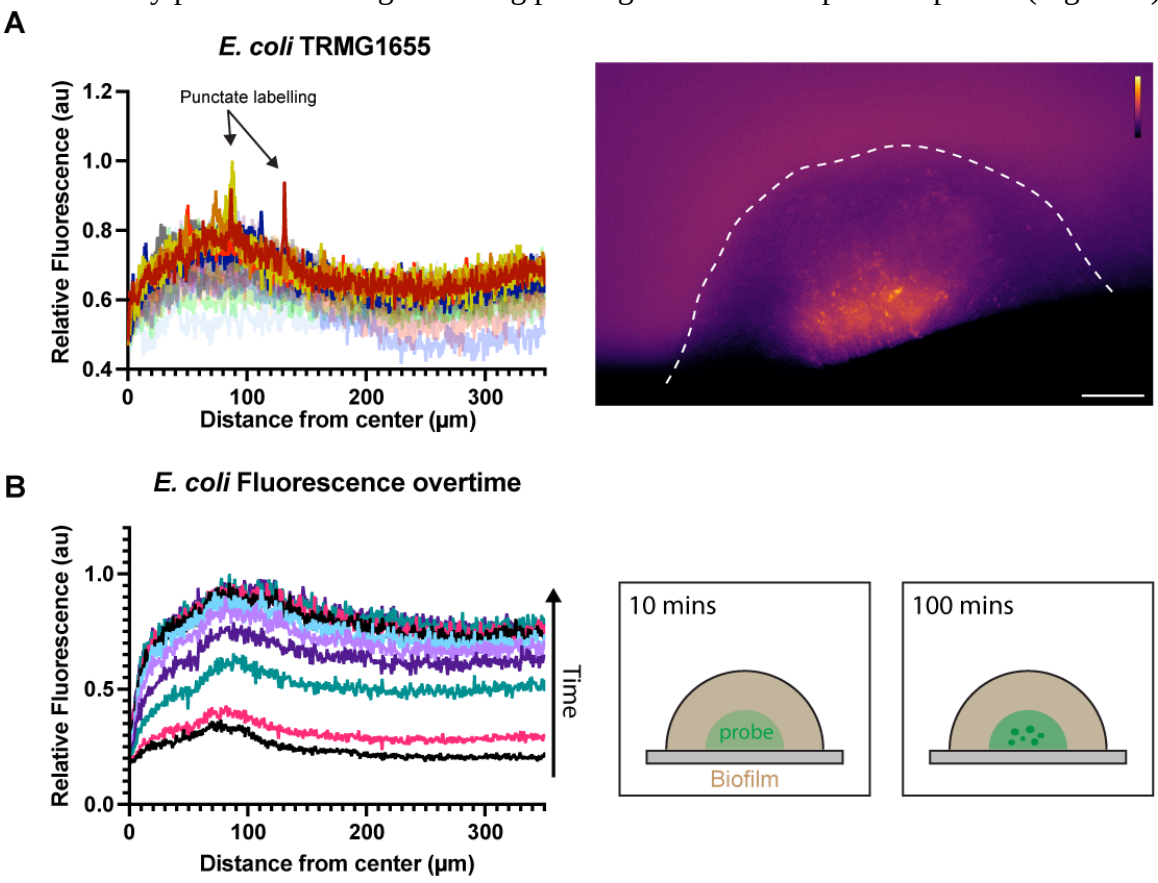

Figure 4.7: Fluorescent signal profiles of E. coli biofilms after labeling with *in*DspB-eGFP (0.2-0.5 µM) for 90mins under continuous flow. Biofilm perimeter is highlighted by white dotted line. A) Larger biofilm sample possessed punctate labeling near center of the structure. B) Smaller, less developed sample retained labeling at the center with no punctate labeling. Scale

4.2.7 Differences in PNAG distribution in *S. epidermidis* vs *E. coli* biofilms

Distinct differences in localization are evident when comparing the PNAG distribution of *S. epidermidis* and *E. coli* biofilms. In *S. epidermidis*, the PNAG concentration is highest in the peripheral zones (Fig 4.8). This localization correlates with the observed dispersal pattern, in which cell shedding was restricted to the outer edges while the primary biofilm body remained intact. These findings suggest that alternative cohesion factors maintain the structural integrity of the *S. epidermidis* core. Previously, Luan Vo from our lab identified the cell surface protein elastin-binding protein (EbpS) as a mediator of cell-matrix interactions in a PNAG-dependent manner, whereas the known *S. epidermidis* biofilm protein Aap does not interact directly with PNAG.[25] These findings, combined with the dispersal patterns observed on our microfluidic platform, highlight the heterogeneity of cohesion factors within a single biofilm structure. The observation that biofilm cross-sectional area expands upon hydrolysis of PNAG suggests that PNAG may play a central role in mediating the compaction and cell–cell interactions within the biofilm. Thus, blocking the interaction of PNAG with other cell surface components like EbpS may prove a viable strategy to prevent efficient biofilm formation in *S. epidermidis*. However, combinations of PNAG hydrolase enzymes with proteins capable of degrading other biofilm protein and nucleic acid components may be required for effective *S. epidermidis* biofilm disruption.

Conversely, *E. coli* biofilm labeling demonstrated that PNAG is predominantly localized within the core. This is consistent with dispersal observations in which *E. coli* biofilms undergo significant biomass loss throughout the biofilm structure and not simply from the periphery. While it was already known that the *pga* operon is required for *E. coli* biofilm formation, the spatial distribution of this polysaccharides throughout the structure had not been previously characterized.[10] The Liu laboratory has performed spatial transcriptomics on *E. coli* MG1655

biofilms by fluorescently tagging cells during biofilm growth, and sorting the cells based on their localization within the biofilm prior to performing RNA-seq.[8] In this study, they were able to identify that some genes that modulate biofilm formation, such as those encoding diguanylate cyclase (DGC) and phosphodiesterase enzymes (PDE) responsible for the production and breakdown of c-di-GMP, differed in their expression profiles in different regions within the biofilm.[8] Their results showed elevated levels of transcripts for diguanylate cyclase enzymes at the *E. coli* biofilm center, which correlates with our observations of concentrated PNAG production in the same region. Moreover, our own analysis of this spatially resolved transcriptomics data suggests that expression of the *pgaABCD* operon responsible for PNAG biosynthesis is also highest in the middle regions of the biofilm.

Beyond the spatial distribution of PNAG, a notable difference in fluorescent intensity for PNAG labeling was also observed between the two species. *S. epidermidis* biofilms exhibited higher probe binding than those of E. *coli*, suggesting increased PNAG biosynthesis in this Gram-

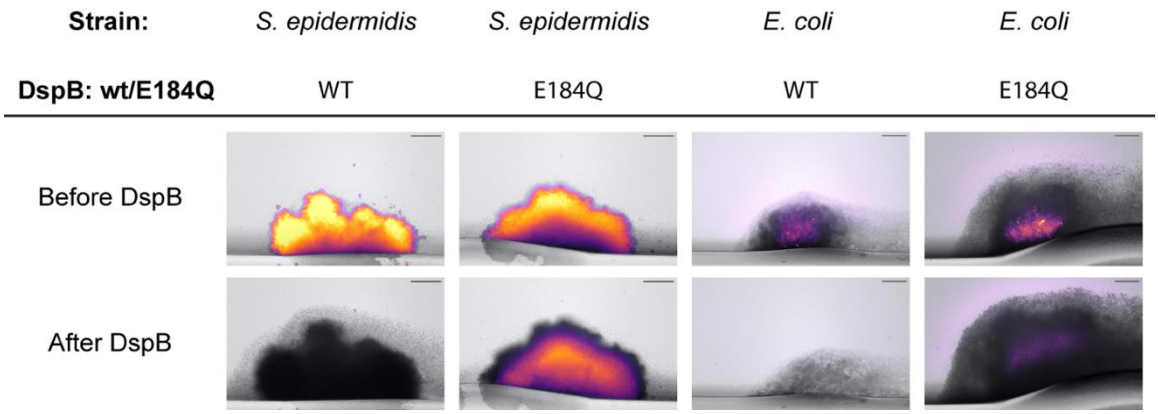

Figure 4.8: Fluorescent signal changes overtime following DspB treatment. Comparison of overlay images from the final frame of the labeling phase (top row) vs the final frame of the dispersal phase (bottom row). Both *S. epidermidis* and *E. coli* biofilms saw a loss in fluorescent signal after DspB treatment. *S. epidermidis* biofilm treated with $DspB_{E184Q}$ shows a lack of labeling at the perimeter of the biofilm and higher labeling near the center while *E.coli* biofilm treated with $DspB_{E184Q}$ exhibited a lower fluorescence signal near the center at significantly lower signal intensity. Scale bar 100 µm.

positive bacteria. Furthermore, *S. epidermidis* biofilms displayed a higher overall cell density than *E. coli* biofilms. This density was evident during the labeling phase, where the fluorescent probe required significantly more time to penetrate the *S. epidermidis* biofilm structure, as documented in the time-lapse data (Appendix). These density variations also impacted probe retention. *E. coli* biofilms lost all observable fluorescence after only 20 minutes of washing, whereas *S. epidermidis* biofilms retained the probe until the onset of the dispersal phase. Since binding between the inDspB-eGFP probe and PNAG and its retention in biofilms is at least partially dependent on the effective PNAG concentration within the biofilms, we can conclude that S. epidermidis biofilms produce significantly greater PNAG than similar sized E. coli biofilms. Although it is important to note that the *E. coli* MG1655Δ*csrA* strain used in these studies is a mutant derived from the laboratory *E. coli* K12 strain MG1655 and thus may not produce PNAG to the same extent as other *E. coli* clinical isolate strains.

During the disruption of *S. epidermidis* biofilms with DspB, the absence of fluorescence within the DspB treated biofilms demonstrates that PNAG has been effectively hydrolyzed throughout the biofilm and that little to no new deposition of PNAG is occurring, despite the observation that the biofilm structure remains largely intact and expands in cross-sectional area during DspB treatment. Interestingly, upon treatment of these same *S. epidermidis* biofilms with $DspB_{E184Q}$ the PNAG labeling around the periphery of the biofilm observed during the initial labeling phase shifted more towards the interior of the biofilm (Fig 4.8). This phenomenon can likely be attributed to the competitive binding between the higher concentration of $DspB_{E184Q}$ (2 μM) and the fluorescent probe (0.5 μM). However, due to the higher density of cells within the *S. epidermidis* biofilm, the rate of rebinding of the larger inDspB-eGFP fluorescent probes likely exceeds the rate of diffusion leading to its retention. Whereas the rate of diffusion of the smaller

unlabeled inactive $DspB_{E184Q}$ protein prevented its similar retention. Thus, this microfluidic labeling approach may provide a mechanism to measure diffusional dynamics within biofilms.

Results for the *E. coli* biofilms followed a similar pattern where samples treated with DspB showed a complete loss of fluorescence signal accompanied by significant dispersal. While biofilms treated with the inactive $DspB_{E184Q}$ mutant exhibited a decrease in signal intensity, likely due to competitive binding between the probe and the mutant enzyme, the overall architecture remained intact and expanded during this period. Collectively, these fluorescence labelling patterns suggest that PNAG mediates the cell-matrix interactions of *S. epidermidis* biofilms primarily at the periphery and does not play a major role in central cohesion. In contrast, PNAG is required for initial cell–cell cohesion in the core of *E. coli* biofilm architecture, serving as a primary cohesion factor for the overall stability of the structure.

4.3 Conclusion

Bacterial biofilms are commonly defined as three-dimensional microbial communities encased within a self-secreted extracellular matrix composed of various components, including EPS and filamentous proteins that contribute structurally.[9,26–28] These macroscopic communities exhibit stratification, creating microenvironments with gradients in oxygen, pH, and nutrients, which influence cellular metabolism and behavior.[29–32] Given these spatial heterogeneities, it is critical to study biofilms *in situ*, without disrupting their architecture, to obtain biologically relevant insights. Understanding the spatial distribution of EPS within biofilms is particularly important, as these polymers are fundamental to biofilm formation and represent potential targets for biofilm inhibition or dispersal strategies.

In this work, we report the cultivation of PNAG-producing bacterial biofilms in microfluidic devices to compare the spatial distribution of the polysaccharide between the Gram-

negative *E. coli* MG1655ΔcsrA and the Gram-positive *S. epidermidis* RP62A.[9,10] Through this approach combined with fluorescence microscopy, we were able to identify the differences in PNAG distribution in different species and its effects on overall biofilm structure when degraded. It is well known that PNAG serves as an important matrix component during biofilm formation and contributes to the three dimensional architecture.[10,33,34] However, the comparative role of PNAG across different bacterial strains has not been thoroughly investigated. Our study suggests that while both species produce PNAG in mature biofilms, the specific role of the polysaccharide differs. *S. epidermidis* biofilms appear to utilize PNAG primarily in the peripheral or growing zones. This suggests that only the more metabolically active cells produce PNAG, likely using the adhesin to anchor themselves to the primary structure as the biofilm expands. Consequently, hydrolyzing these polysaccharides causes the release of peripheral cells while the overall structure remains stable (Fig 4.8). The opposite is true for *E. coli* biofilms, where the polysaccharides concentrate at the center of the structure, corresponding to the region where the translation of diguanylate cyclase enzymes is highest.[8] In this case, PNAG degradation results in significant dissolution of the entire biofilm structure (Fig 4.8).

Although the present study captured the progressive effects of PNAG hydrolysis in *S. epidermidis* and *E. coli* biofilms, the roles of additional matrix components in the overall system remain unclear. For example, extracellular DNA (eDNA) is found ubiquitously in bacterial biofilms and serves as a primary component of the matrix.[27,35,36] Earlier studies of *S. epidermidis* biofilms suggested two distinct pathways: the polysaccharide morphotype and the eDNA/protein morphotype.[37,38] However, recent work by Mlynek and colleagues proposed that these biofilm matrices are not mutually exclusive. Instead, the expression of various matrix materials is governed by specific growth conditions.[22] It is possible that matrix composition varies depending on

environmental factors, creating zones in which certain areas of the biofilm utilize a particular component more than others. This would explain our observation of biofilm stability even during the complete degradation of the PNAG polysaccharide. Additionally, interactions between eDNA and polysaccharides have been reported for other strains, such has *Pseudomonas aeruginosa*, which produces a cationic exopolysaccharide (1→4 glycosidic linkages of N-acetylgalactosamine and N-acetylglucosamine) known as Pel.[39] Jennings and coworkers identified interactions between anionic eDNA and cationic Pel that create an interlocking system serving as a primary structural scaffold.[39] A similar interaction may occur within PNAG-producing biofilms, as one study reported the colocalization of eDNA and PNAG in *Staphylococcus aureus* UAMS-1 under confocal microscopy.[40] These previous studies, however, were performed under static conditions in Petri dishes where old and new cells were indistinguishable. In contrast, spatial mapping of both polysaccharides and eDNA would be possible using our microfluidic approach.

This technique can be extended to study the protein-polysaccharide interactions that occur during biofilm formation. Research into the interplay between proteins and polysaccharides is an expanding field, and several reports have demonstrated the importance of these interactions for robust biofilm development. For instance, CdrA is a large, secreted protein from *Pseudomonas aeruginosa* that serves as a "molecular tether" between Psl and Pel exopolysaccharides.[41] Additionally, our lab recently identified that the cell surface protein EbpS interacts with PNAG to facilitate cell-matrix attachment.[25]

Collectively, this microfluidic device serves as a versatile tool for the reproducible cultivation, labeling, and dispersal of bacterial biofilms. We successfully adapted the system's dimensions to accommodate the formation of larger, more complex three-dimensional biofilm structures. Moving forward, our goal is to expand the labeling and dispersal parameters to include

proteins and eDNA, which will allow us to uncover the specific spatial relationships between each of these critical matrix components.

4.4 Experimental Procedures

Bacteria strains and growth conditions:

Gram-positive (*Staphylococcus epidermidis* RP62A) and Gram-negative (*Escherichia coli* MG1655Δ*crsA*) were chosen for the following labeling experiments. These strains have been used previously to study EPS dependent biofilm formation. *S. epidermidis* biofilms were cultured in Tryptic Soy broth, while *E. coli* biofilms were grown in Tris buffered Luria-Bertani broth, pH 7.

S. epidermidis cultures were grown under continuous shaking at 100 rpm at 37. ^{o}C, overnight before harvesting. *E. coli* MG1655Δ*crsA* were grown in LB shaking at 200 rpm for 5 hours before allowing to grow statically overnight at 37 ^{o}C.

Microfluidic cell device, design and manufacture:

Microfluidic design and manufacture were previously described in with small adaptations to the dimensions.[3] Original study described a 6-micrometer depth for thin uniform biofilm formation. The depth of the device described in this study was increased to 300 micrometers to enable larger 3-dimensional biofilm growth. Devices were made using PDMS and 3M scotch tape (0.5-1mm) was used to mask the seeding zone prior to plasma treatment. Oxygen plasma treatment of both glass and device was performed using the March O2 plasma system (200 V for 30 seconds). The tape was quickly removed, and the device and glass were firmly pushed together for 30 secs before finishing on hot plate 97^{o}C for 5 mins.

Device growth, labeling, and dispersal:

The device was first secured to a flat surface using masking tape and growth media was introducing into the seeding chamber at 60 µL/min. Once the chamber and tubing were filled, the

seeding chamber outlet was closed, and the rate was reduced to 20 µL/hr. The media was introduced until the liquid was observed to enter the main growth chamber at the designated seeding zone. At that time the seeding chamber outlet was opened, and media was introduced to both inlets at 20 µL/min until the device was completed filled.

Overnight starter cultures were harvest and resuspended in 1/10x of final growth media and introduced through the seeding chamber at 20 µL/min. Once the seeding chamber was saturated, the seeding outlet was closed while both inlets are continuously flowing at 5-10 µL/min for 2 mins, allowing cells to enter the growth chamber. The seeding chamber outlet was then opened, and buffer was flown through the seeding chamber at 20 µL/min for 20 min or until most cells were removed.

The cells that were introduced to the device were then left to grow at room temperature for 20 hrs before labeling. Biofilms were grown at a flow rate of 250 µL/hr for 300 µm devices and 85 µL/hr for 100 µm devices, equating to roughly 15 chamber volumes per hour.

Biofilms were labeled using a catalytically inactive hydrolase-fluorescent protein conjugates at 0.2-0.5µM and imaged on through the ECHO revolve microscope. The fluorescent probe was flowed in the device via syringe pump until the fluorescent intensity saturates within the biofilm. Dispersal was conducted with the use of active hydrolase enzymes until biofilm fully dissipates or no continued degradation was observed.

References

1. Merritt, J. H., Kadouri, D. E. & O'Toole, G. A. Growing and Analyzing Static Biofilms. *Curr. Protoc. Microbiol.* 00, 1B.1.1-1B.1.17 (2006).

2. Sternberg, C. & Tolker-Nielsen, T. Growing and Analyzing Biofilms in Flow Cells. *Curr. Protoc. Microbiol.* 00, 1B.2.1-1B.2.15 (2006).

3. Zhang, Y. *et al.* A Microfluidic Approach for Quantitative Study of Spatial Heterogeneity in Bacterial Biofilms. *Small Sci.* 2, (2022).

4. Zhang, R. Y. *et al.* Use of lectins to in situ visualize glycoconjugates of extracellular polymeric substances in acidophilic archaeal biofilms. *Microb. Biotechnol.* 8, 448–461 (2015).

5. Ingino, P., Tiew, K. H. & Obst, M. Suitability of lectin binding studies for the characterization of redox-active microbial environmental biofilms. *AMB Express* 12, 140 (2022).

6. Eddenden, A., Kitova, E. N., Klassen, J. S. & Nitz, M. An Inactive Dispersin B Probe for Monitoring PNAG Production in Biofilm Formation. *ACS Chem. Biol.* 15, 1204–1211 (2020).

7. Pan, M., Zhu, L., Chen, L., Qiu, Y. & Wang, J. Detection Techniques for Extracellular Polymeric Substances in Biofilms: A Review. *BioResources* 11, 8092–8115 (2016).

8. Wang, T., Shen, P., He, Y., Zhang, Y. & Liu, J. Spatial transcriptome uncovers rich coordination of metabolism in E. coli K12 biofilm. *Nat. Chem. Biol.* 19, 940–950 (2023).

9. Joyce, J. G. *et al.* Isolation, structural characterization, and immunological evaluation of a high-molecular-weight exopolysaccharide from Staphylococcus aureus. *Carbohyd Res* 338, 903–922 (2003).

10. Wang, X., Preston, J. F. & Romeo, T. The pgaABCD Locus of Escherichia coli Promotes the Synthesis of a Polysaccharide Adhesin Required for Biofilm Formation. *J. Bacteriol.* 186, 2724–2734 (2004).

11. Jackson, D. W. *et al.* Biofilm Formation and Dispersal under the Influence of the Global Regulator CsrA of Escherichia coli. *J. Bacteriol.* 184, 290–301 (2002).

12. Reisner, A., Krogfelt, K. A., Klein, B. M., Zechner, E. L. & Molin, S. In Vitro Biofilm Formation of Commensal and Pathogenic Escherichia coli Strains: Impact of Environmental and Genetic Factors. *J. Bacteriol.* 188, 3572–3581 (2006).

13. Yakhnin, A. V. *et al.* CsrA activates flhDC expression by protecting flhDC mRNA from RNase E-mediated cleavage. *Mol. Microbiol.* 87, 851–866 (2013).

14. Romeo, T., Gong, M., Liu, M. Y. & Brun-Zinkernagel, A. M. Identification and molecular characterization of csrA, a pleiotropic gene from Escherichia coli that affects glycogen biosynthesis, gluconeogenesis, cell size, and surface properties. *J. Bacteriol.* 175, 4744–4755 (1993).

15. Christensen, G. D. *et al.* Adherence of coagulase-negative staphylococci to plastic tissue culture plates: a quantitative model for the adherence of staphylococci to medical devices. *J. Clin. Microbiol.* 22, 996–1006 (1985).

16. Gill, S. R. *et al.* Insights on Evolution of Virulence and Resistance from the Complete Genome Analysis of an Early Methicillin-Resistant Staphylococcus aureus Strain and a Biofilm-

Producing Methicillin-Resistant Staphylococcus epidermidis Strain. *J. Bacteriol.* 187, 2426–2438 (2005).

17. Panmanee, W. *et al.* High-Throughput Screening for Small-Molecule Inhibitors of Staphylococcus epidermidis RP62a Biofilms. *J. Biomol. Screen.* 18, 820–829 (2013).

18. Kaplan, J. B., Ragunath, C., Velliyagounder, K., Fine, D. H. & Ramasubbu, N. Enzymatic Detachment of Staphylococcus epidermidis Biofilms. *Antimicrob. Agents Chemother.* 48, 2633–2636 (2004).

19. Rohde, H. *et al.* Induction of Staphylococcus epidermidis biofilm formation via proteolytic processing of the accumulation-associated protein by staphylococcal and host proteases. *Mol. Microbiol.* 55, 1883–1895 (2005).

20. Christner, M. *et al.* The giant extracellular matrix-binding protein of Staphylococcus epidermidis mediates biofilm accumulation and attachment to fibronectin. *Mol. Microbiol.* 75, 187–207 (2010).

21. Cucarella, C. *et al.* Bap, a Staphylococcus aureus Surface Protein Involved in Biofilm Formation. *J. Bacteriol.* 183, 2888–2896 (2001).

22. Campoccia, D. *et al.* Exopolysaccharide Production by Staphylococcus Epidermidis and its Relationship with Biofilm Extracellular DNA. *Int. J. Artif. Organs* 34, 832–839 (2011).

23. Schommer, N. N. *et al.* Staphylococcus epidermidis Uses Distinct Mechanisms of Biofilm Formation To Interfere with Phagocytosis and Activation of Mouse Macrophage-Like Cells 774A.1. *Infect. Immun.* 79, 2267–2276 (2011).

24. Yu, S. *et al.* PslG, a self-produced glycosyl hydrolase, triggers biofilm disassembly by disrupting exopolysaccharide matrix. *Cell Res.* 25, 1352–1367 (2015).

25. Vo, L. H. *et al.* Mapping protein–exopolysaccharide binding interaction in Staphylococcus epidermidis biofilms by live cell proximity labeling. *bioRxiv* 2023.08.29.555326 (2023) doi:10.1101/2023.08.29.555326.

26. Garrett, T. R., Bhakoo, M. & Zhang, Z. Bacterial adhesion and biofilms on surfaces. *Prog. Nat. Sci.* 18, 1049–1056 (2008).

27. Limoli, D. H., Jones, C. J. & Wozniak, D. J. Bacterial Extracellular Polysaccharides in Biofilm Formation and Function. *Microbiol Spectr* 3, (2015).

28. Vu, B., Chen, M., Crawford, R. J. & Ivanova, E. P. Bacterial Extracellular Polysaccharides Involved in Biofilm Formation. *Molecules* 14, 2535–2554 (2009).

29. O'Toole, G., Kaplan, H. B. & Kolter, R. BIOFILM FORMATION AS MICROBIAL DEVELOPMENT. *Annu. Rev. Microbiol.* 54, 49–79 (2000).

30. Mukherjee, S. & Bassler, B. L. Bacterial quorum sensing in complex and dynamically changing environments. *Nat. Rev. Microbiol.* 17, 371–382 (2019).

31. Stoodley, P., Sauer, K., Davies, D. G. & Costerton, J. W. BIOFILMS AS COMPLEX DIFFERENTIATED COMMUNITIES. *Annu. Rev. Microbiol.* 56, 187–209 (2002).

32. Vlamakis, H., Aguilar, C., Losick, R. & Kolter, R. Control of cell fate by the formation of an architecturally complex bacterial community. *Genes Dev.* 22, 945–953 (2008).

33. Mack, D. *et al.* The intercellular adhesin involved in biofilm accumulation of Staphylococcus epidermidis is a linear beta-1,6-linked glucosaminoglycan: purification and structural analysis. *J. Bacteriol.* 178, 175–183 (1996).

34. Itoh, Y. *et al.* Roles of pgaABCD genes in synthesis, modification, and export of the Escherichia coli biofilm adhesin poly-beta-1,6-N-acetyl-D-glucosamine. *J Bacteriol* 190, 3670–80 (2008).

35. Chiba, A., Sugimoto, S., Sato, F., Hori, S. & Mizunoe, Y. A refined technique for extraction of extracellular matrices from bacterial biofilms and its applicability. *Microb. Biotechnol.* 8, 392–403 (2015).

36. Campoccia, D., Montanaro, L. & Arciola, C. R. Extracellular DNA (eDNA). A Major Ubiquitous Element of the Bacterial Biofilm Architecture. *Int. J. Mol. Sci.* 22, 9100 (2021).

37. O'Neill, E. *et al.* A Novel Staphylococcus aureus Biofilm Phenotype Mediated by the Fibronectin-Binding Proteins, FnBPA and FnBPB. *J. Bacteriol.* 190, 3835–3850 (2008).

38. Fitzpatrick, F., Humphreys, H. & O'Gara, J. P. Evidence for icaADBC-Independent Biofilm Development Mechanism in Methicillin-Resistant Staphylococcus aureus Clinical Isolates. *J. Clin. Microbiol.* 43, 1973–1976 (2005).

39. Jennings, L. K. *et al.* Pel is a cationic exopolysaccharide that cross-links extracellular DNA in the Pseudomonas aeruginosa biofilm matrix. *Proc. Natl. Acad. Sci.* 112, 11353–11358 (2015).

40. Grande, R. *et al.* Temporal expression of agrB, cidA, and alsS in the early development of Staphylococcus aureus UAMS-1 biofilm formation and the structural role of extracellular DNA and carbohydrates. *Pathog. Dis.* 70, 414–422 (2014).

41. Reichhardt, C. *et al.* The Versatile Pseudomonas aeruginosa Biofilm Matrix Protein CdrA Promotes Aggregation through Different Extracellular Exopolysaccharide Interactions. *J. Bacteriol.* 202, 10.1128/jb.00216-20 (2020).

Chapter 5: Summary and Future Directions

5.1 Summary and Future directions

Bacteria surfaces are predominately composed of polysaccharides that encapsulate cells and are essential of their survival. These surface polysaccharides are highly diverse in structure and play crucial roles in regulating cell permeability and mediating interactions with the surrounding environment.[1] Among these surface polysaccharides are exopolysaccharides (EPS) serve primarily as a cell adhesin during bacterial biofilm formation, often synthesized through the synthase dependent pathway.[2] Given the widespread integration of EPS within bacterial biofilms, the biochemical mechanism that initiates the biosynthesis of these polysaccharides remains an area of active investigation with speculations that synthase-dependent polysaccharide synthesis undergoes self-initiation process. This hypothesis has largely been supported by the reconstitution of activity of synthase dependent glycosyltransferase enzymes such as bacterial cellulose synthase (Bcs) and Hyaluronic acid synthase (HAS).[3,4]

A common EPS found in both Gram-positive and Gram-negative bacteria is Poly-β-(1→6)-N-acetylglucosamine (PNAG), has been proposed to undergo a self-initiation process. However, attempts at rescuing its activity from previously employed strategies has remained unsuccessful suggesting alternative mechanisms for initiation analogous to other surface polysaccharides. Revealing the molecular events underlying the onset of PNAG polymerization and to advance our understanding of synthase-dependent EPS biosynthesis in bacteria. Future studies should focus on the identifying the utilization of lipid substrates by these synthase-dependent pathways.

In additional to PNAG biosynthesis, *E. coli* possesses two additional biosynthetic pathways (Bsc and Nfr) capable to polymerizing alternative forms of EPS. Due to the innate stratification of biofilms and alternative roles of EPS such as the suppression of immune response by cellulose, it is possible that different EPS can also undergo differences in spatial distribution. By unveiling

how these EPS are utilized within biofilms could reveal additional regulatory mechanisms, leading to novel strategies for combating biofilm formations.

5.1.1 Initiation of PNAG biosynthesis by PgaCD complex

PgaCD is a GT2 family enzyme that facilitates the polymerization of PNAG within Gram-negative bacteria by catalyzing the glycosyl transfer from activated sugar nucleotides onto an acceptor substrate.[5] We begin our investigation by obtaining active PgaCD complex through expressing the proteins within the same membrane through a pETduet vector expression system. Generation of the PgaCD fusion protein (PgaCDf) retained its enzymatic activity while ensuring the proper oligomerization of the enzyme. The activity of each protein variant was measured based on conversion of the substrate UDP-GlcNAc to form free UDP upon polymerization of the GlcNAc residues by HPLC through reverse phase chromatography. To confirm the polymerization of the GlcNAc residues, *de novo* synthesized PNAG was isolated and analysis by CP-MAS NMR and revealed δ are characteristic of unsaturated lipid carbons.

Further investigation of the *de novo* PNAG revealed its localization with the membrane after polymerization. To ensure the PNAG association with the membrane was do due to encapsulation within the proteoliposome (PL) IMVs formed during sonication, we treated the reaction with DspB wt. Robust hydrolysis of PNAG in both the crude reaction mixture and the centrifuged membrane pellet without prior membrane disruption indicating the association of PNAG was not due to encapsulation, rather via an alternative mechanism.

Previous evidence of self-initiation involves the hydrolysis of the UDP-sugars, leaving the free sugar to serve as the initial acceptor for polymerization. This concept is supported by the observed activity from purified glycosyl transferase enzymes incubated with just their cognate nucleotide-sugar substrates.[6] However, attempts at reconstituting activity within purified PgaCD

variants did not rescue its activity. Additional incubation of free GlcNAc residues with active PgaCD had no significant impact, suggesting that free GlcNAc monosaccharide does not serve as a primer substrate for PNAG biosynthesis catalyzed by PgaCD.

5.1.2 Spatial distribution of EPS in bacterial biofilms

Due to the stratification of bacterial biofilms, it is important develop techniques that can accurately capture the architecture of the biofilms. Flow-based devices coupled with confocal microcopy has been an emerging strategy for studying biofilms under dynamic conditions without disturbing its architecture.[7,8] Conventional flow devices rely on random adherence of bacterial cells during growth initiation, leading to variances between experiments. Here we were able to incorporate a novel microfluidic device with an integrated cell seeding mechanism to produce predictive biofilm profiles, allowing for direct comparison.

The utilization of the microfluidic device coupled with PNAG specific probe (catalytically inactive PNAG specific hydrolase Dispersin B mutant (DspBE184), fused to eGFP (DspBinactive-eGFP)) unveiled differential PNAG distribution within Gram-positive (*S. epidermidis* RP62A) and Gram-negative (*E. coli* MG1655Δ*csrA*) bacterial biofilms.[9] In *E. coli* biofilms, PNAG predominantly localized within the biofilm core, whereas *S. epidermidis* biofilms showed higher peripheral PNAG concentrations. Biofilm dispersal assays additionally revealed differences in PNAG hydrolysis and biofilm disruption between the two biofilm-forming bacterial species. Compete dissociation was observed for *E. coli* biofilms while the core of the *S. epidermidis* biofilm remained largely intact after initial shedding of the peripheral cells suggesting additional adhesion factors contribute to the cohesion and integrity of the *S. epidermidis* biofilm. We were able to demonstrate the versatility of the microfluidic platform for simultaneous cultivation, imaging, and targeted dispersal of diverse bacterial biofilms.

5.2 Closing remarks

During this dissertation, we investigated the initiation mechanism of PNAG biosynthesis by PgaCD complex through a combination of enzyme kinetics and polysaccharide analysis. Collectively, our results challenged the previous notion of a self-initiating mechanism employed by glycosyl transferases. Specifically, PgaCD activity is not affected by the presence of free GlcNAc residues and *de novo* synthesized PNAG revealed lipid corresponding peaks while demonstrating membrane association after polymerization. Due its prevalence and vital role in promoting biofilm formation identifying how these EPS are initiated would be instrumental in unveiling novel strategies at combating formation. In addition to PNAG initiation, we uncovered differential PNAG distribution and dispersal within commonly studied biofilms by utilizing a microfluidic platform that permitted the cultivation, labeling and dispersal of biofilms *in situ*. Revealing the differences of PNAG utilization between bacterial species demonstrates the diversity of EPS disruption and its role in cellular cohesion.

Appendix

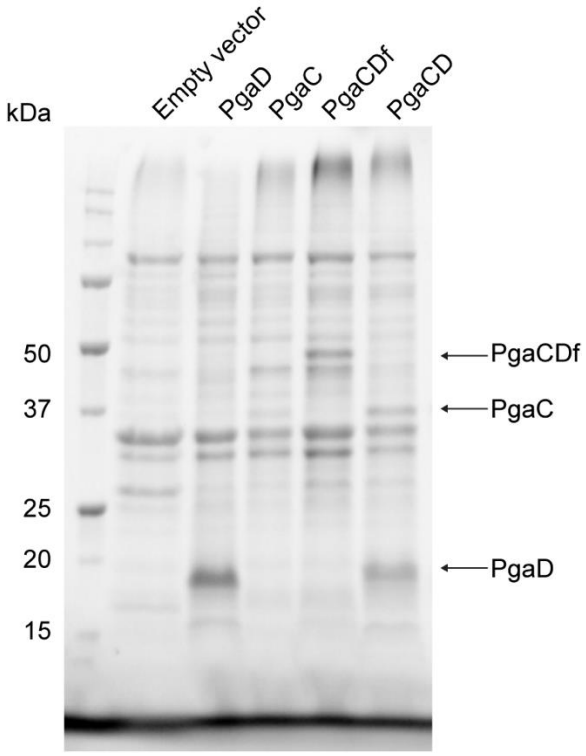

Supplemental Figure 1. Overexpression of pga proteins. Proteins were overexpressed in BL21(DE3) cells. 500mL LB cultures were grown until OD600 reached 0.5-0.6 and cooled on ice for 10-15mins. ITPG (200µM) was added, and the culture was left shaking at 200rpm for 20 hours. Cells were harvested through centrifugation at 5,500 x g and lysed through sonication. Lysate was centrifuged at 13,000 x g to remove large cell debris. The supernatant was floated on top of 1.8M sucrose solution and centrifuged at 60,000 x g for 1 hour. The middle layer was removed and centrifuged at 60,000 x g to pellet the membrane fraction and resuspended to 200mg/mL and stored in -80^{o}C until use.

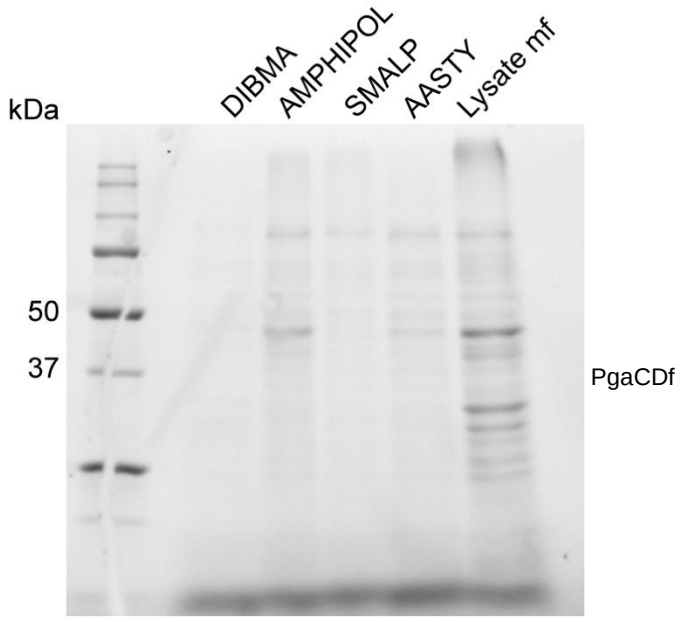

Supplemental Figure 2. Nano-disc solubilization screening of PgaCDf using various polymers. Crude membrane fractions containing PgaCDf were incubated in 1% w/v polymer final concentration in 25mM Tris-HCl 150mM NaCl pH 7.4 at 4^{o}C overnight on rotator. The mixture was centrifuged at 60,000 x g for 1 hour before the supernatant containing the solubilized protein was removed and analyzed by SDS-PAGE. Abbreviations; DIBMA: Diisobutylene-maleic acids, AMPHIPOL: Amphiphilic polymer, SMALP: Styrene maleic anhydride, AASTY: Poly(acrylic acid-co-styrene), mf: membrane fraction.

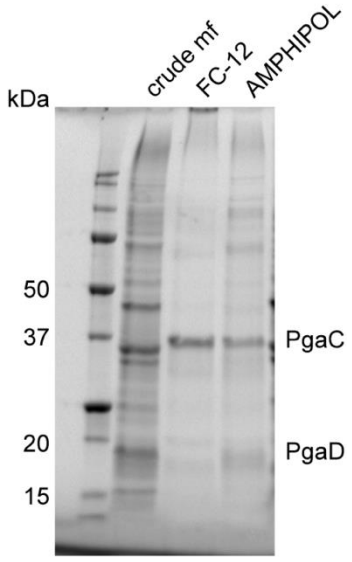

Supplemental Figure 3. Solubilization efficiency of PgaCD in Fos-choline 12 vs AMPHIPOL. Both solubilization strategies were able to co-purify PgaC and PgaD, with AMPHIPOL having efficiency.

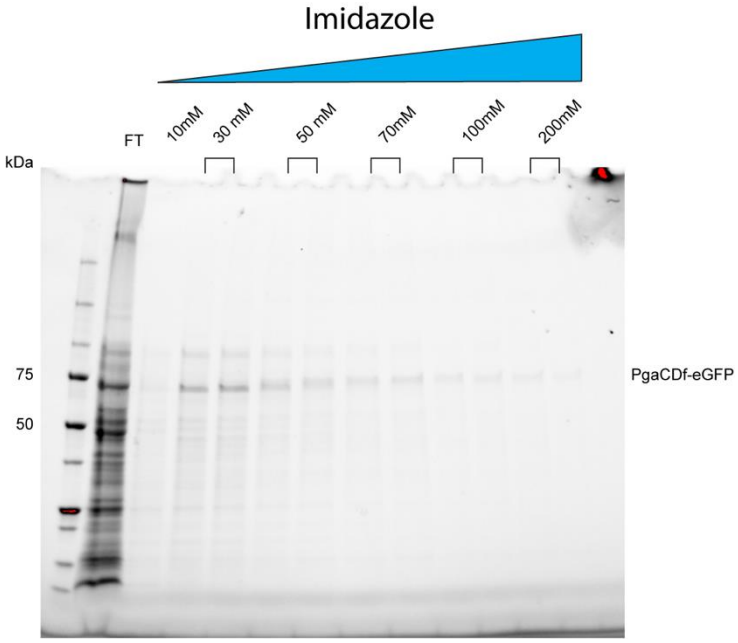

Supplemental Figure 4. Stepwise gradient elution purification. Purification of PgaCDf-eGFP by Ni-NTA column using step gradient elution of imidazole. AMPHIPOL nano discs containing

PgaCDf-eGFP were incubated with Ni-NTA resin overnight at 4^{o}C while rotating. Resin was transferred to spin column and eluted using 400µL of elution buffers. Columns were centrifuged at 0.7 x g for 2 mins. Elution buffer: 25mM sodium phosphate, 150mM NaCl, pH 7.4.

References

1. Cooper, C. A., Mainprize, I. L. & Nickerson, N. N. Prokaryotic Systems Biology. *Adv. Exp. Med. Biol.* 883, 295–315 (2015).

2. Whitney, J. C. & Howell, P. L. Synthase-dependent exopolysaccharide secretion in Gram-negative bacteria. *Trends Microbiol.* 21, 63–72 (2013).

3. Omadjela, O. *et al.* BcsA and BcsB form the catalytically active core of bacterial cellulose synthase sufficient for in vitro cellulose synthesis. *Proc. Natl. Acad. Sci.* 110, 17856–17861 (2013).

4. Hubbard, C., McNamara, J. T., Azumaya, C., Patel, M. S. & Zimmer, J. The Hyaluronan Synthase Catalyzes the Synthesis and Membrane Translocation of Hyaluronan. *J. Mol. Biol.* 418, 21–31 (2012).

5. Itoh, Y. *et al.* Roles of pgaABCD genes in synthesis, modification, and export of the Escherichia coli biofilm adhesin poly-beta-1,6-N-acetyl-D-glucosamine. *J Bacteriol* 190, 3670–80 (2008).

6. Maloney, F. P. *et al.* Structure, substrate recognition and initiation of hyaluronan synthase. *Nature* 604, 195–201 (2022).

7. Schlafer, S. & Meyer, R. L. Confocal microscopy imaging of the biofilm matrix. *J. Microbiol. Methods* 138, 50–59 (2017).

8. Wang, T., Shen, P., He, Y., Zhang, Y. & Liu, J. Spatial transcriptome uncovers rich coordination of metabolism in E. coli K12 biofilm. *Nat. Chem. Biol.* 19, 940–950 (2023).

9. Eddenden, A., Kitova, E. N., Klassen, J. S. & Nitz, M. An Inactive Dispersin B Probe for Monitoring PNAG Production in Biofilm Formation. *ACS Chem. Biol.* 15, 1204–1211 (2020).